SPINODAL INSTABILITIES IN SYMMETRIC NUCLEAR MATTER WITHIN A DENSITY-DEPENDENT RELATIVISTIC MEAN-FIELD APPROACH

A THESIS SUBMITTED TO
THE GRADUATE SCHOOL OF NATURAL AND APPLIED SCIENCES
OF
MIDDLE EAST TECHNICAL UNIVERSITY

BY

BETÜL DANIŞMAN

IN PARTIAL FULFILLMENT OF THE REQUIREMENTS
FOR
THE DEGREE OF MASTER OF SCIENCE
IN
PHYSICS

AUGUST 2011

Approval of the thesis:

SPINODAL INSTABILITIES IN SYMMETRIC NUCLEAR MATTER WITHIN A DENSITY-DEPENDENT RELATIVISTIC MEAN-FIELD APPROACH

submitted by **BETÜL DANIŞMAN** in partial fulfillment of the requirements for the degree of **Master of Science in Physics Department, Middle East Technical University** by,

Prof. Dr. Canan Özgen _____
Dean, Graduate School of **Natural and Applied Sciences**

Prof. Dr. Sinan Bilikmen _____
Head of Department, **Physics**

Prof. Dr. Osman Yılmaz _____
Supervisor, **Physics Department, METU**

Prof. Dr. Şakir Ayık _____
Co-supervisor, **Physics Dept., Tennessee Tech University**

Examining Committee Members:

Prof. Dr. Ahmet Gökalp
Physics Dept., METU _____

Prof. Dr. Osman Yılmaz
Physics Dept., METU _____

Prof. Dr. Şakir Ayık
Physics Dept., Tennessee Tech University _____

Prof. Dr. Gürsevil Turan
Physics Dept., METU _____

Assoc. Prof. Dr. Hüseyin Oymak
Engineering Faculty, Atılım University _____

Date: _____

I hereby declare that all information in this document has been obtained and presented in accordance with academic rules and ethical conduct. I also declare that, as required by these rules and conduct, I have fully cited and referenced all material and results that are not original to this work.

Name, Last Name: BETÜL DANIŞMAN

Signature :

ABSTRACT

SPINODAL INSTABILITIES IN SYMMETRIC NUCLEAR MATTER WITHIN A DENSITY-DEPENDENT RELATIVISTIC MEAN-FIELD APPROACH

Danışman, Betül
M.Sc., Department of Physics
Supervisor : Prof. Dr. Osman Yılmaz
Co-Supervisor : Prof. Dr. Şakir Ayık

August 2011, 78 pages

The nuclear matter liquid-gas phase transition is expected to be a signal of nuclear spinodal instabilities as a result of density fluctuations. Nuclear spinodal instabilities in symmetric nuclear matter are studied within a stochastic relativistic density-dependent model in semi-classical approximation. We use two parameterization for the Lagrange density, DDME1 and TW sets. The early growth of density fluctuations is investigated by employing relativistic Vlasov equation based on QHD and discussed the cluster size of the condensations from the early growth of density correlation functions. Expectations are that hot nuclear matter behaves unstable around $\rho_b \approx \rho_0/4$ (below the saturation density) and at low temperatures. We therefore present our results at low temperature T=1 MeV and at higher temperature T=5 MeV, and also at a lower initial baryon density $\rho_b = 0.2\ \rho_0$ and a higher value $\rho_b = 0.4\ \rho_0$ where unstable behavior is within them.

Calculations in density-dependent model are compared with the other calculations obtained in a relativistic non-linear model and in a Skyrme type non-

relativistic model. Our results are consistent with them. Qualitatively similar results show that the physics of the quantities are model-independent. The size of clusterization is estimated in two ways, by using half-wavelength of the most unstable mode and from the width of correlation function at half maximum. Furthermore, the average speed of condensing fragments during the initial phase of spinodal decomposition are determined by using the current density correlation functions.

Keywords: Spinodal instabilities, nuclear multi-fragmentation, density-dependent relativistic mean-field approach, Vlasov equation.

ÖZ

YOĞUNLUĞA BAĞLI RELATİVİSTİK ORTALAMA ALAN YAKLAŞIMINDA SİMETRİK NÜKLEER MADDENİN SPİNODAL KARARSIZLIKLARI

Danışman, Betül
Yüksek Lisans, Fizik Bölümü
Tez Yöneticisi : Prof. Dr. Osman Yılmaz
Ortak Tez Yöneticisi : Prof. Dr. Şakir Ayık

Ağustos 2011, 78 sayfa

Sonsuz simetrik nükleer maddedeki spinodal kararsızlıklar, yoğunluğa bağlı relativistik stokastik ortalama alan modeli kullanılarak yarı-klasik yaklaşımda çalışıldı. Lagrange yoğunluğu için iki parametri seti olarak DDME1 ve TW setleri kullanıldı. Yoğunluk dalgalanmalarının ilk anlarındaki büyüme QHD'yı esas alan relativistik Vlasov denklemi kullanılarak incelendi ve yoğunluk korelasyon fonksiyonlarının ilk anlarında oluşan yoğunlaşmaların boyutları tartışıldı. Sistemin en kararsız davranışının düşük sıcaklıklarda ve doygunluk değerinin altındada $\rho_b = \rho_0/4$ yoğunluğu etrafında olması beklenir. Bu nedenle, sonuçlar T=1 MeV ve T=5 MeV sıcaklıklarında ve sistemin kararsız olduğu iki farklı başlangıç baryon yoğunlukları olan $\rho_b = 0.2\rho_0$ ve $\rho_b = 0.4\rho_0$ için incelendi.

Yoğunluğa bağlı olarak çalışılan modelde elde edilen sonuçlar, relativistik linear olmayan ve Skyrme-tipi relativisitik olmayan modeller kullanılarak yapılan çalışmalarda elde edilen hesaplarla karşılaştırıldı. Elde edilen sonuçların birbirleriyle uyumlu oldukları gözlendi. Bulunan benzer sonuçlar, niceliklerin fiziğinin

modelden bağımsız olduğunu gösterdi. En kararsız modların yarı-dalgaboylarının yarısı ve korelasyon fonksiyonlarının maximum genişliğinin yarısına karşı gelen mesafelerin, yoğunlaşmaların boyutları olarak elde edildi. Ayrıca, spinodal ayrışmanın ilk evresindeki yoğunlaşan damlacıkların ortalama hızları, akım yoğunluğu korelasyon fonksiyonları kullanılarak elde edildi.

Anahtar Kelimeler: Spinodal kararsızlıklar, nükleer parçalanma, yoğunluğa bağlı relativistik ortalama alan yaklaşımı, Vlasov denklemi.

ACKNOWLEDGMENTS

I would like to express my deepest appreciation to my supervisor Prof. Dr. Osman Yılmaz and my co-supervisor Prof. Dr. Şakir Ayık. With their great efforts to explain things clearly and simply, they helped me to complete this period. Without their guidance and help, this dissertation would not have been possible. I would like to thank Assoc. Prof. Dr. Hüseyin Oymak for teaching me the techniques of programming and writing. Also I want to thank Fatma Acar for endless patience and support. Without her big contribution, it would be very difficult to finish my Ms thesis. I am deeply thankful to my loving husband Rahmi Danışman for helping me to get through the difficult times, for all emotional support and my parents Sevgi and İsmail Hatipoğlu for providing a loving environment for me. They provided me encouragement, sound advice and support in various ways. To my family, my husband and my little daughter, I dedicate this thesis. This work is partially supported by TUBITAK, Turkish Scientific and Technical Research Council, though grant No. 110T274.

TABLE OF CONTENTS

LIST OF TABLES

TABLES

LIST OF FIGURES

FIGURES

CHAPTER 1

INTRODUCTION

The basic interest of the latest nuclear physics research is the investigation of structure and physical properties of atomic nucleus, and to develop the theories explaining these properties in the best way. In other words, the investigation of nuclear matter behavior at different temperature and pressure, and investigation of phase transition depending on temperature and pressure are the basic concern of the nuclear physics. Then, the final goal is to obtain the nuclear matter equation of state (EOS).

Infinite nuclear matter, in which surface effects are ignored, is an idealized system for studying the nucleon-nucleon interaction. On the other hand, symmetric nuclear matter at finite temperature provides a rough picture of hot nuclear systems and the liquid-gas phase transition. Symmetric nuclear matter contains equal number of protons and neutrons, and for simplicity Coulomb interaction between protons is ignored. The investigation of hot nuclear matter is a very important tool to study some astrophysical systems at abnormal densities such as neutron stars or black holes, and to understand the history of the early universe [1].

Heavy ion collisions in existing accelerators are studied to understand the properties of hot nuclear systems on Earth. The phase transition of hot nuclei is studied in multifragmentation events. Hot nuclear matter produced in the early stages collisions of heavy ions at intermediate energies expands, cools down and becomes dynamically unstable at sub-saturation densities. This unstable region

of hot nuclear matter is called spinodal region in which the fragmentation occurs. In this situation, it is important to include fluctuations. In spinodal region, the small density fluctuations grow rapidly and it leads to the system break into fragmentation. [2].

The properties of nuclear matter at equilibrium can be investigated in terms of the equation of state, which is a relation between pressure, density and temperature. The phase of nuclear matter depends on temperature and baryon density. In heavy-ion collisions, nuclear matter is excited and multifragmentation may occur. The process of de-excitation depends on the initial conditions and initial temperature of nuclear matter. If initial pressure and temperature is high enough, the nuclear system completely disintegrate into protons and neutrons; this can be called vaporization. However, when the initial pressure and temperature is not high enough, pressure would be negative after one point and expansion would decrease. So, nuclear matter oscillates around equilibrium density. If initial temperature and pressure are below the critical values, before ending the expansion, the system may enter into the unstable region and breaks up into the big and small mixed fragments. This process is known as multifragmentation. Multifragmentation is considered as a possible signature of the liquid-gas phase transition [1].

Nuclear forces are repulsive at short range and attractive at long and intermediate ranges; so, there is a similarity between the nuclear system and a van der Waals fluid which represents the interaction between neutral atoms or molecules of gases [3]. At normal density and zero temperature, nuclei behave like Fermi liquids and therefore at the lowest energies and at normal states, the nuclear matter shows liquid-like characteristics. After heated at a temperature of a few MeV, some of the nuclei start to evaporate and a liquid-gas phase transition occurs at subnormal densities. In this scale of temperature, the van der Waals type of behavior (a liquid-gas phase transition) is expected to be seen.

Spinodal instabilities arised in heavy ion collision are fast processes (occurred in 10^{-22} s) [4]. If system can stay together sufficiently long time, thermal and

chemical equilibrium may be reached. Therefore, it is not very easy to observe signature of spinodal instabilities.

The experimental phase diagrams based on 8 GeV/c $\pi+$ Au data of the ISIS collaboration are given in [5]. By detecting charge distribution of heaviest fragments in intermediate energy-ion collisions, a signal of phase transition in non extensive system is observed [6]. Furthermore, the observation of charge correlations for fragments in the collisions between ^{129}Xe and ^{nat}Sn at 32 MeV/nucleon is interpreted as a signal of spinodal instabilities in finite system [7, 8].

Mean-field transport theory (MFT) cannot explain the dynamics of density fluctuation process. The single-particle density matrix satisfies the transport equation and the mean-field approximation method involves one-body dissipation mechanism. While Time- Dependent Hartree-Fock (TDHF) gives good description for average evaluation of collective modes, it is insufficient to define the fluctuations of the collective motion. Similarly, the Bolzmann-Uhling-Uhlenbeck (BUU) model can be used for one-body and collisional dissipation, but it is not proper to used for fluctuation mechanism [8]. The stochastic transport theory describes dynamics of density fluctuation more suitably at intermediate energies [9].

Hot nuclear matter and the thermodynamical properties of nucleus are studied with several approaches such as Hartree-Fock Method [10, 11], Thomas-Fermi Approach [12, 13], Relativistic Mean Field Approach [13, 14], non relativistic mean-field calculations with the Skyrme and Gogny type effective forces [15, 16] and relativistic mean-field calculations based on the meson exchange interactions [17, 18, 19]. We use a relativistic stochastic mean-field approach with density dependent coupling parameters in order to investigate nuclear instabilities in spinodal region.

There are theorical investigations about spinodal instabilities based on stochastic transport models [20, 21, 22, 23, 24]. The early development of density fluctuations in spinodal region is studied within a stochastic mean-field approach with

density-dependent Skyrme-type interactions [15, 25], and a similar work is made within the relativistic stochastic mean-field approach [26]. The spinodal instabilities and the evolution of density fluctuations are studied in the stochastic extension of the Walecka-type relativistic mean-field approach [26, 27].

In this thesis, we use the density-dependent stochastic mean-field model with meson-nucleon density-dependent couplings. In Chapter 2, we explain the details of the stochastic extension of the relativistic mean-field theory in the semi-classical approximation. In Chapter 3, the early growth of the correlation function of density fluctuations are discussed in symmetric nuclear matter. Relativistic Vlasov equation and meson field equations are linearized by considering small fluctuations of the mean field around its equilibrium value and obtain three coupled equations for scalar, baryon and current density fluctuations. We solve the equation of motion by employing the method of one sided Fourier transformation and then derive the correlation functions. In Chapter 4, we calculate numerically the growth rates of unstable modes of initial densities fluctuation in spinodal region, in other words unstable solutions of dispersion relations. Also, phase diagrams from dispersion relations are discussed . The size of the primary clusters in spinodal region from baryon density correlation function and the average speed of condensing fragments at the initial phase of spinodal decomposition are determined from current correlation functions. Conclusions are given in Chapter 5.

CHAPTER 2

DENSITY DEPENDENT RELATIVISTIC MEAN-FIELD THEORY

2.1 Density-Dependent Mean-Field Model for Hot Nuclear Matter

2.1.1 Introduction

Nuclei and nuclear matter are complex systems. The strong interaction between nucleons is not known well and therefore different approaches are used for two-body nucleon-nucleon interaction. The One-Boson-Exchange potential (OBE) is an example which depends on the exchange of the non-strange mesons (neutral scalar σ , neutral vector ω, charged scalar δ , charged vector ρ , charged pseudoscalar π and neutral pseudoscalar η).

In 1974, John Dirk Walecka introduced a simple relativistic model for nuclear matter based on the exchange of only a neutral scalar σ meson for the attractive force, and a neutral vector ω meson for the short range repulsion force [14]. The charged mesons, such as rho meson, are not considered in this simplest model. By using this model, the nuclear many-body problem can be described as a relativistic system of nucleons and mesons. This model is called Walecka model (or $\sigma - \omega$ model) in quantum hadrodynamics (QHD). The coupling constants between meson and nucleon fields are unknown parameters and determined by fitting experimental data to the nuclear matter properties, such as saturation density, binding energy and compressibility, to give the saturation properties of

nuclear matter. The in-medium interaction effects are added to the system with density dependent vertices $\Gamma_\alpha(\rho)$,in the density-dependent models. [28, 29, 30, 31].

Since the scalar σ meson and the vector ω meson have different Lorentz structure and they give the correct minimum value $E/B = -15.75MeV/Nucleon$ at saturation density $\rho_0 = 0.16fm^{-3}$ due to a cancelation between the large attractive contribution of the scalar field and a large repulsive contribution from the vector field. In the standard Walecka model, the effective mass value $M^* = 0.55M$ is too small and the nuclear incompressibility $K = 540MeV$ is too high at saturation density. In the density-dependent coupling model and nonlinear model the reduced mass and compressibility are responsible compared with observed value.

In this chapter, we start with a Lorentz-invariant Lagrangian density to derive the eqautions of state at zero and finite temperature in the relativistic density-dependent mean-field model, in which the interaction between nucleons (protons and neutrons) are mediated by neutral scalar σ and neutral vector ω mesons. Since the equations of motion are non-linear coupled equations and the coupling constants in equations are large, perturbation solutions are not practicable. The relativistic mean-field approximation (RMF) is discussed to solve the equations.

2.1.2 Formalism

A Lagrangian density with density-dependent meson-nucleon couplings for a system of nucleons interacting via a neutral scalar meson with mass m_s and a neutral vector meson with mass m_ω is given by

$$\begin{aligned} L_{DDM} &= \overline{\psi}[\gamma^\mu(i\hbar\partial_\mu - \Gamma_\omega(\rho)V_\mu) - (Mc^2 - \Gamma_s(\rho)\phi)]\psi \\ &\quad + \frac{1}{2}(\partial_\mu\phi\partial^\mu\phi - \mu_s^2\phi^2) - \frac{1}{4}\Omega_{\mu v}\Omega^{\mu v} + \frac{1}{2}\mu_v^2 V_\mu V^\mu \end{aligned} \tag{2.1}$$

where ϕ and V_μ denote the scalar and vector meson fields respectively while ψ represents the nucleon field,$\Omega_{\mu v} = \partial_\mu V_v - \partial_v V_\mu$ is the vector field tensor [31]

and $\mu_s = m_s c/\hbar$, $\mu_v = m_\omega c/\hbar$. Here, the scalar density of baryon field is coupled to scalar meson and the conserved baryon current is coupled to vector mesons [14]. The lagrangian density is given in terms of the point couplings as $L_{SWM} = L_{DDM}(\Gamma_\omega(\rho) \to g_\omega, \Gamma_s(\rho) \to g_s)$ in the original Walecka model (SWM) and $L_{NLWM} = L_{DDM}(\Gamma_\omega(\rho) \to g_\omega, \Gamma_s(\rho) \to g_s) - \frac{\kappa}{3!}\phi^3 - \frac{\lambda}{4!}\phi^4$ in the nonlinear Walecka model (NLWM) with non linear self-interaction terms.

In the density-dependent coupling model, density-dependent meson-nucleon couplings for scalar and neutral vector mesons are parameterized by

$$\Gamma_i(\rho) = \Gamma_i(\rho_0) a_i \frac{1 + b_i(\rho/\rho_0 + d_i)^2}{1 + c_i(\rho/\rho_0 + d_i)^2} \tag{2.2}$$

where $i = s, \omega$ (neutral scalar and vector mesons) and ρ_0 is the baryon density at saturation in symmetric nuclear matter. The parameters a_i, b_i, c_i and d_i are real and positive but not independent [14, 29, 30, 31]. The parameter sets, TW introduced by Typel and Wolter [29] and DDME1 [31] that we use in our calculations are given Table 2.1. Fitting properties of nuclear matter are given in Table 2.2.

In this thesis, we use the density dependent model for calculations. The calculations with NL3 set are produced in another work [26]. We use the results obtained in NL3 [31] to compare with our results.

Density dependence of the meson-nucleon coupling constants for the σ and ω mesons in the TW and DDME1 parameterizations are shown in Fig. (2.1). If they are compared around the saturation density, the overall trend is seen to be similar but there is about 25% difference between σ and ω mesons couplings. Γ_s and Γ_ω in both TW and DDME1 are separately consistent at normal and under normal densities. However, they go away from each other at higher densities.

By using the Eurler- Lagrange equation, the field equations (scalar, vector and baryon fields) can be derived as

Table 2.1: Parameters in nonlinear and density-dependent models

	NL3	TW	DDME1
$m_s(MeV)$	508.194	550.0	549.5255
$m_\omega(MeV)$	782.501	783.0	783.0
$\Gamma_s(\rho_0)$	10.217	10.7285	10.4434
$\Gamma_\omega(\rho_0)$	12.868	13.2902	12.8993
$\kappa(fm^{-1})$	10.431	0	0
λ	-28.885	0	0
a_s	1	1.36547	1.3854
b_s	0	0.22606	0.9781
c_s	0	0.40970	1.5342
d_s	0	0.90199	0.4661
a_ω	1	1.40249	1.3879
b_ω	0	0.17258	0.8525
c_ω	0	0.34429	1.3566
d_ω	0	0.98396	0.4957

Table 2.2: Nuclear Matter Properties

	NL3	TW	DDME1
$\rho_0(fm^{-3})$	0.148	0.153	0.152
E/A (MeV)	-16.3	-16.3	-16.20
K (MeV)	272	240	244.5
M^*/M	0.60	0.56	0.578

$$(\partial_\mu \partial^\mu + \mu_s^2)\phi = \Gamma_s \overline{\psi}\psi, \tag{2.3}$$

$$(\partial_\mu \partial^\mu + \mu_v^2)V^\mu = \Gamma_\omega \overline{\psi}\gamma^\mu\psi, \tag{2.4}$$

$$[\gamma^\mu(i\hbar\partial_\mu - \Gamma_\omega V_\mu) - (Mc^2 - \Gamma_s\phi)]\psi = 0. \tag{2.5}$$

The Eq. (2.3) is a Klein-Gordon equation with the baryon scalar density $\overline{\psi}\psi$ as a source term and Eq. (2.4) is the Proca equations with source terms $\overline{\psi}\gamma^\mu\psi$. The last one is the Dirac equation for nucleon field including the interactions with scalar and vector fields.

The Eqs. (2.3-5) are nonlinear coupled equations and there is not a suitable method to solve them exactly. We use the mean-field approximation to solve them. In this theory, all meson field operators are replaced by their ground

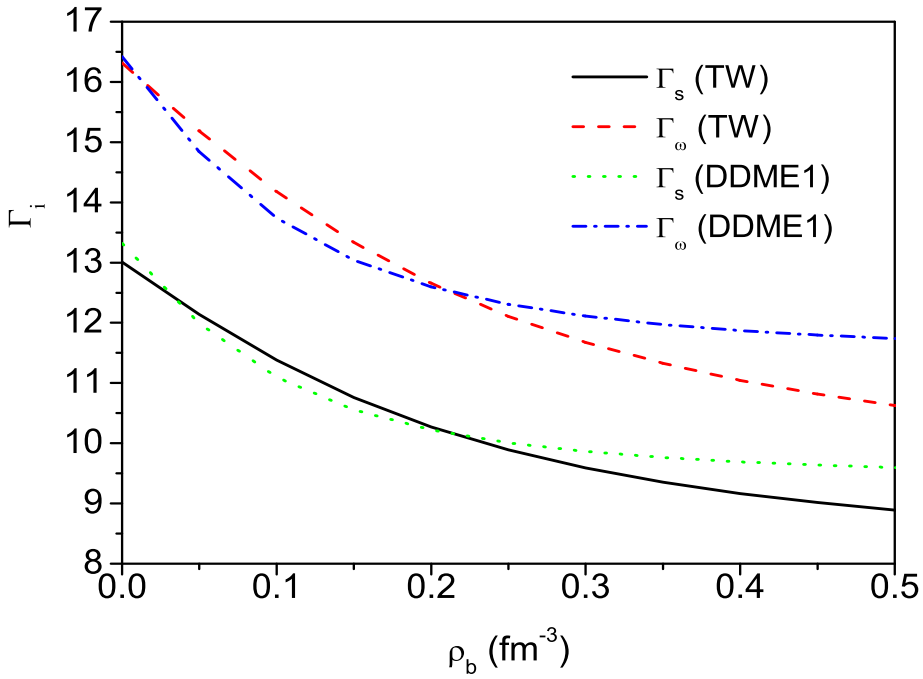

Figure 2.1: Density dependence of the meson-nucleon vertices for σ and ω mesons in the TW and DDME1 parameterizations.

state expectation values of field operators which are treated as classical fields [14] $\phi \to \langle\phi\rangle = \phi_0, V^\mu \to \langle V^\mu\rangle = V_0\Gamma^{\mu 0}$ that are independent of time and the space for a uniform system at equilibrium. So the equations of motion can be solved exactly in the mean-field limit. Here we use that the spatial components of $\langle V^\mu\rangle$ vanishes since the system is static and baryon flux becomes zero [14].

The baryon operators in the source terms are also replaced by their normal order expectation values in the mean-field ground state as $\overline{\psi}\psi \to \langle\overline{\psi}\psi\rangle = \rho_s$ and $\overline{\psi}\gamma^\mu\psi \to \langle\overline{\psi}\gamma^\mu\psi\rangle = g^{\mu 0}\rho_b$. We use the normal ordered expectation values; because, the contributions from the negative energy baryons are neglected. Hence only the positive energy baryon states are considered.

Now, we can write the meson equations in the mean-field approximation as

$$(\partial_\mu\partial^\mu + \mu_s^2)\phi_0 = \Gamma_s\rho_s^0 \tag{2.6}$$

$$(\partial_\mu\partial^\mu + \mu_v^2)\langle V^\mu\rangle = \Gamma_\omega\langle\overline{\psi}\gamma^\mu\psi\rangle \tag{2.7}$$

At the equilibrium as an initial state, the system is static, uniform and independent of position and time. The final equations for meson fields are then found as

$$\phi_0 = \frac{1}{\mu_s^2}\Gamma_s \rho_s^0 \tag{2.8}$$

$$V_0^0 = \frac{\Gamma_\omega}{\mu_v^2}\rho_b^0 \tag{2.9}$$

$$\vec{V_0} = 0 \tag{2.10}$$

We also construct the RMF energy-momentum tensor $T^{\mu\nu}$ of the system, which gives some properties of the system such as energy and pressure. The energy-momentum tensor in continuum mechanics is defined by [32]

$$T^{\mu\nu} = \frac{\partial L}{\partial(\partial q_i/\partial x^\mu)}\frac{\partial q_i}{\partial x_\nu} - \Gamma^{\mu\nu}L \tag{2.11}$$

where q_i denotes physical fields. By using Lagrangian density in Eq. (2.1) we then have

$$T^{\mu\nu} = \overline{\psi}\gamma^\mu i\hbar\partial_\nu\psi - \Gamma^{\mu\nu}\left[-\frac{1}{2}\left[\frac{m_s c}{\hbar}\right]^2\phi_0^2 + \frac{1}{2}\left[\frac{m_\nu c}{\hbar}\right]^2 V_0^2\right] \tag{2.12}$$

An important property of $T^{\mu\nu}$ is energy- momentum conservation. For example, if a field exchange energy and momentum with a particle, particle energy and momentum changing rate must be the same as the change in the rate of the field energy and momentum. By using the baryon field equations given by Dirac equation, we can show that the canonical energy-momentum tensor $T^{\mu\nu}$ is conserved ($\partial_\mu T^{\mu\nu} = 0$) . If the Lagrangian does not depend on space-time coordinates explicitly, energy momentum tensor is conserved. Energy density is the zero component of this tensor $\varepsilon = \langle T^{00}\rangle$, and it can be calculated as

$$\varepsilon = \langle\overline{\psi}\gamma^0 i\hbar\partial_0\psi\rangle + \frac{1}{2}\left[\frac{m_s c}{\hbar}\right]^2\phi_0^2 - \frac{1}{2}\left[\frac{m_\nu c}{\hbar}\right]^2 V_0^2 \tag{2.13}$$

The pressure can be calculated from $P = \frac{1}{3}\langle T^{ii}\rangle$ as

$$P = \frac{1}{3}\langle\overline{\psi}\gamma^i i\hbar\partial_i\psi\rangle - \frac{1}{2}\left[\frac{m_s c}{\hbar}\right]^2\phi_0^2 + \frac{1}{2}\left[\frac{m_\nu c}{\hbar}\right]^2 V_0^2 \tag{2.14}$$

The energy density per nucleon is a starting point to drive the properties of the nuclear matter at different temperatures and densities. While the pressure is defined in terms of the energy density as $p(\rho_b) \equiv \rho_b(\partial\varepsilon/\partial\rho_b) - \varepsilon(\rho_b)$, the binding energy per nucleon is written according to the energy density as $E_B = (\varepsilon/\rho_b) - Mc^2$. Incompressibility is also expressed as the slope of the pressure at saturation density $K = 9\left[\frac{\partial P}{\partial\rho}\right]_{\rho_b=\rho_0}$. In this work, we evaluate and discuss the energy density and pressure of nuclear-matter at zero and finite temperature.

2.1.3 Nuclear Matter at Zero Temperature

The equation of state of nuclear matter (EOS) describes the behavior of a system of nucleons at different temperatures and densities. Also it gives the relation between energy per nucleon and Fermi momentum k_F or baryon density ρ_b. In this thesis, we study both zero and finite temperature cases.

For the final form of the equation of states given in Eqs. (2.13) and Eq.(2.14), we start to derive the equations in the case of zero temperature.

The Dirac field equation in the MFT is written from Eq. (2.5) as

$$[\gamma^\mu i\hbar\partial_\mu - \Gamma_\omega\gamma_0 V_0 - (Mc^2 - \Gamma_s\phi_0)]\psi(x,t) = 0 \tag{2.15}$$

where the effective mass is defined as $M^*c^2 = Mc^2 - \Gamma_s\phi_0$. If we assume the stationary state solution of Dirac equation for a uniform system as $\psi(\vec{x},t) = u(\vec{k},\lambda)e^{i(\vec{k}\vec{x}-\varepsilon(k)t/\hbar)}$, (λ is spin index), we obtain the eigenvalue equation including both positive and negative energies as $\varepsilon^{\pm}(k) = \Gamma_\omega(\rho)V_0 \pm (\vec{p}^2c^2 + M^{*2}c^4)^{1/2}$. The nucleon field operator is written as a superposition of stationary state solutions as

$$\psi(\vec{x},t)=\frac{1}{\sqrt{V}}\sum[A_{\vec{k}\lambda}u(\vec{k},\lambda)e^{i(\vec{k}\vec{x}-i\varepsilon^{+}(k)t/\hbar)}+B^{+}_{\vec{k}\lambda}v(\vec{k},\lambda)e^{i(\vec{k}\vec{x}-i\varepsilon^{-}(k)t/\hbar)}] \quad (2.16)$$

where $u(\vec{k},\lambda)$ and $v(\vec{k},\lambda)$ are the four-component Dirac spinors that satisfy the normalization $u^{\dagger}(\vec{k},\lambda)u(\vec{k},\lambda^{'})=\delta_{\lambda\lambda'}$ and $v^{\dagger}(\vec{k},\lambda)v(\vec{k},\lambda^{'})=\delta_{\lambda\lambda'}$. The terms $A^{\dagger}_{k\lambda},B^{\dagger}_{k\lambda},A_{k\lambda}$ and $B_{k\lambda}$ are creation and destruction operators for baryons and antibaryons satisfying the equal time anticommutation relations. If the Lagrangian density given in Eq. (2.1) is used in the mean-field approximation with Eq. (2.16), the mean-field Hamiltonian and baryon number operator are obtained as [14]

$$\begin{aligned} H_{MFT} &= \left[-\frac{1}{2}(\mu_\nu)^2V_0^2+\frac{1}{2}(\mu_s)^2\phi_0^2\right]+\Gamma_\nu V_0\rho_b \\ &\quad +\frac{1}{V}\sum_{k\lambda}\sqrt{c^2\vec{p}^2+(M^*c^2)^2}[A^{\dagger}_{k\lambda}A_{k\lambda}-B_{k\lambda}B^{\dagger}_{k\lambda}], \end{aligned} \quad (2.17)$$

$$\hat{B}=\sum_{k\lambda}[A^{\dagger}_{k\lambda}A_{k\lambda}+B^{\dagger}_{k\lambda}B_{k\lambda}]. \quad (2.18)$$

Using this general solution given in Eq.(2.16) into Eq. (2.13) and Eq. (2.14), the energy density is obtained as

$$\begin{aligned} \varepsilon(\rho_b) &= \frac{1}{2}\left[\frac{\Gamma_\omega(\rho)}{\mu_\nu}\right]^2\rho_b^2+\frac{1}{2}\left[\frac{\mu_s}{\Gamma_s(\rho)}\right]^2(Mc^2-M^*c^2)^2 \\ &+ \frac{\gamma}{(2\pi\hbar)^3}\int d^3p\sqrt{(c\vec{p})^2+(M^*c^2)^2}. \end{aligned} \quad (2.19)$$

The pressure can be obtained from energy density by using its relation with energy density given by $p(\rho_b)\equiv\rho_b(\partial\varepsilon/\partial\rho_b)-\varepsilon(\rho_b)$

$$
\begin{aligned}
p(\rho_b) &= \frac{1}{2}\left[\frac{\Gamma_\omega(\rho)}{\mu_\nu}\right]^2 \rho_b^2 - \frac{1}{2}\left[\frac{\mu_s}{\Gamma_s(\rho)}\right]^2 (Mc^2 - M^*c^2)^2 \\
&+ \frac{\gamma}{(2\pi\hbar)^3}\frac{1}{3}\int d^3p \frac{(cp)^2}{\sqrt{(c\vec{p})^2 + (M^*c^2)}} \\
&+ \left[\frac{1}{\mu_{(\nu)}}\right]^2 \Gamma_\omega(\rho)\frac{\partial\Gamma_\omega(\rho)}{\partial\rho}\rho^3 - \rho_b\mu_s^2(Mc^2 - M^*c^2)^2\left(\frac{1}{\Gamma_s(\rho)}\right)^3 \frac{\partial\Gamma_\omega(\rho)}{\partial\rho}.
\end{aligned}
\tag{2.20}
$$

The baryon density is obtained from $\rho_b = \langle\psi^\dagger(x,t)\psi(x,t)\rangle$ which is defined by $\rho_b = \frac{\gamma}{(2\pi\hbar)^3}\int_0^{p_F} d^3p$.

Here γ is the degeneracy factor and equals 4 for symmetric nuclear matter (N=Z) and equals 2 for pure neutron matter (Z=0).

Eq. (2.19) and Eq. (2.20) represent the equation of state of nuclear matter at zero temperature in parametric form as $\varepsilon(\rho_b)$ and $P(\rho_b)$. At the end of the calculation, the constant scalar field ϕ_0 or effective mass M^* can be determined thermodynamically by minimizing $\varepsilon(M^*)$ with respect to M^* . This gives rise to the self-consistency condition. At a fixed volume and baryon number, the system will minimize its energy so that $(\partial\varepsilon/\partial M^*)_{V,B} = 0$. We then obtain the effective mass as

$$
M^*c^2 = Mc^2 - \left(\frac{\Gamma_s(\rho)}{\mu_s}\right)^2 \frac{\gamma}{(2\pi\hbar)^3}\int_0^{p_F} d^3p \frac{M^*c^2}{\sqrt{(c\vec{p})^2 + (M^*c^2)^2}} \tag{2.21}
$$

and from the relation $M_0^*c^2 = Mc^2 - (\Gamma_s/\mu_s)^2\rho_s^0$ with $\phi_0 = (\Gamma_s/\mu_s)^2\rho_s^0$ we find the scalar density given by

$$
\rho_s^0 = \frac{\gamma}{(2\pi\hbar)^3}\int_0^{p_F} d^3p \frac{M^*c^2}{\sqrt{(c\vec{p})^2 + (M^*c^2)^2}}. \tag{2.22}
$$

Since the nucleon effective mass depends on meson fields and also meson fields depend on the nucleon effective mass themselves, it is necessary to solve a highly non-linear system of coupled equations by self-consistency procedures.

The effective mass as a function of baryon density in TW, DDME1 and NL3 parameterization are shown in Fig. (2.2). At saturation density, they have almost the same value where M^*/M is less than unity because of the large scalar field effect. The difference is seen above the saturation density.

The binding energy per particle as a function of baryon density in TW, DDME1 and NL3 parameterization are shown in Fig. (2.3). Around and below the saturation density, the curves for the parameter sets have the same trend, however, they represent important differences above the saturation densities as expected. The slope of the curves above saturation density is related to the compressibility and they are consistent with the compressibility values given in Table 2.2.

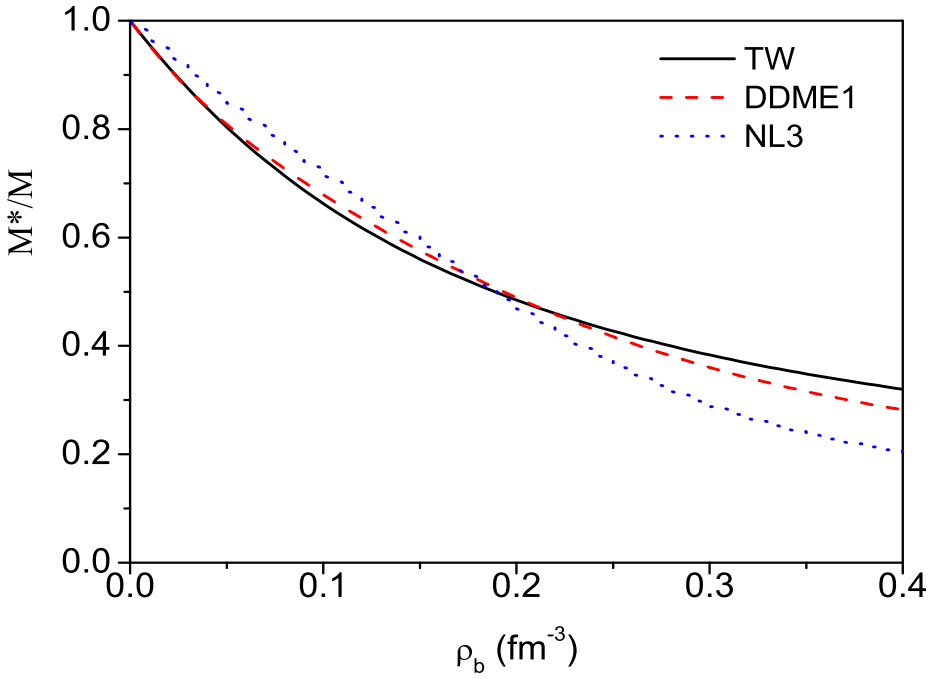

Figure 2.2: The effective mass as a function of baryon density for TW, DDME1 and NL3 parametrization.

2.1.4 Nuclear Matter at Finite Temperature

A fundamental result between the grand partition function Z_G and the thermodynamic potential $\Omega(T, V, \mu)$ in statistical mechanics given by

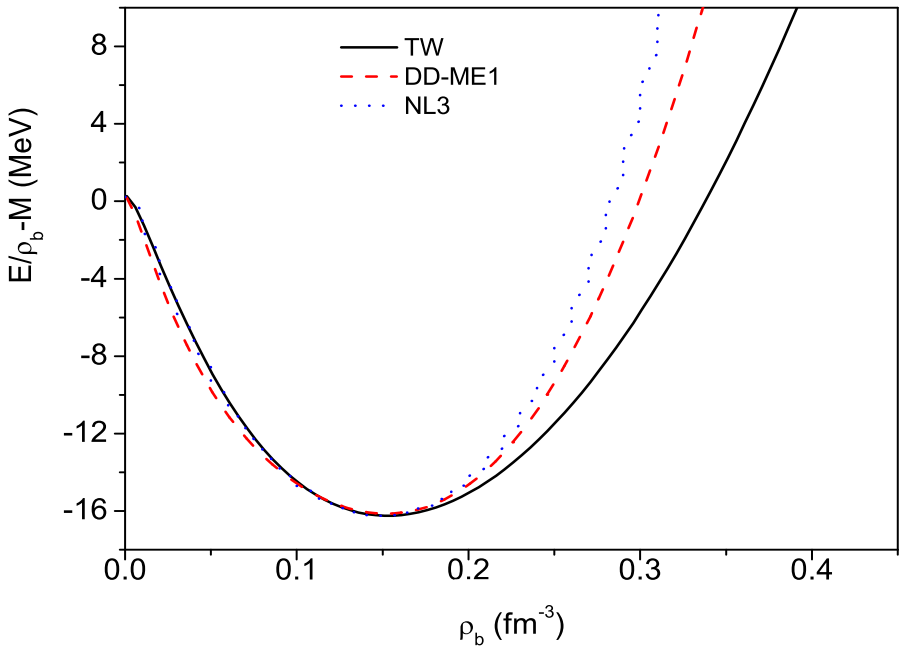

Figure 2.3: The binding energy as a function of baryon density in TW, DDME1 and NL3 parametrization.

$$\Omega(T, V, \mu) = -k_B T \ln Z_G \tag{2.23}$$

allows us to compute all the macroscopic equilibrium thermodynamics from the grand partition function. For an interacting baryon system, the grand partition function is written as $Z_G = \sum_{n_1 \ldots n_\infty} \langle n_1 \ldots n_\infty | e^{-\beta(\hat{H}-\mu\hat{B})} | n_1 \ldots n_\infty \rangle$ where $\beta = \frac{1}{k_B T}$[1]. If we use the MFT Hamiltonian and baryon number operators in Eq. (2.17) and Eq. (2.18), thermodynamic potential becomes

$$\begin{aligned} \Omega(T, V, \mu) &= V\left[-\frac{1}{2}\left(\frac{\Gamma_v}{\mu_v}\right)^2 \rho_b^2 + \frac{1}{2}\left(\frac{\mu_s}{g_s}\right)^2 \left(Mc^2 - M^* c^2\right)^2\right] \\ &\quad -\frac{1}{\beta}\sum_i \ln\left[1 + e^{-\beta(E_i^* - \mu^*)}\right] - \frac{1}{\beta}\sum_j \ln\left[1 + e^{-\beta(E_j^* + \mu^*)}\right] \end{aligned} \tag{2.24}$$

where $\mu^* = \mu - \Gamma_v V_0$ is the reduced chemical potential with $V_0 = (\Gamma_v/\mu_v^2)\rho_b$ and the energy eigenvalue is given by $E_k^* = \sqrt{\vec{p}^2 c^2 + (M^* c^2)^2}$. Baryon density is

found from $\rho_b = -(\partial\Omega/\partial\mu)_{T,V}$ as

$$\rho_b = \frac{\gamma}{(2\pi\hbar)^3}\int d^3p(n_k - \bar{n}_k), \tag{2.25}$$

where n_k and $\bar{n}_k$ are thermal occupation numbers for baryon and antibaryon defined by

$$\begin{aligned} n_k &= \frac{1}{1+e^{\beta(E_i^*-\mu^*)}}, \\ \bar{n}_k &= \frac{1}{1+e^{\beta(E_i^*+\mu^*)}}. \end{aligned} \tag{2.26}$$

The energy density is obtained from $\varepsilon = E/V = (1/V)\partial(\beta\Omega)/\partial\beta + \mu\rho_b$ as

$$\begin{aligned} \varepsilon &= \frac{1}{2}\left(\frac{\Gamma_v}{\mu_v}\right)^2(\rho_b^2) + \frac{1}{2}\left(\frac{\mu_s}{\Gamma_s}\right)^2\left(Mc^2 - M^*c^2\right)^2 \\ &\quad + \frac{\gamma}{(2\pi\hbar)^3}\int d^3p\sqrt{(pc)^2 + (M^*c^2)^2}(n_k + \bar{n}_k). \end{aligned} \tag{2.27}$$

The expression for pressure $p = -\Omega/V$ gives

$$\begin{aligned} p(\rho_b, T) &= \frac{1}{2}\left(\frac{\Gamma_\omega(\rho)}{\mu_v}\right)^2\rho_b^2 - \frac{1}{2}\left(\frac{\mu_s}{\Gamma_s(\rho)}\right)^2\left(Mc^2 - M^*c^2\right)^2 \\ &\quad + \frac{\gamma}{(2\pi\hbar)^3}\frac{1}{3}\int_0^{p_f} d^3p\frac{(c\vec{p})^2}{\sqrt{(c\vec{p})^2 + (M^*c^2)^2}}(n_k + \bar{n}_k) \\ &\quad + \left(\frac{1}{\mu_v}\right)^2\Gamma_\omega(\rho)\frac{\partial\Gamma_\omega(\rho)}{\partial\rho_b}\rho_b^3 - \rho_b\mu_s^2(Mc^2 - M^*c^2)^2\left(\frac{1}{\Gamma_s(\rho)}\right)^3\frac{\partial\Gamma_\omega(\rho)}{\partial\rho_b}. \end{aligned} \tag{2.28}$$

The minimization of the thermodynamical potential at fixed (μ, T, V) gives the self-consistency condition for $M^*c^2 = Mc^2 - \Gamma_s\phi_0$ as

$$\phi_0 = \frac{\Gamma_s(\rho)}{\mu_s^2}\frac{\gamma}{(2\pi\hbar)^3}\int_0^{p_f} d^3p\frac{M^*c^2}{\sqrt{(c\vec{p})^2 + (M^*c^2)^2}}(n_k + \bar{n}_k) \equiv \frac{\Gamma_s(\rho)}{\mu_s^2}\rho_s^0 \tag{2.29}$$

In the numerical calculations, we employ two parameter sets TW and DDME1 given in Table 2.1 and 2.2.

Fig. (2.4) and Fig. (2.5) show the binding energy per nucleon with respect to the the nuclear density ρ_b at different temperatures in TW and DDME1 parameterizations, respectively. In both cases, the nuclear matter represents less bound as temperature is increasing. The energy curves obtained in TW parametrization is softer than the one obtained in DDME1 parametrization.

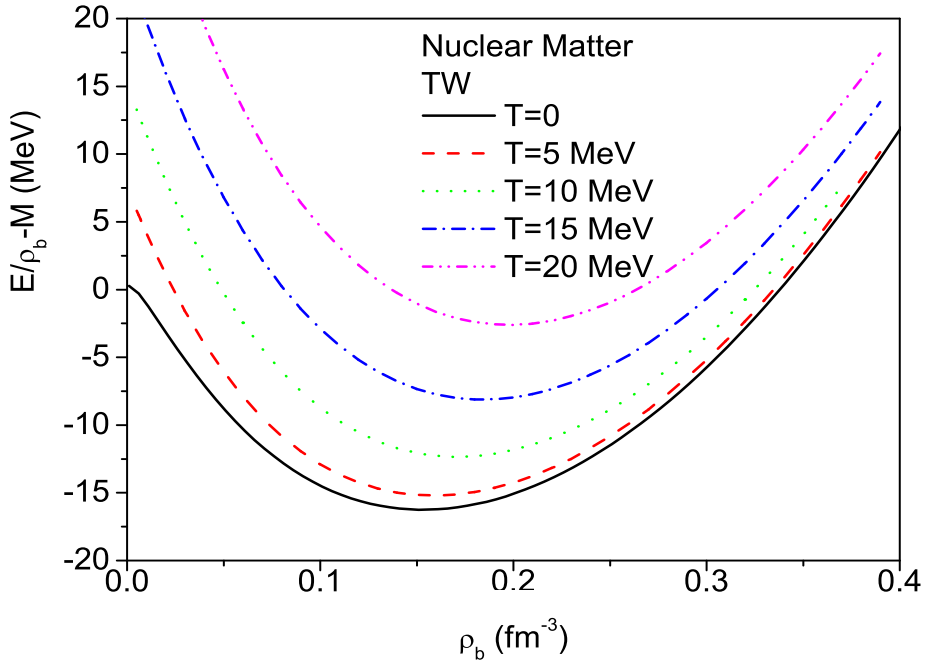

Figure 2.4: The binding energy per nucleon as a function of the baryon density ρ_b for various temperatures, T=0, 5, 10, 15 MeV, in TW parametrization

Pressure as a function of the baryon density at different temperatures calculated in TW and DDME1 parameterizations are presented in Fig. (2.6) and in Fig. (2.7). The value of compressibility, that is defined as the slope of the pressure curve at the saturation density, decreases with the increasing temperature. As a result, we conclude that the compressibility of the nuclear matter decreases as the temperature increases.

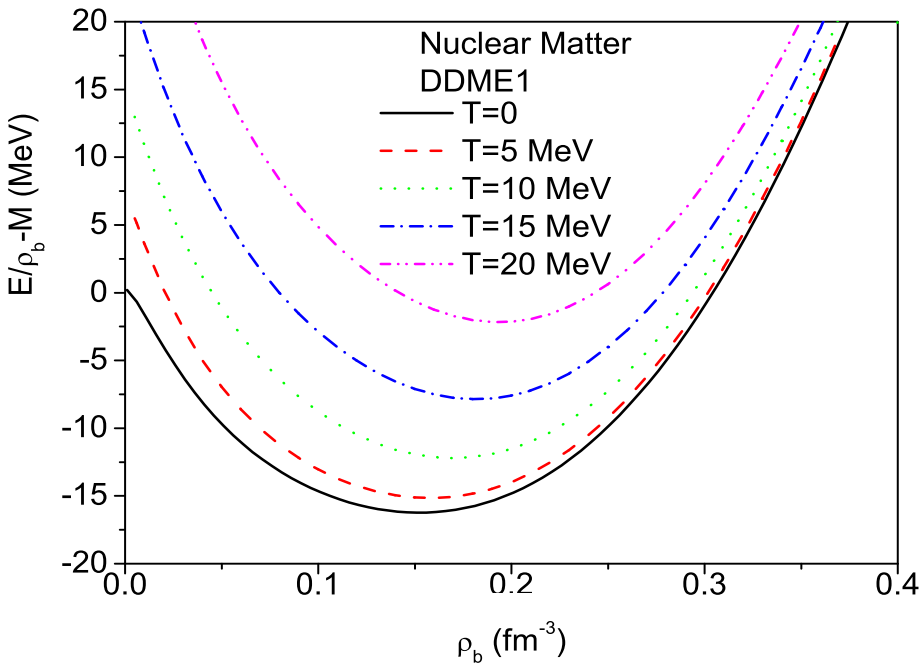

Figure 2.5: The binding energy per nucleon as a function of the baryon density ρ_b for various temperatures , T=0, 5, 10, 15 MeV, in DDME1 parametrization.

There is a phase equilibrium for temperatures above a critical temperature Tc. For below the critical temperatures ($0 < T < T_c$) the pressure curve has a maximum then has a minimum and it has three important densities. One of them corresponds to the maximum of the pressure curve, the second one corresponds to the minimum of the pressure curve and the third density value corresponds to the coexisting phase point. The pressure curve has a negative compressibility between the densities corresponding to maximum and minimum of the curve. This region is called spinodal region where the system is mechanically unstable. The region between spinodal and coexistance boundaries has a mixing of liquid-gas and the compressibility is positive in there. At the critical temperature, there is no surface tension and the distinction between gas and liquid phases disappears [33, 34].

Nuclear matter equation of state depends on the temperature and the density in the spinodal instability region. Spinodal instability of nuclear matter leads

to multifragmentation that may be a possible signature of the liquid-gas phase transformation.

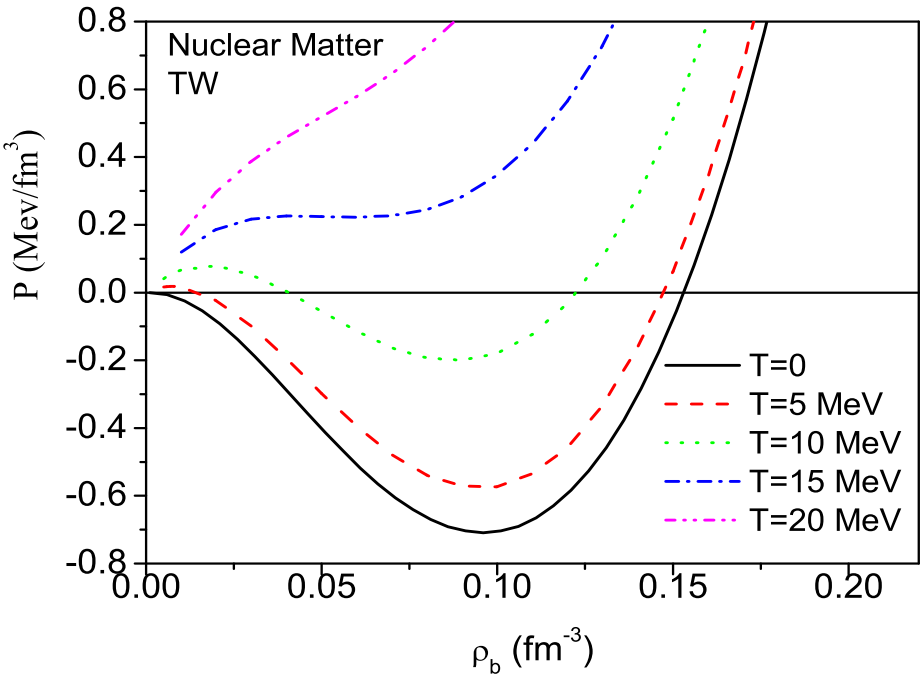

Figure 2.6: Pressure as a function of the baryon density for different fixed temperatures in TW parametrization.

2.2 Stochastic TDHF Approach

As describing the many-body nuclear system, the mean-field approximation is a very important theory. In this theory, the time-dependent wave function is given by a Slater determinant which consists of a number of time-dependent single particle wave functions. These single-particle wave functions are solutions of TDHF with proper initial conditions [9]. While a TDHF equation gives the good description for average behavior of collective motion, it cannot describe the dynamics of density fluctuations.

At low energies dominant mechanism for fluctuations comes from the density fluctuations (quantal or thermal) at the initial state. Recently proposed stochas-

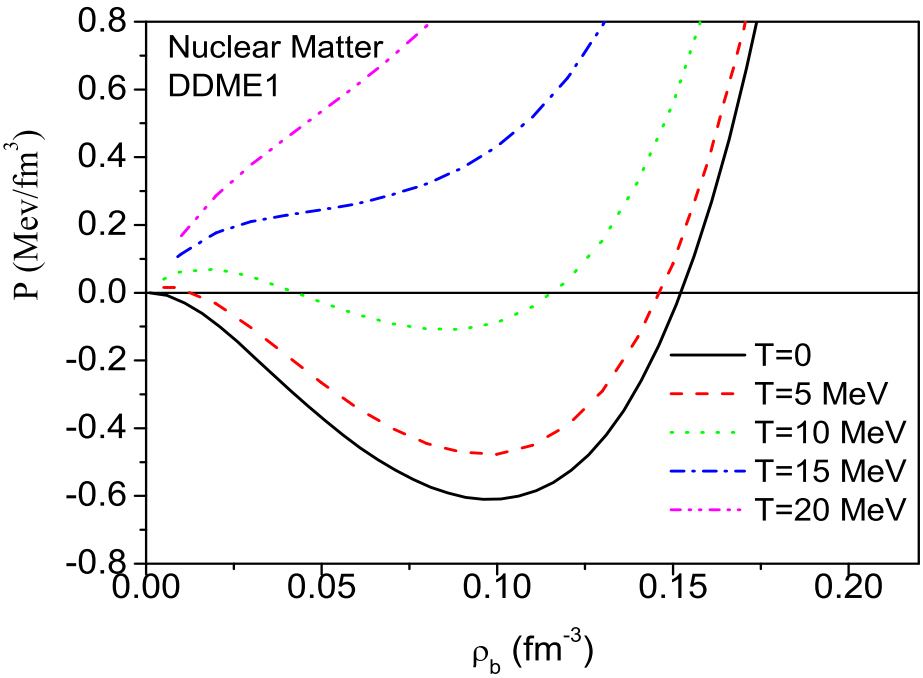

Figure 2.7: Pressure as a function of the baryon density for different fixed temperatures in DDME1 parametrization.

tic Mean-Field approach takes into account for the fluctuations in the initial state in a stochastic approximation [9, 25]. In this approach an ensemble of density matrices are generated according to the initial state fluctuations. A member of the ensemble of single-particle density matrices can be given by,

$$\rho_a(\vec{r},\vec{r}\,',t) = \sum_{ij} \phi_i(\vec{r},t)\rho_{ij}\phi_j^*(\vec{r}\,',t). \tag{2.30}$$

Here indices a indicates the proton and neutron species and ρ_{ij} are the time-independent elements of density matrix defined by the initial conditions. Each matrix element is assumed to be a Gaussian random number defined by an average value $\bar{\rho_{ij}} = \delta_{ij} f_0(j)$ and a variance of $\delta\rho_{ij}$ is determined by

$$\overline{\delta\rho_{ij}(0)\delta\rho_{i'j'}(0)} = \frac{1}{2}\delta_{ii'}\delta_{jj'}\{f_0(i)[1-f_0(j)] + f_0(j)[1-f_0(i)]\}. \tag{2.31}$$

In these expressions $f_0(i)$ denotes the average occupation numbers which are one or zero at zero temperature, and Fermi-Dirac distribution at finite temperature,

$$f_0(j) = \frac{1}{e^{(\epsilon_j - \mu_a)/k_B T} + 1} \tag{2.32}$$

where μ_a is the chemical potential of nucleus and ϵ_j is the Fermi energy at the equilibrium density.

In these theory, time-dependent single-particle wave functions of nucleons in each event are defined by their own self-consistent mean-field,

$$i\hbar \frac{\partial}{\partial t} \phi_j(\vec{r}, t) = h_a \phi_j(\vec{r}, t) \tag{2.33}$$

where $h[\rho] = \frac{p^2}{2M} + U(\rho)$ represents the self-consistent mean-field Hamiltonian and $U(\rho)$ denotes the mean-field potential in the mean-field approach. It is more convenient to express the equation of motion in terms of the single-particle density matrices of nucleons as

$$i\hbar \frac{\partial}{\partial t} \rho(t) = [h[\rho], \rho(t)]. \tag{2.34}$$

An ensemble of single-particle matrices are obtained. By using this approach, probability distribution of observables can be calculated [25]. In spinodal region, the early growth of density fluctuations are studied within the framework of this approach. Details are discussed in reference [25] and [9].

2.3 Relativistic Vlasov Equation

The model based on relativistic Vlasov equation is very useful to describe the dynamics of nuclear systems in the semi-classical calculations. The Vlasov equation is a differential equation describing time evolution of the phase space distribution function.

In the mean field approximation, Walecka model is used to explain the nuclear matter properties as mentioned in introduction and the equations of motion for fields are derived from Euler-Lagrange formalism. Also we introduced the baryon density ρ_b, the scalar density ρ_s and the current density ρ_v . By substituting these equations into the equation of motion and expressing in terms of the large and small components of the nucleon, the nucleons can be described by the Dirac equation for large and small components

$$i\partial_t\psi_L = \vec{\sigma}\cdot c\vec{p}^*\psi_S + \left[\frac{\Gamma_\nu}{\mu_\nu}\rho_b + M^*c^2\right]\psi_L, \tag{2.35}$$

$$i\partial_t\psi_S = \vec{\sigma}\cdot c\vec{p}^*\psi_L + \left[\frac{\Gamma_\nu}{\mu_\nu}\rho_b - M^*c^2\right]\psi_S, \tag{2.36}$$

where $c\vec{p}^* = c\vec{p} - (\Gamma_\nu/\mu_\nu)^2$ and $M^*c^2 = Mc^2 - \Gamma_s\phi$.

In the local-density approximation, the nucleons are assumed to be moving in constant fields and approximate relations between their small and large components are given by

$$\psi_S \approx [\vec{\sigma}\cdot c\vec{p}^*/(e^* + M^*c^2)]\psi_L \tag{2.37}$$

$$\psi_L \approx [\vec{\sigma}\cdot c\vec{p}^*/(e^* - M^*c^2)]\psi_S \tag{2.38}$$

where $e^* = (\vec{p}^{*2}c^2 + M^{*2}c^4)^{1/2}$ with the value of the local momentum $\vec{p}^*$. With the help of these equations, the coupling between the small and large components reduces equations in Eq (2.34):

$$i\hbar\partial_t\psi(\vec{x},t) = \{E^* + (\Gamma_v/\mu_\nu)^2\rho_b\}\psi(\vec{x},t), \tag{2.39}$$

where $E^* = (P^{*2}c^2 + M^{*2}c^4)^{1/2}$ with the effective one-body Hamiltonian $h = E^* + (\Gamma_\nu/\mu_\nu)^2\rho_b$.

From Eq. (2.39), we get the TDHF equation

$$i\partial_t \left[\psi(\vec{r}_1,t)\psi^\dagger(\vec{r}_2,t)\right] = h(\vec{r}_1)\psi(\vec{r}_1,t)\psi^\dagger(\vec{r}_2,t) - \psi(\vec{r}_1,t)\psi^\dagger(\vec{r}_2,t)h(\vec{r}_2). \quad (2.40)$$

In the Eq. (2.40), $\psi(\vec{r},t)$ and $\psi^\dagger(\vec{r},t)$ represent the single particle wave functions not field operators and the single particle density matrix is defined as $\psi^\dagger(\vec{r}_1,t)\psi(\vec{r}_2,t) = \rho(\vec{r}_1,\vec{r}_2,t)$. To derive a Vlasov equation, we consider a phase space distribution function $f(\vec{p},\vec{r},t)$ which is defined as Wigner transform of density matrix

$$f(\vec{p},\vec{r},t) = \int \frac{d^3s}{2\pi\hbar} e^{-i\vec{p}\cdot\vec{s}/\hbar}\rho(\vec{r}+\frac{1}{2}\vec{s},\vec{r}-\frac{1}{2}\vec{s},t) \quad (2.41)$$

by using a transformation $\vec{r} = (\vec{r}_1+\vec{r}_2)/2$ and $\vec{s} = (\vec{r}_1-\vec{r}_2)$. Wigner transform of the Hartree-Fock Hamiltonian $h[\rho]$ is given by

$$h(\vec{p},\vec{r},t) = \int \frac{d^3s}{2\pi\hbar} e^{-i\vec{p}\cdot\vec{s}/\hbar}h(\vec{r}+\frac{1}{2}\vec{s},\vec{r}-\frac{1}{2}\vec{s},t) \quad (2.42)$$

where $h(\vec{r}+\frac{1}{2}\vec{s},\vec{r}-\frac{1}{2}\vec{s},t) = \left\langle \vec{r}+\frac{1}{2}\vec{s}|h[\rho]|\vec{r}-\frac{1}{2}\vec{s}\right\rangle$. The Wigner transform of Eq. (2.40) with Eq. (2.41) gives the following equation

$$i\hbar\frac{\partial}{\partial t}f(\vec{p},\vec{r},t) = (h[\rho]\rho(t))_W - (\rho(t)h[\rho])_W. \quad (2.43)$$

Wigner transform of the products of two single-particle operators $\hat{A}$ and $\hat{B}$ is defined by $(\hat{A}\hat{B})_W = \hat{A}(\vec{p},\vec{r})e^{i\frac{\hbar}{2}\overline{\wedge}}\hat{B}(\vec{p},\vec{r})$ with $\overline{\wedge} = \overleftarrow{\nabla}_r\overrightarrow{\nabla}_p - \overleftarrow{\nabla}_p\overrightarrow{\nabla}_r$. If we apply this definition into the terms in Eq. (2.43), we obtain an equation including $\hbar$

$$\begin{aligned} i\hbar\partial_t f(\vec{r},\vec{p}) &= h(\vec{r},\vec{p})e^{i\frac{\hbar}{2}\overline{\wedge}}f(\vec{r},\vec{p},t) - h(\vec{r},\vec{p})e^{-i\frac{\hbar}{2}\overline{\wedge}}f(\vec{r},\vec{p},t) \\ &= 2i\hbar(\vec{r},\vec{p})\sin\left[\frac{\hbar}{2}\overline{\wedge}\right]f(\vec{p},\vec{r},t) \end{aligned} \quad (2.44)$$

By using the Taylor expansion for $\sin\left[\frac{\hbar}{2}\overleftrightarrow{\wedge}\right]$, we then obtain an expression that includes the expression of $\hbar$

$$\frac{\partial}{\partial t}f(\vec{p},\vec{r},t) = 2h(\vec{p},\vec{r},t)\left[\frac{1}{2}\overleftrightarrow{\wedge} + \frac{\hbar^2}{3!}\left(\frac{1}{2}\overleftrightarrow{\wedge}\right)^3 + ...\right] f(\vec{r},\vec{p},t) \tag{2.45}$$

At the semi classical limit $\hbar \to 0$, only the first term in the expression in Eq.(2.45) contributes so that the final form of the relativistic Vlasov equation itakes the form

$$\frac{\partial}{\partial t}f(\vec{r},\vec{p},t) + \vec{\nabla}_p h(\vec{r},\vec{p},t)\cdot\vec{\nabla}_r f(\vec{r},\vec{p},t) - \vec{\nabla}_r h(\vec{r},\vec{p},t)\cdot\vec{\nabla}_p f(\vec{r},\vec{p}) = 0, \tag{2.46}$$

where $\vec{v} = \vec{\nabla}_p h(\vec{r},\vec{p},t)$ denotes the velocity. This equation is used to investigate the dynamics of the system and its evoluation in time. TDHF is a quantal equation, however, Vlasov equation is obtained in classical limit and therefore it is a semi-classical equation.

CHAPTER 3

EARLY GROWTH OF DENSITY FLUCTUATIONS

The understanding of nuclear matter and its phase diagram are important in heavy ion physics and nuclear astrophysics. The detailed structure of the phase diagram and the exact locations where phase transitions takes place are still debated. A description of small amplitude oscillations around an initial state in nuclear matter is formulated in the context of the relativistic Vlasov equation. In this section, we linearize the relativistic Vlasov equation given in Eq. (2.46) for the study of the early growth effects in spinodal region from density fluctuations in symmetric nuclear matter. In this chapter, we derive the equations of density fluctuations and then density correlation functions for the hot nuclear matter in a stochastic mean-filed approach. Correlation functions of density fluctuation gives important information about the unstable dynamics of the nuclear matter in the spinodal region.

3.1 Linearization of Meson Field Equations

We start to linearize the meson field equations given in Eqs. (2.6) and (2.7). In these equations, the meson fields are linearized around their initial values as $\phi = \phi_0 + \delta\phi(\vec{r},t)$ and $V^\mu = V_0^\mu + \delta V^\mu(\vec{r},t)$ and the source terms around their initial values as $\rho_s(\vec{r},t) = \rho_s^0 + \delta\rho_s(\vec{r},t), \rho_b(\vec{r},t) = \rho_b^0 + \delta\rho_b(\vec{r},t)$ and $\vec{\rho}_v(\vec{r},t) = \vec{\rho}_v^0 + \delta\vec{\rho}_v(\vec{r},t)$. The meson field fluctuations are found in terms of the related density fluctuations. Although the initial values of the meson fields ϕ_0 and V_0^μ

are constants, the fluctuations $\delta\phi(\vec{r},t)$ and $\delta V^{\mu}(\vec{r},t)$ depend on space and time. The vector density is zero $\vec{\rho_v}^0 = 0$, so the vector field $\vec{V_0} = 0$ is also zero . However, the fluctuation of vector meson field $\delta\vec{V}(\vec{r},t)$ do not vanish since it includes nonzero $\delta\vec{\rho}_v(\vec{r},t)$ fluctuation. If there is a variation on dynamics of nuclear system such as fragmentation, this variation becomes in the direction of $\delta\vec{V}(\vec{r},t)$.

After the linearization of the scalar field equation, we obtain two expressions. One of them is

$$\mu_s^2\phi_0 = \Gamma_s(\rho_b^0)\rho_s^0 \tag{3.1}$$

where ρ_0 and ρ_b^0 represent the baryon density at saturation and the baryon density in the initial state, respectively. We use the initial value $\rho_b^0 = \eta\rho_0$ where $\eta = 0.2$ and $\eta = 0.4$ in our numerical calculations. The density ρ_s^0 denotes the scalar density in the initial state. The linearized equation becomes as

$$\left(\partial_\mu\partial^\mu + \mu_{\rm s}^2\right)\delta\phi = \Gamma_{\rm s}(\rho_b^0)\delta\rho_s^0 + \rho_s^0\left[\frac{\partial\Gamma_{\rm s}}{\partial\rho}\right]_0\delta\rho_b. \tag{3.2}$$

The term $\left(\frac{\partial\Gamma_{\rm s}}{\partial\rho}\right)_0$ comes from the density dependency of the scalar coupling corresponding to the values at the initial state defined by ρ_b (not saturation density)

$$\left(\frac{\partial\Gamma_s}{\partial\rho}\right)_0 = \Gamma_s(\rho_0)a_s \times \frac{\frac{2}{\rho_0}b_s\left(\frac{\rho_b^0}{\rho_0}+d_s\right)\left[1+c_s\left(\frac{\rho_b^0}{\rho_0}+d_s\right)^2\right] - \frac{2}{\rho_0}c_s\left(\frac{\rho_b^0}{\rho_0}+d_s\right)\left[1+b_s\left(\frac{\rho_b^0}{\rho_0}+d_s\right)^2\right]}{\left[1+c_s\left(\frac{\rho_b^0}{\rho_0}+d_s\right)^2\right]^2}. \tag{3.3}$$

In a similar manner, the linearizations of the vector field equation give the following expressions

$$\mu_{\rm v}^2 V_0 = \Gamma_\omega(\rho_b^0)\rho_0, \tag{3.4}$$

$$\left(\partial_\mu\partial^\mu + \mu_{\rm s}^2\right)\delta V_0 = \Gamma_\omega(\rho_b^0)\delta\rho_b + \rho_0\left[\frac{\partial\Gamma_\omega}{\partial\rho}\right]_0\delta\rho_b, \tag{3.5}$$

$$\left(\partial_\mu\partial^\mu + \mu_{\rm s}^2\right)\delta\vec{V} = \Gamma_\omega(\rho_b^0)\delta\vec{\rho}_v. \tag{3.6}$$

The term $\left(\frac{\partial\Gamma_\omega}{\partial\rho}\right)_0$ comes from the density dependency of the vector coupling corresponding to the values at the initial state:

$$\left(\frac{\partial\Gamma_\omega}{\partial\rho}\right)_0 = \Gamma_\omega(\rho_0)a_\omega \times\frac{\frac{2}{\rho_0}b_\omega\left(\frac{\rho_b^0}{\rho_0}+d_\omega\right)\left[1+c_\omega\left(\frac{\rho_b^0}{\rho_0}+d_\omega\right)^2\right]-\frac{2}{\rho_0}c_\omega\left(\frac{\rho_b^0}{\rho_0}+d_\omega\right)\left[1+b_\omega\left(\frac{\rho_b^0}{\rho_0}+d_\omega\right)^2\right]}{\left[1+c_\omega\left(\frac{\rho_b^0}{\rho_0}+d_\omega\right)^2\right]^2}. \tag{3.7}$$

As we see below, we solve the linearized equations by taking Fourier transforms in space and one-sided Fourier transforms in time. As a result we can relate the Fourier transforms of fluctuating fields to the Fourier transforms of fluctuating scalar $\delta\tilde{\rho}_s(\vec{k},\omega)$, baryon $\delta\tilde{\rho}_b(\vec{k},\omega)$ and current $\delta\tilde{\vec{\rho}}_b(\vec{k},\omega)$ densities as

$$\delta\phi(\vec{k},\omega) = \left[\frac{1}{-(w/c)^2+k^2+{\mu_s}^2}\right]\left[\Gamma_s(\rho_b^0)\delta\tilde{\rho}_s(\vec{k},\omega)+\rho_s^0\left(\frac{\partial\Gamma_s}{\partial\rho}\right)_0\delta\tilde{\rho}_b(\vec{k},\omega)\right] \tag{3.8}$$

$$\delta V_0(\vec{k},\omega) = \left[\frac{1}{-(w/c)^2+k^2+{\mu_v}^2}\right]\left[\Gamma_\omega(\rho_b^0)\delta\tilde{\rho}_b(\vec{k},\omega)+\rho_0\left(\frac{\partial\Gamma_\omega}{\partial\rho}\right)_0\delta\tilde{\rho}_s(\vec{k},\omega)\right] \tag{3.9}$$

$$\delta\vec{V}(\vec{k},\omega) = \frac{\Gamma_\omega(\rho_b^0)}{-(w/c)^2 + k^2 + {\mu_v}^2}\delta\tilde{\rho}_v(\vec{r},\omega). \tag{3.10}$$

For the reduced mass we have $M^*c^2 = Mc^2 - \Gamma_s(\rho_b^0)\phi_0$ and from Eq. (3.1) the initial scalar field $\phi_0 = \Gamma_s(\rho_b^0)\rho_s^0/\mu_s^0$.

3.2 Linearization of Vlasov Equation

In order to find the linearization of Vlasov equation, we use the small fluctuations of the phase space distribution function around a homogeneous initial sate $f_0(\vec{p})$ as $f(\vec{r},\vec{p},t) = f_0(\vec{p}) + \delta f(\vec{r},\vec{p},t)$. The fluctuation of the Hamiltonian obtained from Eq. (2.5) is written as $U(\vec{r},\vec{p},t) = U_0 + \delta U(\vec{r},\vec{p},t)$ and for the velocity $\vec{\mathrm{v}} = \vec{\mathrm{v}_0} + \delta\vec{\mathrm{v}}$ is used. The second and higher order fluctuations are neglected in the linearization. The linearized Vlasov equation is then obtained in the form

$$\frac{\partial}{\partial t}\delta f(\vec{r},\vec{p},t) + \vec{\mathrm{v}}_0 \cdot \vec{\nabla}_r \delta f(\vec{r},\vec{p},t) - \vec{\nabla}_r \delta U(\vec{r},\vec{p},t) \cdot \vec{\nabla}_p f_0(\vec{p}) = 0. \tag{3.11}$$

where the mean-field Hamiltonian that is obtained from Dirac equation based on Eq. (2.5) in given by

$$U = \sqrt{\left(c\vec{p} - \Gamma_\omega(\rho)\vec{V}\right)^2 + \left(Mc^2 - \Gamma_s(\rho)\phi_0\right)^2} + \Gamma_\omega(\rho)V_0. \tag{3.12}$$

Its value at the initial state is written as

$$U^0 \equiv (U)_{\rho_b=\rho_b^0} = \sqrt{(c\vec{p})^2 + \left(Mc^2 - \Gamma_s(\rho)\phi_0\right)^2} + \Gamma_\omega(\rho)V_0^0 \tag{3.13}$$

where ρ_b is now the baryon density in the initial state. In Eq. (3.11), the initial velocity is found as

$$\vec{v}_0 = c\vec{p}/\sqrt{(c\vec{p})^2 + \left(Mc^2 - \Gamma_s(\rho_b^0)\phi_0\right)^2}. \tag{3.14}$$

The fluctuation of the Hamiltonian around the initial state is written in terms of field fluctuations as

$$\begin{aligned}\delta U &= \left(\frac{\partial U}{\partial V_i}\right)_0 \delta V_i + \left(\frac{\partial U}{\partial V_0}\right)_0 \delta V_0 + \left(\frac{\partial U}{\partial \phi}\right)_0 \delta\phi + \left(\frac{\partial U}{\partial \Gamma_s(\rho)}\right)_0 \delta\Gamma_s(\rho) \\ &\quad + \left(\frac{\partial U}{\partial \Gamma_\omega(\rho)}\right)_0 \delta\Gamma_\omega(\rho) \qquad (3.15)\end{aligned}$$

where $\delta\Gamma_s(\rho) = \left(\frac{\partial\Gamma_s}{\partial\rho}\right)_0 \delta\rho_b$ and $\delta\Gamma_\omega(\rho) = \left(\frac{\partial\Gamma_\omega}{\partial\rho}\right)_0 \delta\rho_b$. The terms $()_0$ in Eq. (3.15) are derived by using Hamiltonian in Eq. (3.12) below

$$\left(\frac{\partial U}{\partial V_0}\right)_0 = \Gamma_\omega(\rho_b^0) \qquad (3.16)$$

$$\left(\frac{\partial U}{\partial \phi}\right)_0 = \frac{-\Gamma_{\rm s}(\rho_b^0)(Mc^2 - \Gamma_{\rm s}(\rho_b^0)\phi_0)}{\sqrt{(c\vec{p})^2 + (Mc^2 - \Gamma_{\rm s}(\rho_b^0)\phi_0)^2}} = -\Gamma_{\rm s}(\rho_b^0)\frac{M_0^* c^2}{\varepsilon_0^*} \qquad (3.17)$$

$$\left(\frac{\partial U}{\partial V_i}\right)_0 = \frac{-\Gamma_\omega(\rho_b^0) c p_i}{\sqrt{(c\vec{p})^2 + (Mc^2 - \Gamma_{\rm s}(\rho_b^0)\phi_0)^2}} = -\Gamma_\omega(\rho_b^0)\frac{c p_i}{\varepsilon_0^*} \qquad (3.18)$$

$$\left(\frac{\partial U}{\partial \Gamma_\omega}\right)_0 = V_0^0 \qquad (3.19)$$

$$\left(\frac{\partial U}{\partial \Gamma_{\rm s}}\right)_0 = \frac{-\phi_0(\rho_b^0)(M^* c^2 - \Gamma_{\rm s}(\rho_b^0)\phi_0)}{\sqrt{(c\vec{p})^2 + (Mc^2 - \Gamma_{\rm s}(\rho_b^0)\phi_0)^2}} = -\phi_0\frac{M_0^* c^2}{\varepsilon_0^*} \qquad (3.20)$$

where $\varepsilon^* = \sqrt{(c\vec{p^*})^2 + (M^* c^2)^2} = \sqrt{(c\vec{p} - \Gamma_\omega(\rho)\vec{V})^2 + (Mc^2 - \Gamma_{\rm s}(\rho)\phi)^2}$ is the energy of the system. We then find the fluctuation δU in terms of field fluctuations as

$$\begin{aligned}\delta U &= -\Gamma_\omega(\rho_b^0)\frac{c\vec{p}\cdot\delta\vec{V}}{\varepsilon_0^*} + \Gamma_\omega(\rho_b^0)\delta\vec{V_0} - \Gamma_s(\rho_b^0)\frac{M_0^* c^2}{\varepsilon_0^*}\delta\phi \\ &\quad -\phi_0\frac{M_0^* c^2}{\varepsilon_0^*}\left(\frac{\partial\Gamma_s}{\partial\rho}\right)_0 \delta\rho_b + V_0^0\left(\frac{\partial\Gamma_\omega}{\partial\rho}\right)_0 \delta\rho_b. \qquad (3.21)\end{aligned}$$

Using Eqs. (3.8), (3.9) and (3.10), space-time Fourier transform of the fluctuation on the mean field potential is written in terms of Fourier transforms of density fluctuations as

$$
\begin{aligned}
\delta\tilde{U} &= -G_\omega^2 \frac{c\vec{p}}{\varepsilon_0^*}\cdot\delta\tilde{\rho}_{\rm v} - G_\sigma^2\frac{M_0^*c^2}{\varepsilon_0^*}\delta\tilde{\rho}_s\left\{G_\omega^2 + \frac{\Gamma_\omega(\rho_b^0)}{-(w/c)^2+k^2+{\mu_v}^2}\rho_b^0\left(\frac{\partial\Gamma_\omega}{\partial\rho}\right)_0\right. \\
&- \frac{\Gamma_s(\rho_b^0)}{-(w/c)^2+k^2+{\mu_s}^2}\frac{M_0^*c^2}{\varepsilon_0^*}\rho_s^0\left(\frac{\partial\Gamma_s}{\partial\rho}\right)_0 \\
&- \left.\phi_0\frac{M_0^*c^2}{\varepsilon_0^*}\left(\frac{\partial\Gamma_s}{\partial\rho}\right)_0 + V_0^0\left(\frac{\partial\Gamma_\omega}{\partial\rho}\right)_0\right\}\delta\tilde{\rho}_b
\end{aligned}
\tag{3.22}
$$

where the fields at initial state are $\phi_0 = \Gamma_s(\rho_b^0)\rho_s^0/\mu_s^2$,$V_0^0 = \Gamma_\omega(\rho_b^0)\rho_b^0/\mu_v^2$ and the scalar density at initial state becomes $\rho_s^0 = \mu_s^2(Mc^2 - M_0^*c^2)/[\Gamma_s(\rho_b^0)]^2$. We also used the following definitions in Eq. (3.22)

$$
G_\omega^2 = \frac{[\Gamma_\omega(\rho_b^0)]^2}{-(w/c)^2+k^2+{\mu_\omega}^2} \tag{3.23}
$$

$$
G_\sigma^2 = \frac{[\Gamma_s(\rho_b^0)]^2}{-(w/c)^2+k^2+{\mu_s}^2}. \tag{3.24}
$$

If we define the term in front of the baryon density fluctuation $\delta\rho_b(\vec{r},\omega)$ as below

$$
\begin{aligned}
G_\Gamma &= \frac{\Gamma_\omega(\rho_b^0)}{-(w/c)^2+k^2+{\mu_v}^2}\rho_b^0\left(\frac{\partial\Gamma_\omega}{\partial\rho}\right)_0 \\
&- \frac{\Gamma_s(\rho_b^0)}{-(w/c)^2+k^2+{\mu_s}^2}\frac{M_0^*c^2}{\varepsilon_0^*}\rho_s^0\left(\frac{\partial\Gamma_\omega}{\partial\rho}\right)_0 \\
&- \phi_0\frac{M_0^*c^2}{\varepsilon_0^*}\left(\frac{\partial\Gamma_s}{\partial\rho}\right)_0 + V_0^0\left(\frac{\partial\Gamma_\omega}{\partial\rho}\right)_0
\end{aligned}
\tag{3.25}
$$

we then have a simple form of Eq. (3.22)

$$
\delta\tilde{U} = -G_\omega^2\frac{c\vec{p}}{\varepsilon_0^*}\cdot\delta\vec{\rho}_{\rm v} - G_\sigma^2\frac{M_0^*c^2}{\varepsilon_0^*}\delta\tilde{\rho}_s + \{G_\omega^2 + G_\Gamma\}\delta\tilde{\rho}_b. \tag{3.26}
$$

We want to solve scalar density fluctuation $\delta\rho_s(\vec{r},t)$, baryon density fluctuation $\delta\rho_b(\vec{r},t)$ and current density fluctuation $\delta\vec{\rho}_v(\vec{r},t)$ based on the Vlasov equation. In order achieve this task, we first take space Fourier transform of the in linearized Vlasov equation,

$$\frac{\partial}{\partial t}\int \frac{d^3k}{(2\pi)^3}e^{i\vec{k}\cdot\vec{r}}\delta f(\vec{k},\vec{p},t) + \vec{v}_0\cdot\vec{\nabla}_r\int \frac{d^3k}{(2\pi)^3}e^{i\vec{k}\cdot\vec{r}}\delta f(\vec{k},\vec{p},t) - \vec{\nabla}_r f_0(p)\cdot\vec{\nabla}_r$$
$$\times\left\{-G_\omega^2\frac{c\vec{p}}{\varepsilon_0^*}\cdot\int\frac{d^3k}{[2\pi]^3}e^{i\vec{k}\cdot\vec{r}}\delta\vec{\rho}_v(\vec{k},t) + (G_\omega^2+G_\Gamma)\int\frac{d^3k}{2\pi^3}e^{i\vec{k}\cdot\vec{r}}\delta\rho_b(\vec{k},t)\right.$$
$$\left.-G_\sigma^2\frac{M_0^*c^2}{\varepsilon_0^*}\int\frac{d^3k}{(2\pi)^3}e^{i\vec{k}\cdot\vec{r}}\delta\rho_s(\vec{k},t)\right\} = 0 \qquad (3.27)$$

where the Fourier expansions $\delta f(\vec{r},\vec{p},t) = \int_{-\infty}^{\infty}\frac{d^3k}{(2\pi)^3}e^{i\vec{k}\cdot\vec{r}}\delta f(\vec{k},\vec{p},t)$ and $\delta\rho_\alpha(\vec{r},t) = \int_{-\infty}^{\infty}\frac{d^3k}{(2\pi)^3}e^{i\vec{k}\cdot\vec{r}}\delta\rho_\alpha(\vec{k},t)$ are used. After the spatial derivatives of the last two terms in Eq. (3.27), we find

$$\frac{\partial}{\partial t}\delta f(\vec{k},\vec{p},t) + i\vec{v}_0\cdot\vec{k}\delta f(\vec{k},\vec{p},t) = [i\vec{\nabla}_p f_0(p)\cdot\vec{k}]$$
$$\times\left\{-G_\omega^2\frac{c\vec{p}}{\varepsilon_0^*}\delta\vec{\rho}_{\rm v}(\vec{k},t) + (G_\omega^2+G_\Gamma)\delta\rho_b(\vec{k},t) - G_\sigma^2\frac{M_0^*c^2}{\varepsilon_0^*}\delta\rho_{\rm s}(\vec{k},t)\right\}. \qquad (3.28)$$

Here $f_0(p)$ is the Fermi-Dirac distribution function given by $f_0(p) = 1/[e^{\beta(\varepsilon_0^*-\mu_0^*)}+1]$, the energy $\varepsilon_0^* = \sqrt{(c\vec{p})^2 + (Mc^2-\Gamma_s(\rho_b^0)\phi_0)^2}$ and the reduced chemical potential $\mu_0^* = \mu - \Gamma_v^2\rho_b^0/\mu_v^2$.

In order to solve the resultant equation, we employ the method of the one-sided Fourier transforms, $\delta\tilde{f}(\vec{k},\vec{p},\omega) = \int_0^\infty dt e^{i\omega t}\delta f(\vec{k},\vec{p},t)$ and $\delta\tilde{\rho}_i(\vec{k},\omega) = \int_0^\infty dt e^{i\omega t}$ $\delta\rho_\alpha(\vec{k},t)$.

One-side Fourier transformation of the first term in Eq. (3.28) gives

$$\int_0^\infty\frac{\partial}{\partial t}\delta f(\vec{k},\vec{p},t)e^{i\omega t}dt = -\delta f(\vec{k},\vec{p},0) - i\omega\delta f(\vec{k},\vec{p},\omega) \qquad (3.29)$$

where $\delta\tilde{f}(\vec{k},\vec{p},0)$ denotes the initial fluctuations of phase space distribution function. Finally we obtain an expression for $\delta\tilde{f}(\vec{k},\vec{p},\omega)$ in the form

$$\delta\tilde{f}(\vec{k},\vec{p},\omega)=\frac{-\vec{\nabla}_p\tilde{f}_0\cdot\vec{k}}{\omega-\vec{\mathrm{v}}_0\cdot\vec{k}}\left\{-G_\omega^2\frac{c\vec{p}}{\varepsilon_0^*}\cdot\delta\vec{\tilde{\rho}}_{\mathrm{v}}(\vec{k},\omega)\right.$$
$$\left.+(G_\omega^2+G_\Gamma)\delta\tilde{\rho}_b(\vec{k},\omega)-G_\sigma^2\frac{M_0^*c^2}{\varepsilon_0^*}\delta\tilde{\rho}_{\mathrm{s}}(\vec{k},\omega)\right\}+i\frac{\delta\tilde{f}(\vec{k},\vec{p},0)}{\omega-\vec{\mathrm{v}}_0\cdot\vec{k}}. \quad (3.30)$$

3.3 Density Fluctuation Equations

In order to solve Eq. (3.30) for density fluctuations, we recall definitions of baryon, scalar and current densities,

$$\rho_b(\vec{k},\omega) = \gamma\int\frac{d^3p}{(2\pi\hbar)^3}f(\vec{k},\vec{p},\omega) \quad (3.31)$$
$$\rho_{\mathrm{s}}(\vec{k},\omega) = \gamma\int\frac{d^3p}{(2\pi\hbar)^3}\frac{M^*c^2}{\varepsilon^*}f(\vec{k},\vec{p},\omega) \quad (3.32)$$
$$\vec{\rho}_{\mathrm{v}}(\vec{k},\omega) = \gamma\int\frac{d^3p}{(2\pi\hbar)^3}\frac{c\vec{p}^*}{\varepsilon^*}f(\vec{k},\vec{p},\omega) \quad (3.33)$$

where γ represents the spin-isospin factor that is 2 for neutron matter and 4 for nuclear matter.

Firstly, from Eq. (3.31) the fluctuation of baryon density is written as

$$\delta\rho_b(\vec{k},\omega) = \gamma\int\frac{d^3p}{(2\pi\hbar)^3}\delta f(\vec{k},\vec{p},\omega) \quad (3.34)$$

Eq. (3.30) is used into Eq. (3.34) and the following equation is obtained

$$\delta\rho_b(\vec{k},\omega)\left\{1+\gamma\int\frac{d^3p}{(2\pi\hbar)^3}\frac{\vec{\nabla}_p f_0\cdot\vec{k}}{\omega-\vec{\mathrm{v}}_0\cdot\vec{k}}(G_\omega^2+G_\Gamma)\right\}=-\gamma\int\frac{d^3p}{(2\pi\hbar)^3}\frac{\vec{\nabla}_p f_0\cdot\vec{k}}{\omega-\vec{\mathrm{v}}_0\cdot\vec{k}}$$
$$\times\left\{-G_\omega^2\frac{c\vec{p}}{\varepsilon_0^*}\cdot\delta\vec{\rho}_v(\vec{k},\omega)-G_\sigma^2\frac{M_0^*c^2}{\varepsilon_0^*}\delta\rho_b(\vec{k},s)\right\}+\gamma\int\frac{d^3p}{(2\pi\hbar)^3}\frac{i\delta f(\vec{k},\vec{p},0)}{\omega-\vec{\mathrm{v}}_0\cdot\vec{k}}. \quad (3.35)$$

This is first relation between density fluctuations including an initial fluctuations. Secondly, the scalar density fluctuations can be written as

$$\delta\rho_s(\vec{k},\omega) = \gamma \int \frac{d^3p}{(2\pi\hbar)^3} \delta\left[\left(\frac{M^*c^2}{\varepsilon^*}\right) f(\vec{k},\vec{p},\omega)\right] \tag{3.36}$$

where $\delta\left[\left(\frac{M^*c^2}{\varepsilon^*}\right) f(\vec{k},\vec{p},\omega)\right] = \left(\frac{M^*c^2}{\varepsilon^*}\right)_0 \delta f(\vec{k},\vec{p},\omega) + f_0\delta\left(\frac{M^*c^2}{\varepsilon^*}\right)$. After a few steps we find

$$\begin{aligned}\delta\left(\frac{M^*c^2}{\varepsilon^*}\right) &= G_\sigma^2\left[-\frac{(c\vec{p})^2}{\varepsilon_0^{*3}}\right]\delta\rho_s + G_\omega^2\frac{M_0^*c^2}{\varepsilon_0^{*3}}c\vec{p}\cdot\delta\vec{\rho}_{\rm v} \\ &\quad +\phi_0\left[-\frac{1}{\varepsilon_0^*}+\frac{(M_0^*c^2)^2}{\varepsilon_0^{*3}}\right]\left(\frac{\partial\Gamma_s}{\partial\rho}\right)_0\delta\rho_b \end{aligned} \tag{3.37}$$

and a second relation between density fluctuations becomes

$$\begin{aligned}&\delta\vec{\rho}_{\rm v}\cdot\gamma\int\frac{d^3p}{(2\pi\hbar)^3}\left\{\frac{c\vec{p}}{\varepsilon_0^*}\left[\frac{M^*c^2}{\varepsilon_0^*}\right]\frac{\vec{\nabla}_p f_0\cdot\vec{k}}{\omega-\vec{\rm v}_0\cdot\vec{k}}[-G_\omega^2] - f_0G_\omega^2\frac{M^*c^2}{\varepsilon_0^{*3}}c\vec{p}\right\} \\ +\;&\delta\rho_{\rm s}(\vec{k},\omega)\left\{1-\gamma\int\frac{d^3p}{(2\pi\hbar)^3}\left\{G_\sigma^2\left[\frac{M_0^*c^2}{\varepsilon_0^*}\right]^2\frac{\vec{\nabla}_p f_0\cdot\vec{k}}{\omega-\vec{\rm v}_0\cdot\vec{k}} + f_0G_s^2\frac{-(c\vec{p})^2}{\varepsilon_0^{*3}}\right\}\right\} \\ +\;&\delta\rho_b(\vec{k},\omega)\gamma\int\frac{d^3p}{(2\pi\hbar)^3} \\ &\times\left\{\frac{(M_0^*c^2)}{\varepsilon_0}\frac{\vec{\nabla}_p f_0\cdot\vec{k}}{\omega-\vec{\rm v}_0\cdot\vec{k}}(G_\omega^2+G_\Gamma) - f_0\phi_0\left[-\frac{1}{\varepsilon_0^*}+\frac{(M_0^*c^2)^2}{\varepsilon_0^{*3}}\right]\left(\frac{\partial\Gamma_s}{\partial\rho}\right)_0\right\} \\ =\;&\gamma\int\frac{d^3p}{(2\pi\hbar)^3}\frac{(M_0^*c^2)}{\varepsilon_0^*}\frac{i\delta f(\vec{k},\vec{p},0)}{\omega-\vec{\rm v}_0\cdot\vec{k}}. \end{aligned} \tag{3.38}$$

For a third relation between density fluctuations can be obtained by deducing current fluctuations from Eq. (3.33),

$$\delta\vec{\rho}_{\rm v}(\vec{k},\omega) = \gamma\int\frac{d^3p}{(2\pi\hbar)^3}\left[f_0\delta\left(\frac{c\vec{p}^*}{\varepsilon^*}\right)+\left(\frac{c\vec{p}^*}{\varepsilon_0^*}\right)\delta f(\vec{k},\vec{p},\omega)\right] \tag{3.39}$$

with

$$\frac{c\vec{p}^*}{\varepsilon^*} = \frac{c\vec{p} - \Gamma_\omega(\rho)\vec{V}}{\sqrt{(c\vec{p})^2 + \Gamma_\omega^2(\rho)\sum_i V_i^2 - 2\Gamma_\omega(\rho)\sum_i c\vec{p}_i V_i + (Mc^2 - \Gamma_s(\rho)\phi)^2}} \tag{3.40}$$

and

$$\begin{aligned}\delta\left(\frac{c\vec{p}^*}{\varepsilon^*}\right) &= G_\sigma^2\left[\frac{M_0^* c^2}{\varepsilon_0}\right] c\vec{p}\delta\rho_s + G_\omega^2\left[-\frac{1}{\varepsilon_0^*} + \frac{c\vec{p}}{\varepsilon_0^{*3}}c\vec{p}^*\right]\delta\vec{\rho}_{\rm v} \\ &\quad + \phi_0\frac{c\vec{p}(M_0^* c^2)}{\varepsilon_0^{*3}}\left(\frac{\partial\Gamma_s}{\partial\rho}\right)_0\delta\rho_b.\end{aligned} \tag{3.41}$$

We obtain a third relation as

$$\begin{aligned}&\delta\tilde{\vec{\rho}}_{\rm v}(\vec{k},\omega)\left\{1 - \gamma\int\frac{d^3p}{(2\pi\hbar)^3}G_\omega^2\left[f_0\left(-\frac{1}{\varepsilon_0^*} + \frac{(c\vec{p})^2}{\varepsilon_0^{*3}}\right) + \frac{(c\vec{p})^2}{\varepsilon_0^{*2}}\frac{\vec{\nabla}_p f^0\cdot\vec{k}}{\omega - \vec{\rm v}_0\cdot\vec{k}}\right]\right\} \\ &+\delta\tilde{\rho}_s(\vec{k},\omega)\gamma\int\frac{d^3p}{(2\pi\hbar)^3}\left\{f^0 G_\sigma^2\frac{M_0^* c^2}{\varepsilon_0^3}c\vec{p} + \frac{c\vec{p}}{\varepsilon_0^*}\frac{\vec{\nabla}_p f^0\cdot\vec{k}}{\omega - \vec{\rm v}_0\cdot\vec{k}}G_\sigma^2\frac{M_0^* c^2}{\varepsilon_0^*}\right\} \\ &+\delta\tilde{\rho}_b(\vec{k},\omega)\gamma\int\frac{d^3p}{(2\pi\hbar)^3}\left\{(G_\omega^2 + G_\Gamma)\frac{c\vec{p}}{\varepsilon_0^*}\frac{-\vec{\nabla}_p f_0\cdot\vec{k}}{\omega - \vec{\rm v}_0\cdot\vec{k}} + f^0\phi_0\frac{c\vec{p}(M_0^* c^2)}{\varepsilon_0^{*3}}\left(\frac{\partial\Gamma_s}{\partial\rho}\right)_0\right\} \\ &= -i\gamma\int\frac{d^3p}{(2\pi\hbar)^3}\frac{c\vec{p}}{\varepsilon_0^*}\frac{\delta\tilde{f}(\vec{k},\vec{p},0)}{\omega - \vec{\rm v}_0\cdot\vec{k}}.\end{aligned} \tag{3.42}$$

Now we have three independent equations that are given by Eq. (3.35), (3.38) and (3.42) for density fluctuations $\delta\tilde{\rho}_s(\vec{k},\omega)$, $\delta\tilde{\rho}_b(\vec{k},\omega)$ and $\delta\tilde{\rho}_{\rm v}(\vec{k},\omega)$. They are solved by using these coupled relations. These relations contain the initial fluctuation of phase-space distribution function.

We are interested in description of longitudinal unstable modes within this work that requires $\delta\vec{\rho}_{\rm v} = \delta\rho_{\rm v}\hat{k}$, in which the current density oscillates along the propagation axis. Therefore, some terms in Eq. (3.35), (3.38) and (3.42) becomes $\vec{\nabla}_p f_0\cdot\vec{k} = (\nabla_p f_0)k\cos\theta$ and $\vec{v}_0\cdot\vec{k} = v_0 k\cos\theta$. Some of angular integrals for $\cos\theta$ vanish that are

$$\delta\vec{\rho}_{\rm v}\cdot\int\frac{d^3p}{(2\pi\hbar)^3}G_\omega^2\frac{c\vec{p}}{\varepsilon_0^*}\left[f^0\left(\frac{M_0^*c^2}{\varepsilon_0^2}\right)\right]\sim\int_{-1}^{1}d(\cos\theta)\cos\theta=0 \tag{3.43}$$

and

$$\delta\rho_s(\vec{k},w)\left\{-\gamma\frac{d^3p}{(2\pi\hbar)^3}G_\sigma^2f^0\frac{c\vec{p}}{\varepsilon_0^*}\frac{M_0^*c^2}{\varepsilon_0^2}\right\}\sim\hat{k}\int_{-1}^{1}d(\cos\theta)\cos\theta=0 \tag{3.44}$$

Finally the set of coupled equations given in Eq. (3.35), (3.38) and (3.42) can be written in a matrix form

$$\begin{pmatrix}A_1&A_2&A_3\\B_1&B_2&B_3\\C_1&C_2&C_3\end{pmatrix}\begin{pmatrix}\delta\tilde{\rho}_{\rm v}(\vec{k},\omega)\\\delta\tilde{\rho}_{\rm s}(\vec{k},\omega)\\\delta\tilde{\rho}_b(\vec{k},\omega)\end{pmatrix}=i\begin{pmatrix}\tilde{S}_b(\vec{k},\omega)\\\tilde{S}_{\rm s}(\vec{k},\omega)\\\tilde{S}_{\rm v}(\vec{k},\omega)\end{pmatrix} \tag{3.45}$$

where

$$\begin{pmatrix}A_1&A_2&A_3\\B_1&B_2&B_3\\C_1&C_2&C_3\end{pmatrix}=$$
$$\begin{pmatrix}-G_\omega^2\chi_{\rm v}&-G_\sigma^2\chi_{\rm s}&[1+(G_\omega^2+G_{\Gamma V})\chi_b+G_{\Gamma s}\chi_{\rm s}]\\-G_\omega^2\tilde{\chi}_{\rm v}(\vec{k},\omega)&1+G_\sigma^2\tilde{\chi}_{\rm s}&[(G_\omega^2+G_{\Gamma V})\chi_s+G_{\Gamma s}\chi_{2\rm s}+\chi_{1s}]\\1+G_\omega^2\tilde{\chi}_b&-G_\sigma^2\chi_{\rm v}&[(G_\omega^2+G_{\Gamma V})\chi_{\rm v}+G_{\Gamma s}\chi_{{\rm v}s}]\end{pmatrix}. \tag{3.46}$$

where Lindhard functions are functions of $\vec{k}$ and ω. We use $G_\Gamma = G_{\Gamma V} + (M_0^*/\varepsilon_0^*)G_{\Gamma s}$ with

$$G_{\Gamma V}=\left[\frac{1}{-(w)^2+k^2+{m_\omega}^2}+\frac{1}{m_\omega^2}\right]\rho_b^0\Gamma_\omega(\rho_b^0)(\partial\Gamma_\omega/\partial\rho)_0 \tag{3.47}$$

$$G_{\Gamma s} = -\phi_0(\partial\Gamma_s/\partial\rho)_0 \left(1 + \frac{m_s^2}{-(w)^2 + k^2 + {m_s}^2}\right) \tag{3.48}$$

The functions $S_\alpha(\vec{k},\omega)$ in Eq. (3.45) denote the fluctuating source terms arising from initial $\delta f(\vec{k},\vec{p},0)$ given by

$$\begin{pmatrix} \tilde{S}_{\rm v}(\vec{k},\omega) \\ \tilde{S}_{\rm s}(\vec{k},\omega) \\ \tilde{S}_b(\vec{k},\omega) \end{pmatrix} = \gamma \int \frac{d^3p}{(2\pi\hbar)^3} \begin{pmatrix} \vec{p}\cdot\vec{k}/\varepsilon_0^* \\ M_0^* c^2/\varepsilon_0^* \\ 1 \end{pmatrix} \frac{\delta\tilde{f}(\vec{k},\vec{p},0)}{\omega - \vec{\rm v}_0\cdot\vec{k}}. \tag{3.49}$$

The functions $\chi_\alpha(\vec{k},\omega)$ are the long wavelength limit of relativistic Lindhard functions associated with baryon, scalar and current densities

$$\begin{pmatrix} \chi_{\rm v}(\vec{k},\omega) \\ \chi_{\rm s}(\vec{k},\omega) \\ \chi_b(\vec{k},\omega) \end{pmatrix} = \gamma \int \frac{p^2dp}{(2\pi)^2} \left(\frac{p}{\varepsilon_0^*}k\right) \frac{\partial f_0}{\partial\varepsilon_0^*} \begin{pmatrix} \frac{p}{\varepsilon_0^*}K_2(\vec{k},\omega) \\ \frac{M_0^*}{\varepsilon_0^*}K_1(\vec{k},\omega) \\ K_1(\vec{k},\omega) \end{pmatrix}. \tag{3.50}$$

The other terms in Eq. (3.46) are given by

$$\begin{pmatrix} \chi_{1s}(\vec{k},\omega) \\ \chi_{2s}(\vec{k},\omega) \\ \chi_{\rm vs}(\vec{k},\omega) \end{pmatrix} = \gamma \int \frac{p^2dp}{(2\pi)^2} \begin{pmatrix} \left(\frac{p^2}{\varepsilon_0^{*3}}\right)\phi_0 f_0(p)\left(\frac{\partial\Gamma_s}{\partial\rho}\right)_0 \\ \left(\frac{{M_0^*}^2}{\varepsilon_0^*}\right)\left(\frac{p}{\varepsilon_0^*}k\right)\frac{\partial f^0}{\partial\varepsilon_0^*}K_1(\vec{k},\omega) \\ \left(\frac{M_0^*}{\varepsilon_0^*}\right)\left(\frac{p^2}{\varepsilon_0^{*2}}k\right)\frac{\partial f^0}{\partial\varepsilon_0^*}K_2(\vec{k},\omega) \end{pmatrix}, \tag{3.51}$$

and

$$\begin{pmatrix} \tilde{\chi}_s(\vec{k},\omega) \\ \tilde{\chi}_{\rm v}(\vec{k},\omega) \\ \tilde{\chi}_b(\vec{k},\omega) \end{pmatrix} = \gamma \int \frac{p^2dp}{(2\pi)^2} \begin{pmatrix} \frac{2}{\varepsilon_0^*}\left(\frac{p}{\varepsilon_0^*}\right)^2 f_0(p) - \left(\frac{M_0^*}{\varepsilon_0^*}\right)^2\left(\frac{p}{\varepsilon_0^*}k\right)\frac{\partial f_0}{\partial\varepsilon_0^*}K_1(\vec{k},\omega) \\ \left(\frac{M_0^*}{\varepsilon_0^*}\right)\frac{1}{k}\left(\frac{p}{\varepsilon_0^*}k\right)^2\frac{\partial f_0}{\partial\varepsilon_0^*}K_2(\vec{k},\omega) \\ \frac{2}{\varepsilon_0^*}f_0(p) - \frac{2}{3\varepsilon_0^*}\left(\frac{p}{\varepsilon_0^*}\right)^2 f_0(p) - k\left(\frac{p}{\varepsilon_0^*}\right)^3\frac{\partial f_0}{\partial\varepsilon_0^*}K_3(\vec{k},\omega) \end{pmatrix}, \tag{3.52}$$

where

$$K_q \equiv \int_{-1}^{1} dx \frac{x^q}{w - k(p/\varepsilon_0^*)x}. \tag{3.53}$$

The baryon $\delta\tilde{\rho}_b(\vec{k},\omega)$, the scalar $\delta\tilde{\rho}_s(\vec{k},\omega)$ and the current $\delta\tilde{\vec{\rho}}_{\rm v}(\vec{k},\omega)$ density fluctuations can then be obtained from Eq. (3.45) as

$$\begin{pmatrix} \delta\tilde{\rho}_b(\vec{k},\omega) \\ \delta\tilde{\rho}_s(\vec{k},\omega) \\ \delta\tilde{\vec{\rho}}_{\rm v}(\vec{k},\omega) \end{pmatrix} = \frac{i}{\varepsilon(\vec{k},\omega)} \begin{pmatrix} D_1^b\tilde{S}_{\rm b}(\vec{k},\omega) + D_2^b\tilde{S}_{\rm s}(\vec{k},\omega) + D_3^b\tilde{S}_{\rm v}(\vec{k},\omega) \\ D_1^s\tilde{S}_{\rm b}(\vec{k},\omega) + D_2^s\tilde{S}_{\rm s}(\vec{k},\omega) + D_3^s\tilde{S}_{\rm v}(\vec{k},\omega) \\ D_1^v\tilde{S}_{\rm b}(\vec{k},\omega) + D_2^v\tilde{S}_{\rm s}(\vec{k},\omega) + D_3^v\tilde{S}_{\rm v}(\vec{k},\omega) \end{pmatrix}. \tag{3.54}$$

Here, we use the following short hand definitions:$D_1^b = B_1C_2 - B_2C_1$, $D_2^b = C_1A_2 - C_2A_1$, $D_3^b = A_1B_2 - A_2B_1$, $D_1^s = C_1B_3 - B_1C_3$, $D_3^s = B_1A_3 - A_1B_3$, $D_2^s = A_1C_3 - C_1A_3$, $D_1^v = B_2C_3 - C_2B_3$, $D_2^v = C_2A_3 - A_2C_3$, $D_3^v = A_2B_3 - B_2A_3$ and the quantity $\varepsilon(\vec{k},\omega) = A_3D_1^b + B_3D_2^b + C_3D_3^b$ defines the susceptibility which is determinant of the matrix given in Eq. (3.46). In the spinodal region, frequency is imaginary. Therefore we interested in the unstable behavior at $\omega \to -i\Gamma$.

If we use $\omega \to -i\Gamma$, we have $A_1 \to -A_1, B_1 \to -B_1, C_2 \to -C_2, C_3 \to -C_3$. . However, the determinant of the matrix becomes the same with the case of $\omega \to +i\Gamma$. For both cases, $\omega = \pm i\Gamma$, the susceptibility can be calculated numerically. The growth and decay rates of the unstable modes are calculated from the roots of the dispersion relation $\varepsilon(\vec{k},\omega) = 0$ with $\omega = \pm i\Gamma$.

The dispersion relation gives the important information about the behavior of the system when it is affected dynamically; such as phase transition. In nuclear matter, unstable modes are plane waves. Wave lengths and growth rates of dominant modes are determined by solving the dispersion relation. In the nuclear matter, collective modes are characterized by the wave number, and the solution of the dispersion relation gives the characteristic frequencies for every wave numbers. If we use $\omega = i\Gamma$ to find the unstable region, we obtain the wave numbers at which the system is the most unstable. In our calculations, we analyze the spinodal instabilities for different initial baryon densities $\rho_b = 0.4\rho_0 fm^{-3}$ and

$\rho_b = 0.2\rho_0 fm^{-3}$ where the saturation baryon density $\rho_b = 0.16 fm^{-3}$ for both DDME1 and TW sets.

3.4 Density Correlation functions

The baryon $\delta\tilde{\rho}_b(\vec{k},\omega)$, the scalar $\delta\tilde{\rho}_s(\vec{k},\omega)$ and the current $\delta\tilde{\vec{\rho}}_v(\vec{k},\omega)$ density fluctuations given in Eq. (3.54) are used to find the evolution of density fluctuations in time. The inverse Fourier transformation of $\delta\tilde{\rho}_\alpha(\vec{k},\omega)$ in time is written as $\delta\tilde{\rho}_\alpha(\vec{k},t) = \int \frac{d\omega}{2\pi}\delta\tilde{\rho}_\alpha(\vec{k},\omega)e^{-i\omega t}$. Cauchy-Residue theorem is applied to the counter integral for [35]

$$\delta\tilde{\rho}_\alpha(\vec{k},t) = \int_C \frac{d\omega}{2\pi} i \left[\frac{D_1^\alpha \tilde{S}_b(\vec{k},\omega) + D_2^\alpha \tilde{S}_{\rm s}(\vec{k},\omega) + D_3^\alpha \tilde{S}_{\rm v}(\vec{k},\omega)}{\varepsilon(\vec{k},\omega)} \right] e^{-i\omega t} \qquad (3.55)$$

We are interested only in the collective poles of the susceptibility $\varepsilon(\vec{k},\omega)$. Cauchy-Residue theorem for a counter integral $\int_C \frac{g(z)}{h(z)}dz$, if $g(z_0) \neq 0$, $h(z_0) = 0$ and , $h' = (\partial h/\partial z)_{z=z_0} \neq 0$ gives [35]

$$\int_C \frac{g(z)}{h(z)}dz = 2\pi i {\rm Res}[f(z), z = z_0] = 2\pi i \sum_k A_{-1}(k) \qquad (3.56)$$

where the residue of the function is determined by $A_{-1}(k) = \lim_{z\to z_0} \frac{g(z)}{h'(z)}$. There are two collective poles of susceptibility $\varepsilon(\vec{k},\omega)$ at $\omega = \pm i\Gamma$. After residue integral of Eq. (3.55), $\delta\rho_\alpha(\vec{k},t)$ is written in terms of growing and decaying collective modes corresponding to the poles $\omega = \pm i\Gamma$ as

$$\delta\tilde{\rho}_\alpha(\vec{k},t) = \delta\rho_\alpha^+(\vec{k})e^{+\Gamma_k t} + \delta\rho_\alpha^-(\vec{k})e^{-\Gamma_k t} \qquad (3.57)$$

where $\alpha = b, s, {\rm v}$ shows baryon, scalar and current indices. The density fluctuations related to growing and decaying modes at the initial are determined by

$$\delta\rho_\alpha^{\mp}(\vec{k}) = -\left\{ \frac{D_1^\alpha \tilde{S}_b(\vec{k},\omega) + D_2^\alpha \tilde{S}_s(\vec{k},\omega) + D_3^\alpha \tilde{S}_v(\vec{k},\omega)}{\partial\varepsilon(\vec{k},\omega)/\partial\omega} \right\}_{\omega=\mp i\Gamma_k} \tag{3.58}$$

The terms are classified as real or pure imaginary. The terms $A_2, A_3, B_2, B_3, C_1, D_1, D_2$ are real and the others A_1, B_1, C_2, C_3, D_3 are pure imaginary that comes from $\omega = \pm i\Gamma$. As a result, we may understand the behavior of the terms corresponding to $\omega = \pm i\Gamma$. For both roots the susceptibility can be calculated numerically

$$\begin{aligned} \varepsilon(k,\omega) &= A_3D_1 + B_3D_2 + C_3D_3 \\ &= A_{13}(i^2B_{11}C_{12} - C_{11}B_{12}) + B_{13}(C_{11}A_{12} - i^2A_{11}C_{12}) \\ &\quad + iC_{13}(iA_{11}B_{12} - iB_{11}A_{12}) \end{aligned} \tag{3.59}$$

where $A_{\alpha\beta}, B_{\alpha\beta}$ and $C_{\alpha\beta}$, are defined as real numbers. After a straightforward calculation we can find the derivative of $\varepsilon(\vec{k},\omega)$ at $\omega \to -i\Gamma$ as

$$\left(\frac{\partial\varepsilon(k,\omega)}{\partial\omega}\right)_{\omega=-i\Gamma} = -\left(\frac{\partial\varepsilon(k,\omega)}{\partial\omega}\right)_{\omega=+i\Gamma} \tag{3.60}$$

Spectral intensity of the density correlation function, $\tilde{\sigma}_{\alpha\alpha}(\vec{k},t)$, is determined as the second moment of Fourier transformation of the density fluctuation

$$\overline{\delta\tilde{\rho}_\alpha(\vec{k},t)(\delta\tilde{\rho}_\alpha(\vec{k'},t))^*} = (2\pi)^3\delta^3(\vec{k}-\vec{k'})\tilde{\sigma}_{\alpha\alpha}(\vec{k},t) \tag{3.61}$$

where time-dependent baryon density functions are defined in Eq. (3.57). We derive $\tilde{\sigma}_{\alpha\alpha}(\vec{k},t)$ by using the definitions in Eq. (3.57) and Eq. (3.58). Firstly, we write the second moment of the density fluctuation in terms $\delta\rho_\alpha^{\mp}(\vec{k})$ as

$$\begin{aligned} \overline{\delta\tilde{\rho}_\alpha(\vec{k},t)(\delta\tilde{\rho}_\alpha(\vec{k'},t))^*} &= \overline{\delta\rho_\alpha^+(\vec{k})(\delta\rho_\alpha^+(\vec{k}))^*}e^{2\Gamma_k t} + \overline{\delta\rho_\alpha^-(\vec{k})(\delta\rho_\alpha^-(\vec{k}))^*}e^{-2\Gamma_k t} \\ &\quad + \overline{\delta\rho_\alpha^+(\vec{k})(\delta\rho_\alpha^-(\vec{k}))^*} + \overline{\delta\rho_\alpha^-(\vec{k})(\delta\rho_\alpha^+(\vec{k}))^*} \end{aligned} \tag{3.62}$$

Secondly, we write the explicit forms of $\delta\rho_\alpha^{\mp}(\vec{k})$ including source terms into Eq. (3.62). The source terms contain initial fluctuations $\delta\tilde{f}(\vec{k},\vec{p},0)$. Using the variance relation of initial fluctuations as

$$\overline{\delta\tilde{f}(\vec{k},\vec{p},0)(\delta\tilde{f}(\vec{k'},\vec{p'},0))^*} = (2\pi)^3\delta^3(\vec{k}-\vec{k'})(2\pi\hbar)^3\delta^3(\vec{p}-\vec{p'})f_0(p)(1-f_0(p)) \quad (3.63)$$

we then obtain the average correlations of source terms. As a result, we find density correlation function as

$$\begin{aligned}
&(2\pi)^3\delta^3(\vec{k}-\vec{k'})\tilde{\sigma}(\vec{k}-\vec{k'}) = \\
&\gamma^2(2\pi)^3\delta^3(\vec{k}-\vec{k'})\{[K_{11}^+ + |D_1|^2 + K_{22}^+ + |D_2|^2 + K_{33}^+ + |D_3|^2 \\
&+2K_{12}^+ D_1 D_2]/(N^2)\}[e^{2\Gamma_k} + e^{-2\Gamma_k}] \\
&-\gamma^2(2\pi)^3\delta^3(\vec{k}-\vec{k'})[K_{11}^- + |D_1|^2 + K_{22}^- + |D_2|^2 - K_{33}^- + |D_3|^2 \\
&+2K_{12}^- D_1 D_2]/(-N^2)
\end{aligned} \quad (3.64)$$

where N^2 represents the value of $|[\partial\varepsilon(\vec{k},\omega)/\partial/\omega]_{\omega=i\Gamma_k}|^2$

The spectral functions are found in the final form

$$\tilde{\sigma}_{\alpha\alpha}(\vec{k},t) = \frac{E_\alpha^+(\vec{k})}{|[\partial\varepsilon(\vec{k},\omega)/\partial/\omega]_{\omega=i\Gamma_k}|^2}(e^{2\Gamma_k t} + e^{-2\Gamma_k t}) + \eta\frac{2E_\alpha^-(\vec{k})}{|[\partial\varepsilon(\vec{k},\omega)/\partial/\omega]_{\omega=i\Gamma_k}|^2} \quad (3.65)$$

where

$$E_\alpha^{\mp}(\vec{k}) = |D_1^\alpha|^2 K_{11}^{\mp} + |D_2^\alpha|^2 K_{22}^{\mp} + |D_3^\alpha|^2 K_{33}^{\mp} + 2D_1^\alpha D_{2^\alpha} K_{12}^{\mp} \quad (3.66)$$

and

$$\begin{pmatrix} K_{11}^{\mp} \\ K_{22}^{\mp} \\ K_{33}^{\mp} \\ K_{12}^{\mp} \end{pmatrix} = \gamma^2 \int \frac{d^3p}{(2\pi\hbar)^3} \begin{pmatrix} 1 \\ (M_0^*/\epsilon_0^*)^2 \\ \left(\vec{p}\cdot\hat{k}/\epsilon_0^*\right)^2 \\ M_0^*/\epsilon_0^* \end{pmatrix} \frac{\Gamma_k^2 \mp (\vec{v}_0\cdot\vec{k})^2}{[\Gamma_k^2 + (\vec{v}_0\cdot\vec{k})^2]^2} f_0(\vec{p})[1 - f_0(\vec{p})] \tag{3.67}$$

In Eq. (3.65), $\eta = +1$ is used for baryon and scalar, $\eta = -1$ is used current spectral intensities, respectively. Detailed calculations of equations are given in Appendix B and C.

Local density fluctuations $\delta\rho_\alpha(\vec{r},t)$ are determined by the Fourier transformation of $\delta\rho_\alpha(\vec{k},t)$. Equal time density correlation function for baryon, scalar and current densities as a function of distance between two space locations can be evaluated from the spectral intensity as

$$\sigma_{\alpha\alpha}(|\vec{r}-\vec{r}'|,t) = \overline{\delta\rho_\alpha(\vec{r},t)\delta\rho_\alpha(\vec{r}',t)} = \int \frac{d^3k}{(2\pi)^3} e^{i\vec{k}\cdot\vec{x}} \tilde{\sigma}_{\alpha\alpha}(\vec{k},t). \tag{3.68}$$

CHAPTER 4

NUMERICAL RESULTS AND DISCUSSIONS

In chapter 3, we calculate the linearization of Vlasov equation to find the early growth effects from density fluctuations and density correlation functions for hot nuclear matter. In this section, we calculate numerically the early development of spinodal dynamics of nuclear matter within a semi-classical approximation, by using the expressions evaluated in Chapter 3. We calculate essentially the growth rates and phase diagrams of dominant modes in spinodal region for symmetric nuclear matter, and early growth of the correlation function of density fluctuations. In section 4.1 we show the growth rates of unstable modes depending on the wave number and growth rates of most unstable modes as a function of density. In section 4.2, by using temperature versus density graphs, the spinodal boundary is determined for different wavelengths and section in 4.3 and in section 4.4, we calculate early evaluation of the density correlation function.

4.1 Unstable Solutions of Dispersion Relations

In these section, we calculete the growth rates of collective modes which are obtained from the roots of dispersion relation $\varepsilon(\vec{k},\omega) = 0$, determinant of the matrix given in Eq. (3.46), with $\omega = \pm\Gamma$. Fig. 4.1 shows the changing of the growth rates of unstable modes depending on the wave number k in the spinodal region for the two different density dependent sets (DDME1, TW) and two different initial baryon densities ($\rho_b = 0.4\rho_0$, $\rho_b = 0.2\rho_0$) at different

temperatures. For each temperature, the growth rates raises linearly from origin to a maximum value at a definite wave number, then drops to zero because of the non-local effects and effect of k^2 term in the dispersion relation. In the relativistic calculations, the most growing modes are concentrated around the wave numbers $k = 0.6\ fm^{-1}$, $\lambda \approx 10\ fm$ for $\rho_b = 0.4\rho_0$ and $k = 0.8\ fm^{-1}$, $\lambda \approx 8\ fm$ for $\rho_b = 0.2\rho_0$. It can be averaged out $k \approx 0.7\ fm^{-1}$ and with the help of the graph, the wavelength of most growing modes is found $\lambda \approx 9\ fm$. Also, the time constant can be calculated by using inverse of the growth rate $\tau = 1/\Gamma_k$, and it specifies the initial growth of the density fluctuations. For example, the shortest growth time is changing 30-50 fm/c for $\rho_b = 0.4\rho_0$ and 20-50 fm/c for $\rho_b = 0.2\rho_0$ in both two sets. Also, by using both of these graphs, it can be understood that increasing temperature causes the growing rates occurred at lower wave numbers and the increasing in the initial baryon density affects in the same way. Fig. 4.2 determines the growth rates of the most unstable

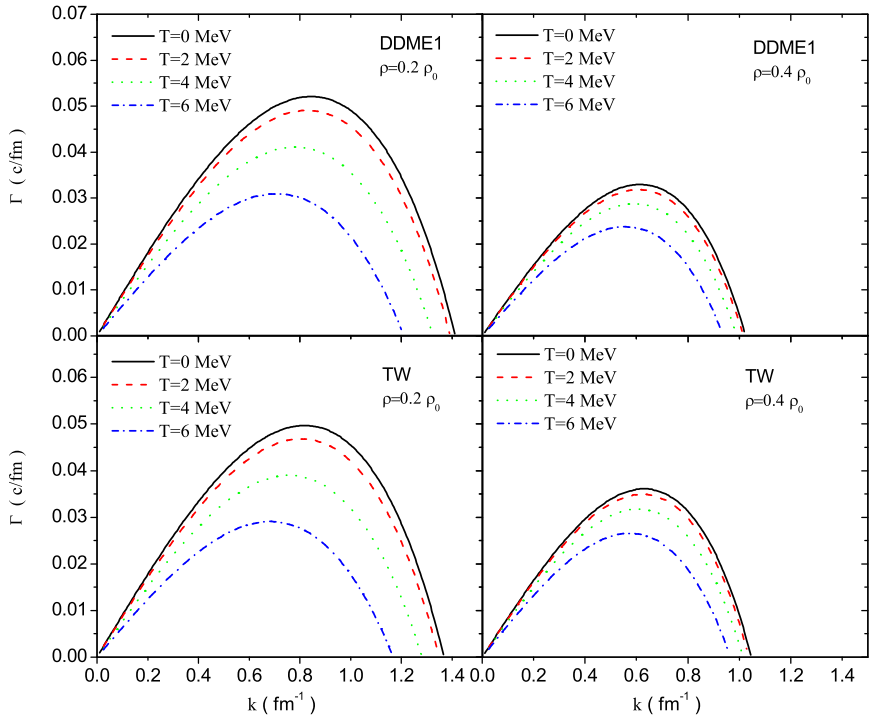

Figure 4.1: The growth rates of unstable modes as a function of wave number in the spinodal region at baryon densities $\rho = 0.2\rho_0$ and $\rho = 0.4\rho_0$ at temperatures $T = 0 - 6\ MeV$ for DDME1 and TW sets.

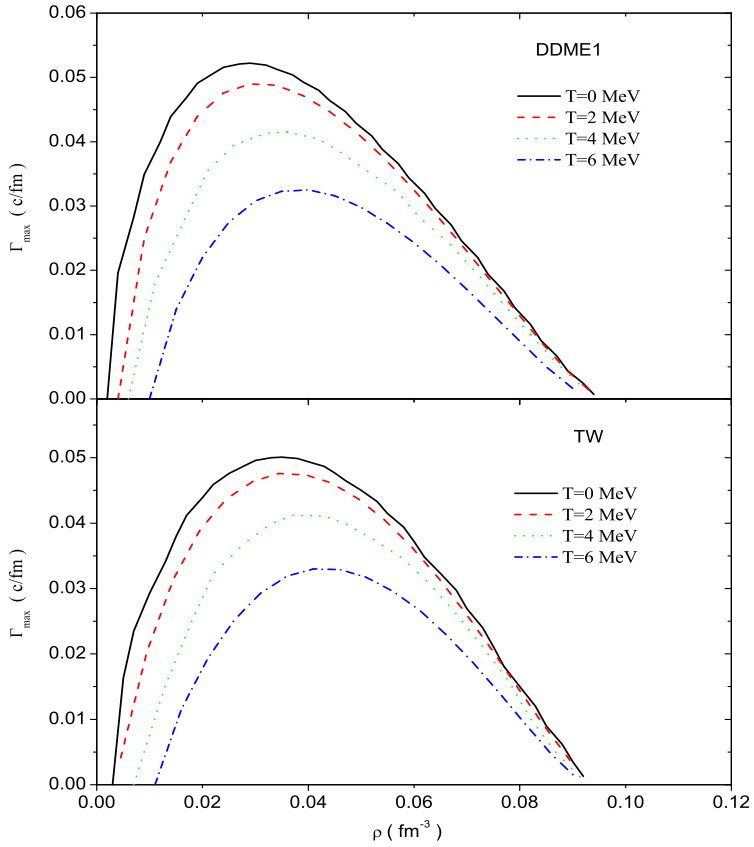

Figure 4.2: Dependence of the growth rates of the most unstable modes on initial baryon densities for DDME1 and TW with T=0, 2, 4, 6 MeV.

modes as a function of density for DDME1 and TW at T=2, 4, 6 MeV. As it can be seen from figure, the most unstable response shifts towards at higher densities when temperature increases in both sets. The maximum growth rate of most unstable modes is around $\rho_b \approx 0.03$ for DDME1 and $\rho_b \approx 0.04$ for TW. We may say that the system shows the most unstable behavior around $\rho_b \approx \rho_0/4$.

Figure 4.3 helps us to compare two sets with non-relativistic calculation [15, 25] and relativistic calculation [36] at temperature T=5 MeV. The form of the curves are comparable in both non-relativistic and the relativistic models. The relativistic with non-linear self interaction of scalar meson and relativistic with density-dependent couplings models exhibit the most unstable behavior around $\rho_b \approx 0.25\rho_0$ while it occurs around $\rho_b = 0.2\rho_0$ in the non-relativistic calculation.

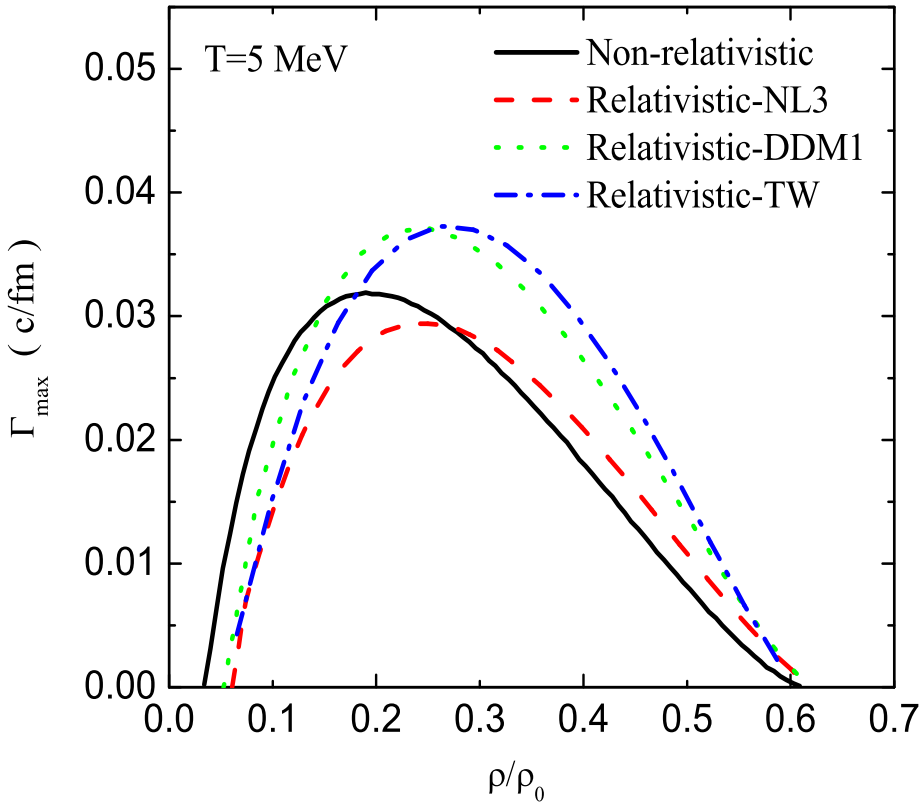

Figure 4.3: Comparison of growth rates of the most unstable modes calculated in different models at T= 5 MeV.

4.2 Phase Diagrams

In this section, we illustrate the spinodal region boundaries by using temperature versus density graph. Fig. 4.4 shows the boundary of the spinodal region of the unstable modes for $\lambda = 9\ fm$ and $\lambda = 12\ fm$ wavelengths calculated in the relativistic models with NL3, DDME1 and TW parameters. The parabola-like curves are consistent with each other obtained from different models. When the wavelength increases, the critical temperature increases and density region spreads. The region under the curve has fragmentations; in other words, mixture of liquid-gas phases. The maximum of the spinodal line is called the critical temperature for the liquid-gas phase transition [37]. Above this point, system is in only gas-phase. In the density dependent models, the critical temperature is around 14 MeV for $\lambda = 12\ fm$ and the corresponding baryon density is

approximately 0.04, however, for $\lambda = 9\ fm$, the critical temperature is around 12 MeV and the baryon density is again 0.04 that corresponds to $\rho_b \approx \rho_0/4$. In the case of NL3, the critical temperature is found less than the value in density-dependent approach, but their most unstable densities are comparable.

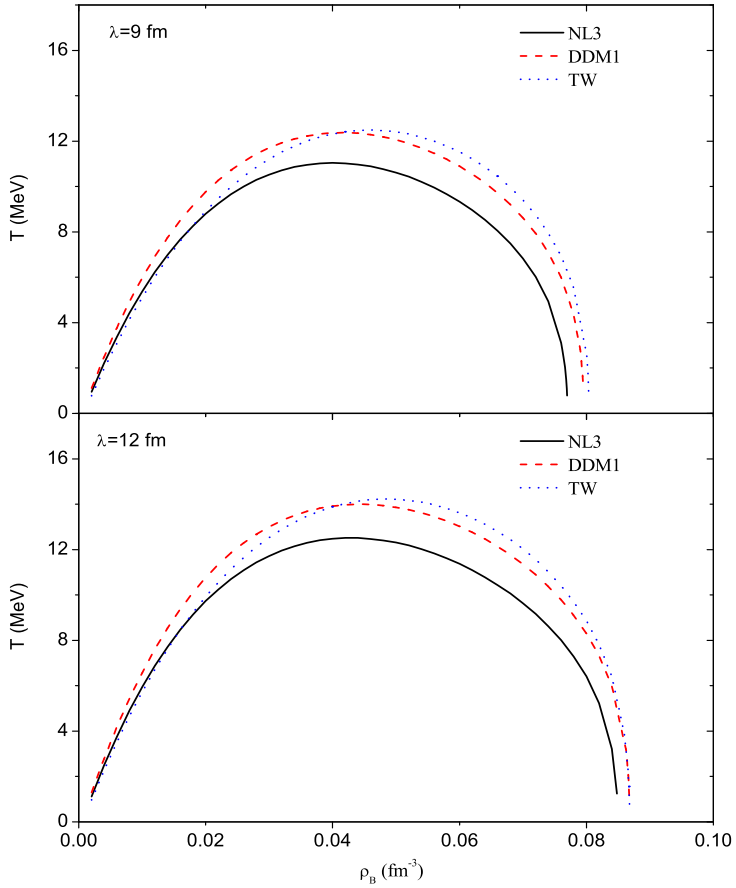

Figure 4.4: Phase diagrams in the spinodal region corresponding to the unstable modes $\lambda = 9\ fm$ and $\lambda = 12\ fm$ calculated in relativistic models.

4.3 Early Condensation in Spinodal Region

In this section, the initial cluster sizes are estimated. Fig. 4.5 shows the change in the half-wavelengths of the most unstable collective modes with respect to baryon density at different temperatures and in two different sets. We can obtain the information about emerging cluster size by using half-wavelengths. The curves reduce to minimum values around baryon densities $\rho_b = 0.2\rho_0$. Then we find the half-wavelength about $\lambda_0/2 \approx 4.5\ fm$ for DDME1 and TW which becomes the estimated value of the diameter of the primary fragments . Increasing in temperature also makes the size of cluster increase.

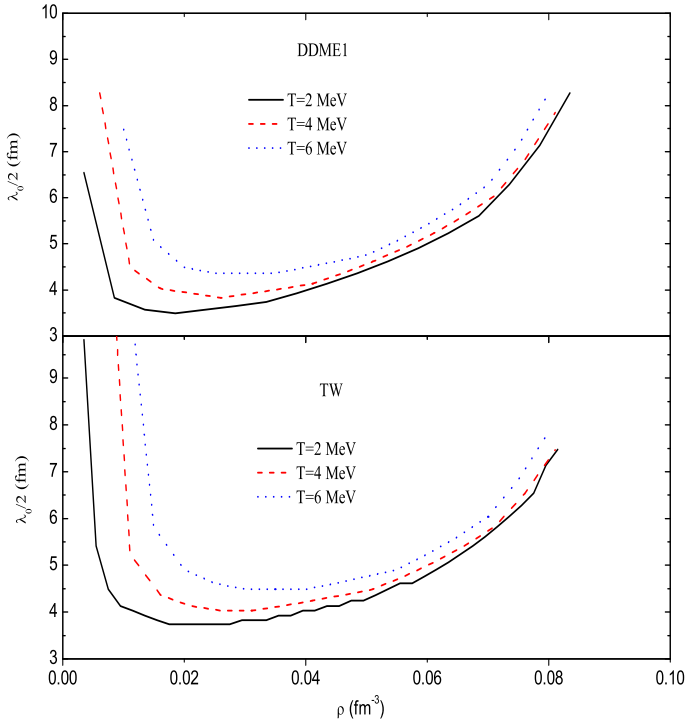

Figure 4.5: Size of the primary clusters in the spinodal region at T= 2, 4, 6 MeV for DDME1 and TW.

In Fig. 4.6, we compare the estimated cluster sizes in relativistic approaches at T=5 MeV. We observed that the results are comparable with the value about 4.5 fm and are model independent.

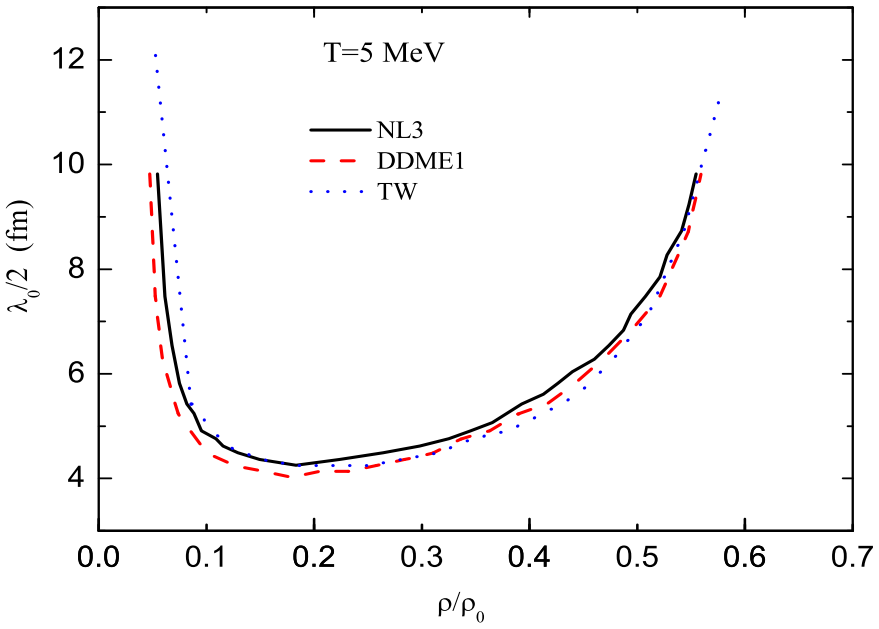

Figure 4.6: Comparison of the size of the primary clusters in the spinodal region in relativistic and non-relativistic approaches.

4.4 Density Correlation Functions

4.4.1 Correlation Functions depending on Wave number

For the investigation of initial development of baryon density fluctuations, the correlation functions are defined in Eq. (3.65). In Fig. 4.7 and Fig. 4.8, the spectral intensity of the baryon density correlation function depending on wave number is given at five different times (t=0, t=20 fm/c, t= 30 fm/c, t= 40 fm/c and t=50 fm/c) and at initial baryon densities $\rho_b = 0.2\rho_0$ and $\rho_b = 0.4\rho_0$ below normal density at temperature T= 1 MeV and temperature T=5 MeV, respectively.

By using Cauchy-Residue theorem, the evolution of baryon density fluctuation $\delta\tilde{\rho}_b(\vec{k},\omega)$ given in Eq. (3.54) are calculated. However; by that way, there are contributions from non-collective poles of $\varepsilon(\vec{k},\omega)$ and source term. These contributions are important and effective for large wave number at the initial state;

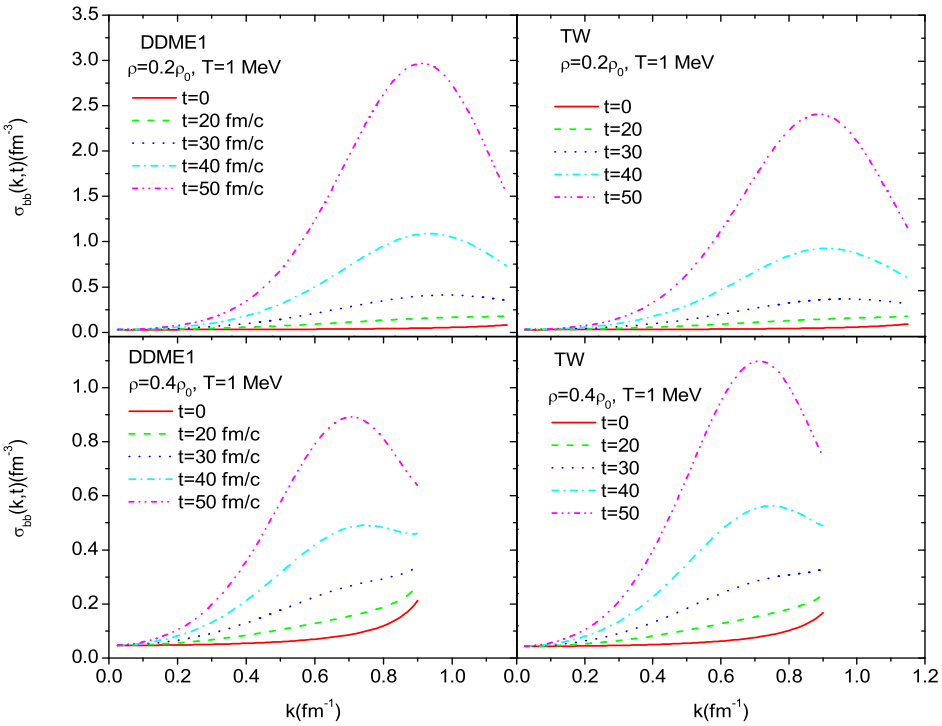

Figure 4.7: Spectral intensity of baryon density correlation function as a function of wave number at temperature T=1 MeV and time t= 0, 20, 30, 40, 50 fm/c calculated with DDME1 and TW sets.

however, they disappear in a short time interval. We don't use non-collective effects in our calculations; so, wave number is cut off 0.8 $fm^{-3} - 1.15\ fm^{-3}$ in our graphs. In conclusion, calculated baryon density correlation function $\tilde{\sigma}_{bb}(\vec{k}, t)$ is a good approximation for long wavelengths below critical wave number k_c.

In these graphs, the largest growth takes place at the wave numbers, which overlap the range of dominant unstable modes in Fig. 4.1. We may discuss the situations due to the initial baryon densities and temperatures. In Fig. 4.7 and Fig. 4.8, we observe the same trend of the growth of baryon density correlation function for both parameter sets. When the initial baryon density increases, the spectral intensity grows smaller, however, the growth is larger at high temperature case. While the early growth of baryon density correlation

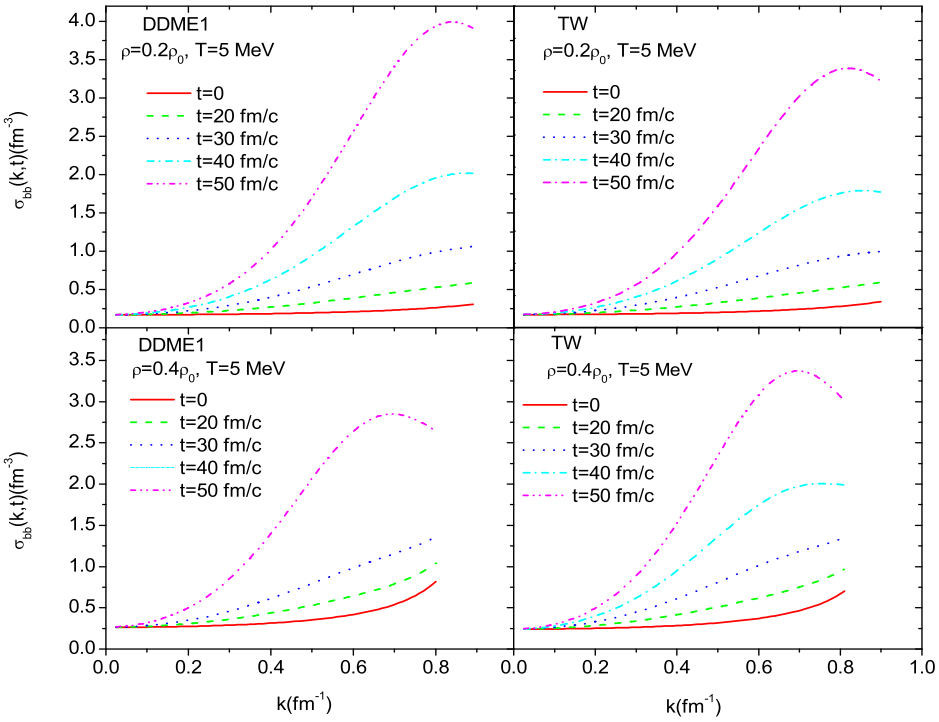

Figure 4.8: Spectral intensity of baryon density correlation function as a function of wave number at temperature T=5 MeV and time t= 0, 20, 30, 40, 50 fm/c calculated with DDME1 and TW sets.

function $\overline{\sigma}_{bb}(\vec{k},t)$ is 1.5 times larger at $\rho_b = 0.2\rho_0$ than at $\rho_b = 0.4\rho_0$ in the case of higher temperature T=5 MeV, it is 3 times larger at low temperature T=1 MeV. As a result, we deduce that the early growth of the baryon density correlation function $\tilde{\sigma}_{bb}(\vec{k},t)$ becomes faster at lower densities and lower temperatures.

On the other side, at T=1 MeV, the growth of baryon density correlation function reaches a maximum around $k = 0.9\ fm^{-1}$ at $\rho_b = 0.2\rho_0$ and $k = 0.7\ fm^{-1}$ at $\rho_b = 0.4\rho_0$. At higher temperature T=5 MeV, the growth of baryon density correlation function $\tilde{\sigma}_{bb}(\vec{k},t)$ reaches maximum around shorter wave length as $k = 0.8\ fm^{-1}$ at $\rho_b = 0.2\rho_0$ and $k = 0.6\ fm^{-1}$ at $\rho_b = 0.4\rho_0$.

Fig. 4.9 and Fig. 4.10 show the spectral intensity of the scalar density correlation

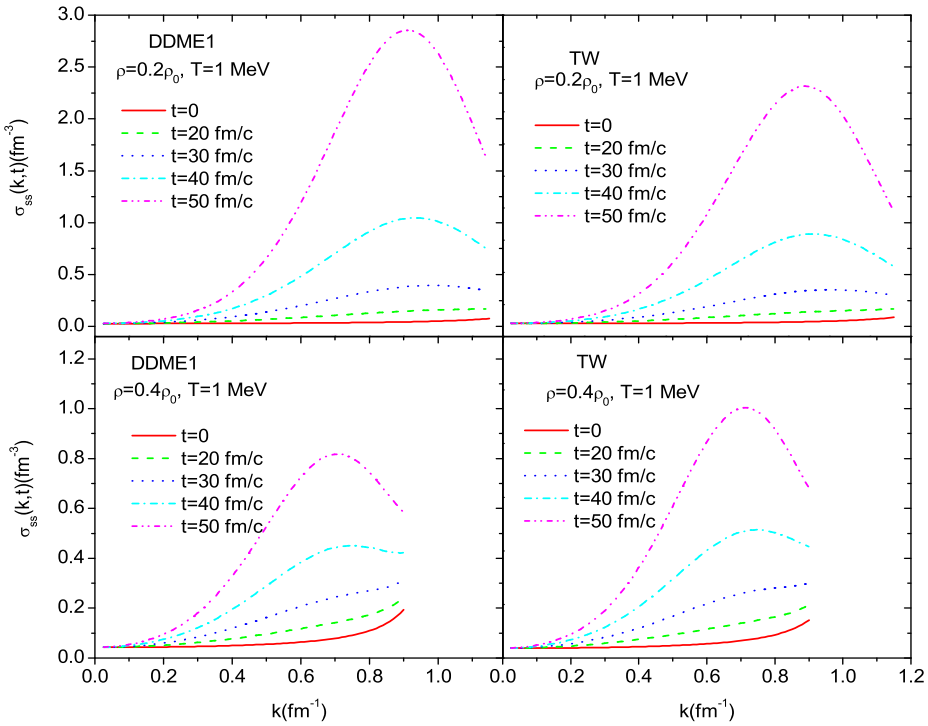

Figure 4.9: Spectral intensity of scalar density correlation function as a function of wave number at temperature T=1 MeV and time t= 0, 20, 30, 40, 50 fm/c with DDME1 and TW set.

function as a function of the wave number for different times at initial densities $\rho_b = 0.2\rho_0$, $\rho_b = 0.4\rho_0$ and at temperature T= 1 MeV, T= 5 MeV by using DDME1 and TW parameter sets. The values of wave numbers at which scalar density correlation function $\tilde{\sigma}_{ss}(\vec{k}, t)$ reaches maximum are the same as baryon density functions. The early growth rates are almost the same with baryon case.

By using the same chosen values, the spectral intensity of the current density correlation function as a function of the wave number are shown in Fig. 4.11 and Fig. 4.12 at temperatures T= 1 MeV and T= 5 MeV, respectively. At low temperature T=1 MeV, the k values corresponding to the maximum growth of current density correlation function $\tilde{\sigma}_{vv}(\vec{k}, t)$ are observed $k = 0.8\ fm^{-1}$ at $\rho_b = 0.2\rho_0$ and $k = 0.6\ fm^{-1}$ at $\rho_b = 0.4\rho_0$. At higher temperature T=5 MeV,

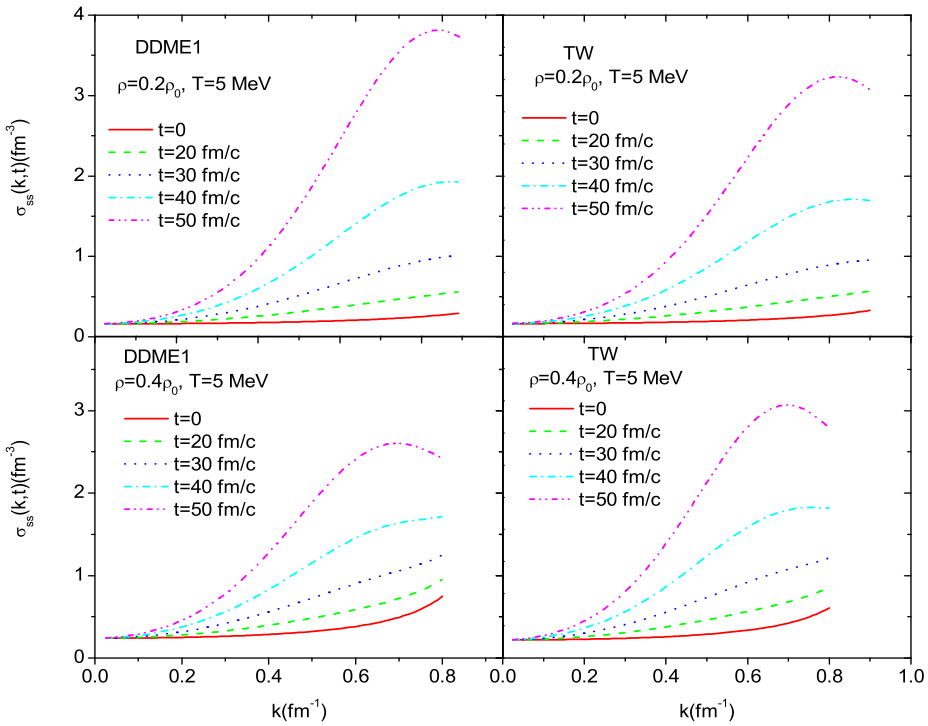

Figure 4.10: Spectral intensity of scalar density correlation function as a function of wave number at temperature T=5 MeV and time t= 0, 20, 30, 40, 50 fm/c with DDME1 and TW sets.

they become $k = 0.6\ fm^{-1}$ at $\rho_b = 0.2\rho_0$ and $k = 0.5\ fm^{-1}$ at $\rho_b = 0.4\rho_0$. The decaying of the curves at larger wave numbers is observed well in the current density case. The growth rate of current density correlation function $\tilde{\sigma}_{vv}(\vec{k}, t)$ is the same for baryon and scalar cases.

4.4.2 Correlation Functions depending on Distance

In chapter 3, space dependent baryon density fluctuations $\delta\rho_b(\vec{r}, t)$ are found out by Fourier transform of momentum dependent $\delta\rho_b(\vec{k}, t)$. Equal time correlation function of baryon density fluctuations is represented as a function of distance between two space locations in Eq. (3.68). In this expression, the distance dependency of the correlation function is important so that correlation function

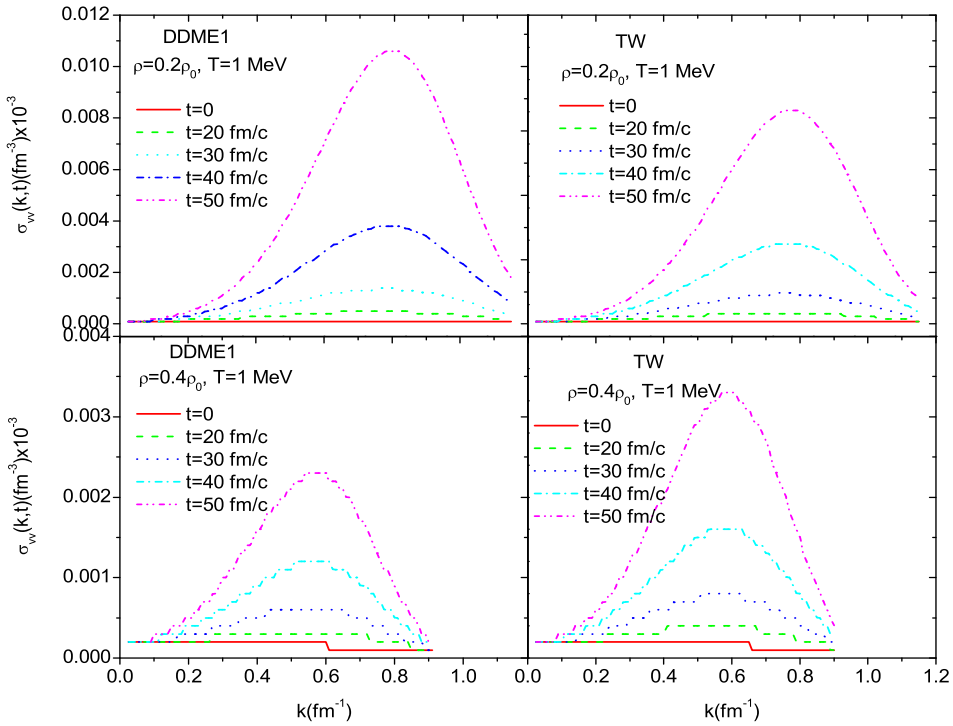

Figure 4.11: Spectral intensity of current density correlation function as a function of wave number at temperature T=1 MeV and time t= 0, 20, 30, 40, 50 fm/c with DDME1 and TW sets.

becomes zero when the magnitude of distance goes to the infinity. At these points, the fluctuations are statistically independent [25]. Baryon density correlation function gives valuable information about the dynamics of the system in the spinodal region. Figure 4.13 shows the relation between baryon density correlation function as a function of distance between two space points $\mid \vec{x} - \vec{x}' \mid$ at T=1 MeV calculated for DDME1 and TW sets at different times, and at two initial baryon densities $\rho_b = 0.2\rho_0$ and $\rho_b = 0.4\rho_0$. We can obtain initial information about the average size of clusters by using this graph. The width of correlation function at half maximum gives approximately the size of cluster. Correlation length of density fluctuations is obtained about 3.0 fm in both case of densities $\rho_b = 0.2\rho_0$, $\rho_b = 0.4\rho_0$. In Fig. 4.5, we also find $\lambda/2 \approx 4.5\ fm$

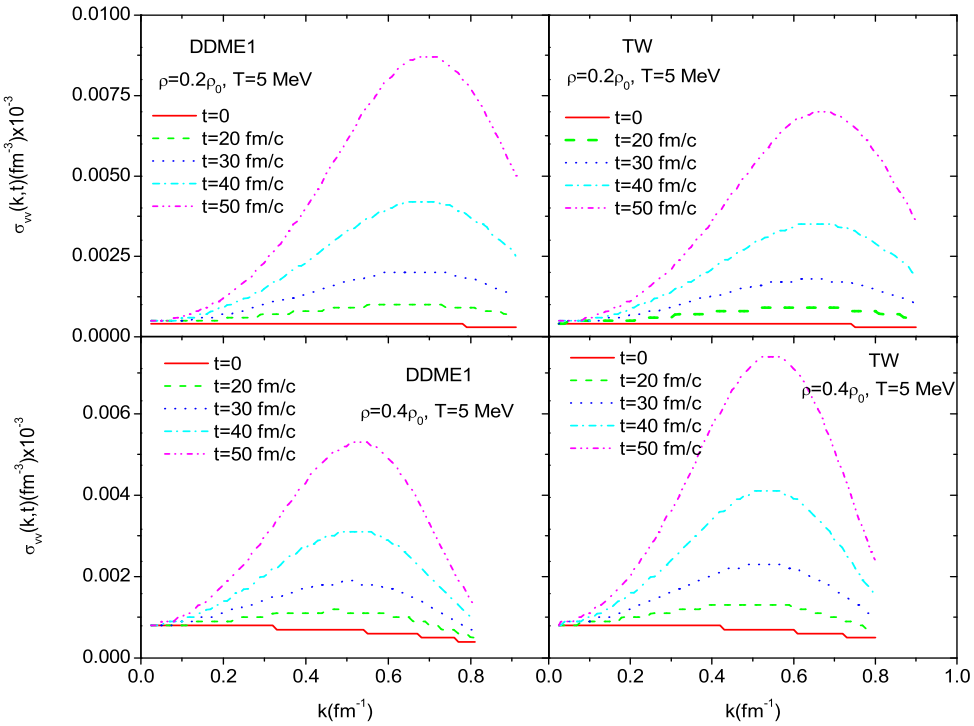

Figure 4.12: Spectral intensity of current density correlation function as a function of wave number at temperature T=5 MeV and time t= 0, 20, 30, 40, 50 fm/c with DDME1 and TW1 set.

for $\rho_b = 0.2\rho_0$. If it is accepted that Fig. 4.5 gives the diameter and Fig. 4.12 gives the size of the initial condensation region, these values are consistent with each other. At the same temperature, baryon density fluctuations grow faster with larger densities. On the other hand, the evaluation of baryon density correlation function in time is faster at lower densities. In the DDME1 case, $\sigma_{bb}(x = 0, t = 50\ fm/c) \approx 0.055\ fm^{-6}$ at initial baryon density $\rho_b = 0.2\rho_0$ and $\sigma_{bb}(x = 0, t = 50\ fm/c) \approx 0.009\ fm^{-6}$ at $\rho_b = 0.4\rho_0$ that show six times faster at $\rho_b = 0.2\rho_0$. In the TW case, $\sigma_{bb}(x = 0, t = 50\ fm/c) \approx 0.045\ fm^{-6}$ at initial baryon density $\rho_b = 0.2\rho_0$ and $\sigma_{bb}(x = 0, t = 50\ fm/c) \approx 0.012\ fm^{-6}$ at $\rho_b = 0.4\rho_0$ that show four times faster at $\rho_b = 0.2\rho_0$.

Fig. 4.14 shows baryon density correlation function as a function of distance at

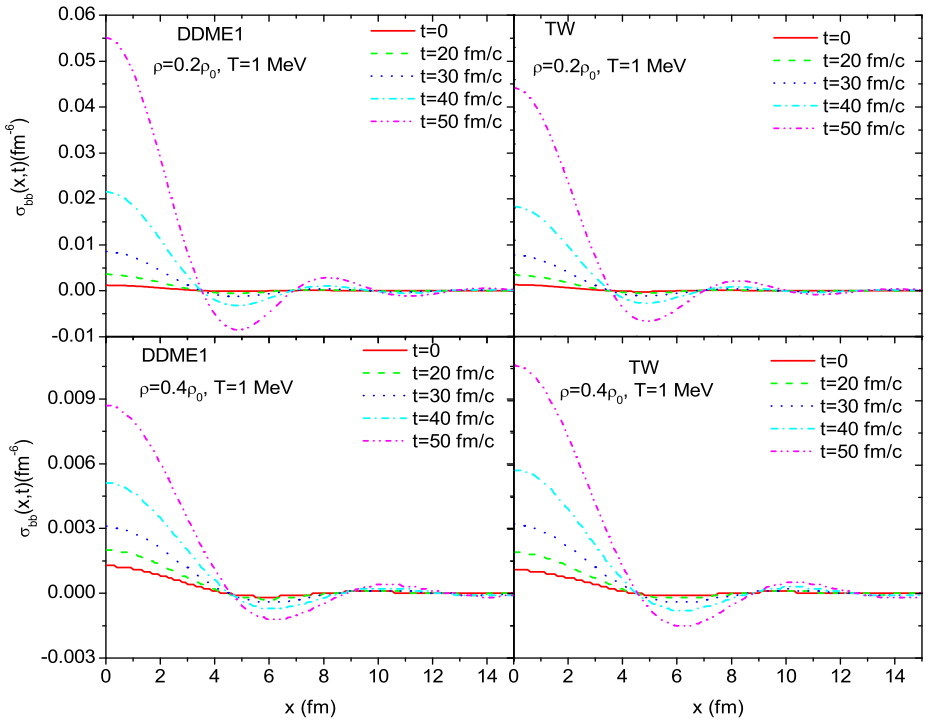

Figure 4.13: Baryon density correlation function as a function of distance at times t= 0, t= 20 fm/c, 30 fm/c, 40 fm/c and 50 fm/c at temperature T=1 MeV at density $\rho_b = 0.2\rho_0$ and $\rho_b = 0.4\rho_0$ calculated with DDME1 and TW

the different initial baryon densities but higher temperature T=5 MeV for the same initial times as given in Fig. 4.13. At this temperature, the growth rate in time is slower than T=1 MeV case. The ratio is about two. Correlation length of density fluctuations is also obtained about 3.0 fm from Fig. 4.14 for both densities and both sets.

Fig. 4.15 and Fig. 4.16 present the scalar density correlation function as a function of distance between two space points at different initial times and the initial baryon densities at $\rho_b = 0.2\rho_0$ and $\rho_b = 0.4\rho_0$ temperature T=1 MeV and T=5 MeV, respectively. The scalar correlation function give again information about the size of condensation that is found about 2.5 fm which is considerable value with the estimated one from baryon density correlation function.

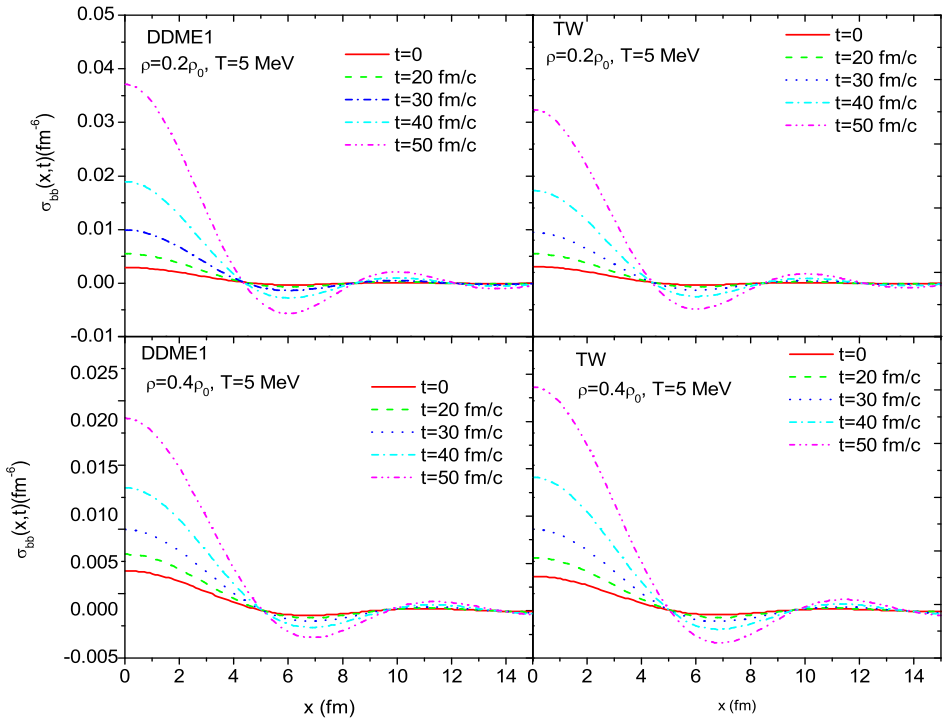

Figure 4.14: Baryon density correlation function as a function of distance at times t= 0, t= 20 fm/c, 30 fm/c, 40 fm/c and 50 fm/c at temperature T=5 MeV at density $\rho_b = 0.2\rho_0$ and $\rho_b = 0.4\rho_0$ calculated with DDME1 and TW

Fig. 4.17 and Fig. 4.18 show the current density correlation function as a function of distance under similar conditions with other calculations. Current density has an additional factor ε^*/M^* in the definition; so, it is reduced by a factor of 1000. By using current density correlation, the variance of the local velocity fluctuations of initial cluster can be estimated. The local velocity fluctuations are proportional to the current density fluctuations $\delta\vec{\rho}_v(\vec{r},t) \approx \delta\vec{u}(\vec{r},t)\rho_b$. And the equation which satisfies the relation between equal time correlation function and the local velocity fluctuations given by $\overline{\delta\vec{u}(\vec{r},t)\delta\vec{u}(\vec{r}',t)} = \sigma_{vv}(\mid \vec{x}-\vec{x}' \mid,t)/\rho_b^2$.

The variance of local velocity fluctuations are obtained by taking $\mid \vec{x}-\vec{x}' \mid = 0$ and average speed of initial fragments of spinodal decomposition is then calculated from the formula of root-mean-square value $u_{rms} = (c/\rho_b)\sqrt{\sigma_{vv}(0,t)}$.

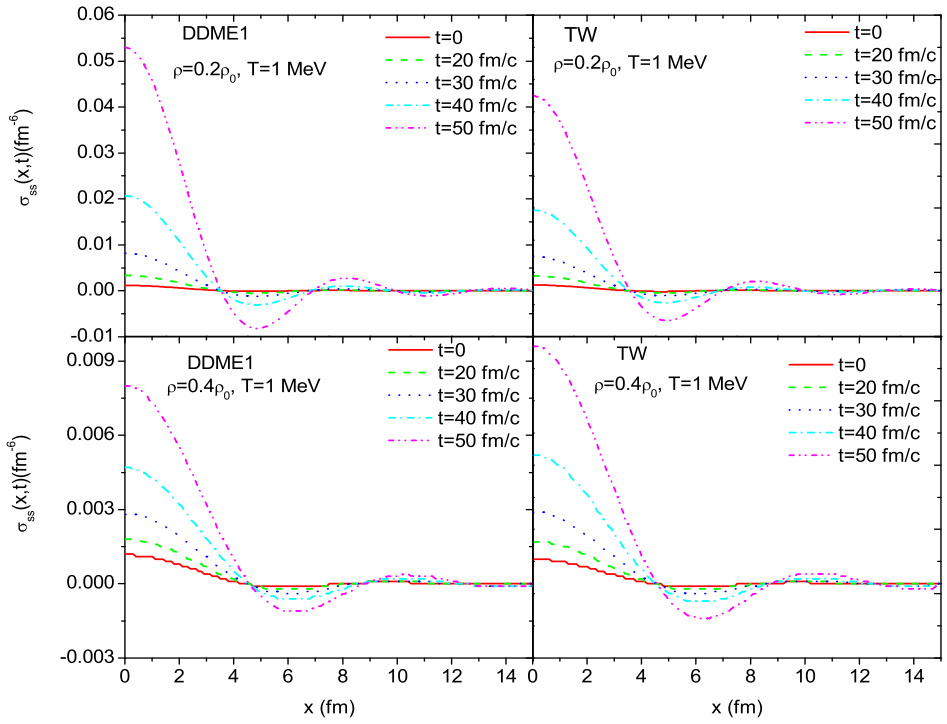

Figure 4.15: Scalar density correlation function as a function of distance at times t= 0, t= 20 fm/c, 30 fm/c, 40 fm/c and 50 fm/c at temperature T=1 MeV at density $\rho_b = 0.2\rho_0$ and $\rho_b = 0.4\rho_0$ calculated with DDME1 and TW

For example, for DDME1, at time t=0 fm/c to t= 50 fm/c and at T=5 MeV, the rms value changes from $u_{rms} = 0.04c$ to $u_{rms} = 0.09c$ for baryon density $\rho_b = 0.4\rho_0 = 0.06\ fm^{-3}$ and for $\rho_b = 0.2\rho_0 = 0.03\ fm^{-3}$, it changes $u_{rms} = 0.08c$ to $u_{rms} = 0.31c$ during 50 fm/c. In the case of parameter TW, we found approximately values.

We estimate the evolution of the root-mean-square value in time considering Fig. 4. 17 and Fig. 4.18 and give the results in Table 4.1 and Table 4.2 for DDME1 and TW sets, respectively.

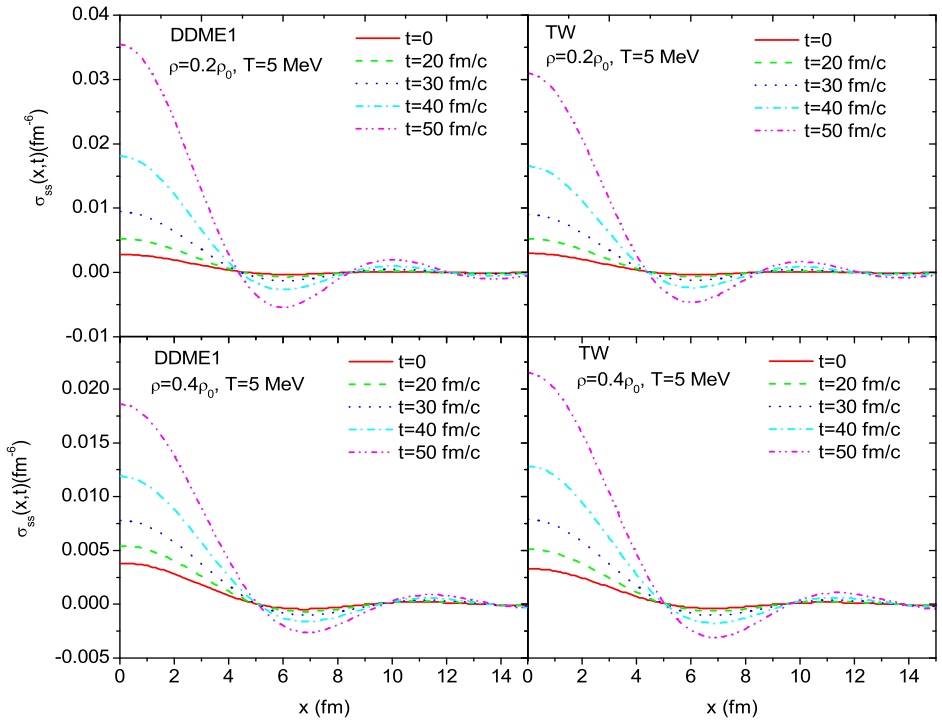

Figure 4.16: Scalar density correlation function as a function of distance at times t= 0, t= 20 fm/c, 30 fm/c, 40 fm/c and 50 fm/c at temperature T=5 MeV at density $\rho_b = 0.2\rho_0$ and $\rho_b = 0.4\rho_0$ calculated with DDME1 and TW

Table 4.1: The average speed of initial fragments of spinodal decomposition at T=1 MeV and T=5 MeV for DDME1

DDME1	T=1 MeV			T=5 MeV		
	t (fm/c)	$\sigma_{vv}(0,t)(fm^{-6})$	u_{rms}	t (fm/c)	$\sigma_{vv}(0,t)(fm^{-6})$	u_{rms}
	0	0.002×10^{-3}	$0.05c$	0	0.005×10^{-3}	$0.075c$
	20	0.009×10^{-3}	$0.1c$	20	0.011×10^{-3}	$0.11c$
$\rho_b = 0.2\rho_0$	30	0.024×10^{-3}	$0.16c$	30	0.021×10^{-3}	$0.15c$
	40	0.064×10^{-3}	$0.27c$	40	0.042×10^{-3}	$0.22c$
	50	0.167×10^{-3}	$0.43c$	50	0.085×10^{-3}	$0.31c$
	t (fm/c)	$\sigma_{vv}(0,t)(fm^{-6})$	u_{rms}	t (fm/c)	$\sigma_{vv}(0,t)(fm^{-6})$	u_{rms}
	0	0.0016×10^{-3}	$0.020c$	0	0.005×10^{-3}	$0.04c$
	20	0.0029×10^{-3}	$0.028c$	20	0.008×10^{-3}	$0.047c$
$\rho_b = 0.4\rho_0$	30	0.0051×10^{-3}	$0.038c$	30	0.012×10^{-3}	$0.058c$
	40	0.0091×10^{-3}	$0.050c$	40	0.02×10^{-3}	$0.07c$
	50	0.0165×10^{-3}	$0.068c$	50	0.032×10^{-3}	$0.094c$

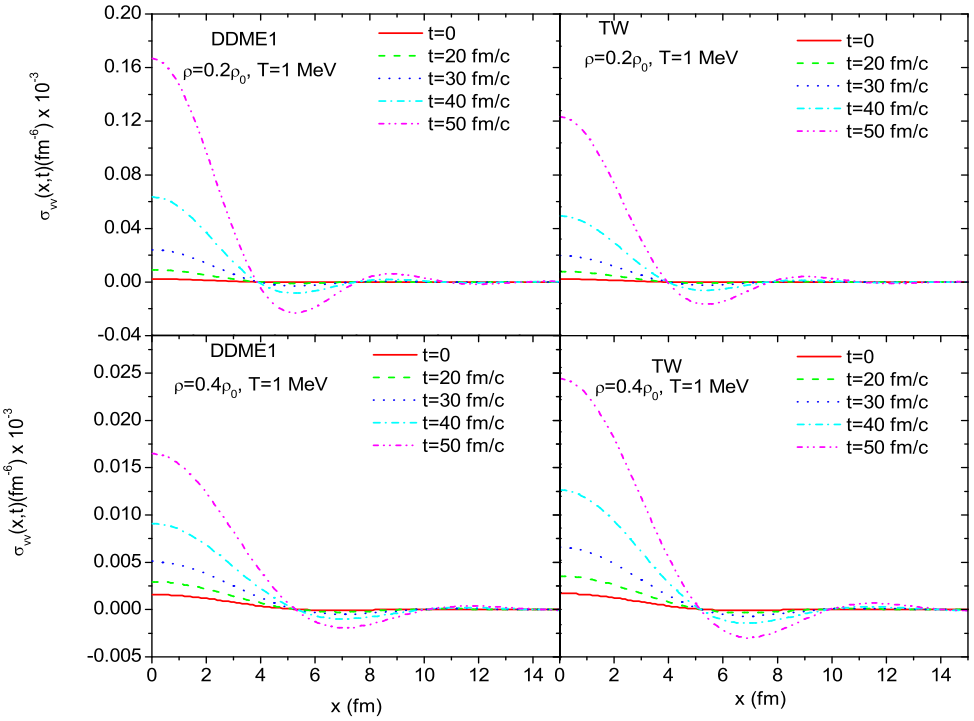

Figure 4.17: Current density correlation function as a function of distance at times t= 0, t= 20 fm/c, 30 fm/c, 40 fm/c and 50 fm/c at temperature T=1 MeV at density $\rho_b = 0.2\rho_0$ and $\rho_b = 0.4\rho_0$ calculated with DDME1 and TW

Table 4.2: The average speed of initial fragments of spinodal decomposition at T=1 MeV and T=5 MeV for TW

DDME1	T=1 MeV			T=5 MeV		
	t (fm/c)	$\sigma_{vv}(0,t)(fm^{-6})$	u_{rms}	t (fm/c)	$\sigma_{vv}(0,t)(fm^{-6})$	u_{rms}
	0	0.002×10^{-3}	$0.05c$	0	0.004×10^{-3}	$0.07c$
	20	0.008×10^{-3}	$0.09c$	20	0.010×10^{-3}	$0.11c$
$\rho_b = 0.2\rho_0$	30	0.020×10^{-3}	$0.15c$	30	0.018×10^{-3}	$0.14c$
	40	0.049×10^{-3}	$0.23c$	40	0.035×10^{-3}	$0.20c$
	50	0.123×10^{-3}	$0.37c$	50	0.067×10^{-3}	$0.27c$
	t (fm/c)	$\sigma_{vv}(0,t)(fm^{-6})$	u_{rms}	t (fm/c)	$\sigma_{vv}(0,t)(fm^{-6})$	u_{rms}
	0	0.0017×10^{-3}	$0.022c$	0	0.005×10^{-3}	$0.04c$
	20	0.0035×10^{-3}	$0.031c$	20	0.009×10^{-3}	$0.05c$
$\rho_b = 0.4\rho_0$	30	0.0066×10^{-3}	$0.043c$	30	0.015×10^{-3}	$0.065c$
	40	0.0126×10^{-3}	$0.059c$	40	0.027×10^{-3}	$0.086c$
	50	0.0244×10^{-3}	$0.082c$	50	0.045×10^{-3}	$0.11c$

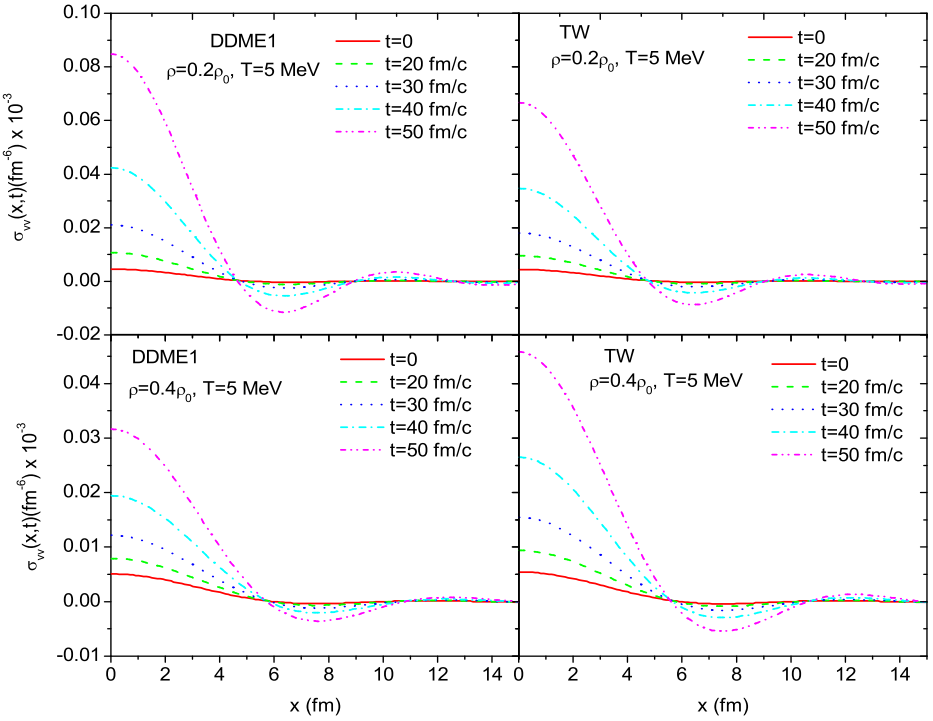

Figure 4.18: Current density correlation function as a function of distance at times t= 0, t= 20 fm/c, 30 fm/c, 40 fm/c and 50 fm/c at temperature T=5 MeV at density $\rho_b = 0.2\rho_0$ and $\rho_b = 0.4\rho_0$ calculated with DDME1 and TW

CHAPTER 5

CONCLUSION

We study the nuclear spinodal instabilities in the framework of a stochastic relativistic density-dependent mean-field theory with density-dependent coupling constants. The stochastic relativistic mean-field approach with density-dependent version is a valid model for investigating density fluctuation dynamics in the spinodal region. We use DDME1 and TW parameter sets in our numerical calculations. We start with Lorentz invariance Lagrangian, and the relativistic field equations are derived from Euler-Lagrange formalism. In the mean-field approach, the meson fields are defined in terms of densities. We use the relativistic Vlasov equation for a phase space distribution function and use the definitions of the baryon, scalar and current densities related by the phase space distribution function. Since we would like to investigate the early stage of density fluctuations, we linearize the quantities around their initial values. Finally, three coupled equations of density fluctuations are obtained by including initial information of the system.

In the first part of this thesis, we analyze the growth rates of unstable collective modes with respect to the wave number or wave length from a dispersion relation at two different initial densities below the normal density and at low temperatures. We study with the collective modes and due to the effects of non-collective modes after a certain wave numbers; growth rates of unstable modes are suppressed. We choose low temperature because we realize from pressure figure that the instability occurs below a critical temperature about $T_c \approx 14\ MeV$.

Spinodal decomposition of nuclear matter and nuclear fragmentation is the low energy processes. We also choose the initial baryon densities as $\rho_b = 0.2\rho_0$, $\rho_b = 0.4\rho_0$ in order to compare with previous calculations obtained in other models. Corresponding to the most unstable mode, we find a phase picture that exhibits a boundary of spinodal region. We also calculate a measure for the size of primary fragments in the spinodal region from half-wavelength at different temperature around $\rho_b \approx 0.3\rho_0$. We observe that the size of the clusters increases as temperature increases.

In the second part, we investigate the behavior of the spectral density correlation functions as a function of wave numbers at early times of fragmentation. Spectral density represents an increasing behavior at low wave number and a decreasing behavior at long wave number as expected. At different times, we calculate the baryon, scalar and current density correlation functions as a function of a distance between two space locations at temperatures T=1 MeV and T=5 MeV and at two initial baryon densities $\rho_b = 0.2\rho_0$, $\rho_b = 0.4\rho_0$. Stochastic mean field approach enables us to calculate early development of density correlation functions in spinodal region; they provide important information about the size of the early condensation regions and the current correlation function give the information about the average speed of condensing fragments.

Our results are in agreement with the results obtained in a nonrelativistic calculation with an effective Skyrme force [15, 25] and in the nonlinear relativistic Walecka model with NL3 parametrization [26, 36]. Our stochastic relativistic density-dependent approach is suitable for investigating the spinodal instability of hot nuclear matter occurred in heavy ion reactions.

We use a semi-classical model of a relativistic mean-field approach with density dependent couplings for a hot symmetric nuclear matter. We do not consider the quantum statistical effects on the density correlation functions which give considerable contributions, in particular, at low temperatures and at low densities. The charge asymmetric nuclear matter, which is studied by including the charged vector meson , is worked within this approach. It would become impor-

tant to understand the isospin dependence of the spinodal dynamics in multi-fragmentation reactions of neutron rich nuclear systems and for astrophysical processes.

REFERENCES

[1] Ph. Chomaz, M. Colonna and J. Randrup, Phys. Rep. **389** (2004) 263.

[2] G. Bertsh and P.J. Siemens, Phys. Lett. **B126** (1983) 9.

[3] G.F. Bertsch and S. das Gupta, Phys. Rep. **160** (1988) 189.

[4] A. Corbone et al, Phys. Rev. **C 83** (2011) 024308.

[5] J. B. Elliott et al, Phys. Rev. Lett.**88** (2002) 042701.

[6] E. Bonnet et al, Phys. Rev. Lett.**103** (2009) 072701.

[7] B. Borderie et all, Phys. Rev. Lett. **86** (2001) 3252.

[8] B. Borderie et al, Nucl. Phys.**A 734** (2004) 495.

[9] S. Ayik, Phys. Lett. **B 658** (2008) 174.

[10] G. Sauer, H. Chandra ve U. Mosel, Nucl. Phys.**A 264** (1976) 221-243.

[11] P. Bonche, S. Levit and D. Vautherin, Nucl. Phys.**A 427** (1984) 278-296.

[12] E. Suraud, Nucl. Phys. **A 462** (1987) 109- 149.

[13] H. Müller, ve B. D. Serot, Phys. Rev.**C 52** (1995) 2072-2091.

[14] B. D. Serot, and J. D. Walecka, "Advances in Nuclear Physics Vol.16", Plenium Press, New York-London, 1968.

[15] S.Ayik, N. Er, O. Yilmaz, A. Gökalp, Nucl. Phys. **812** (2008) 44.

[16] A A. Rios, Nucl. Phys. **A 845** (2010) 58.

[17] S. S. Avancini, L. Brito, D. P. Menezes and C. Providencia, Phys. Rev. **C 71** (2005) 044323.

[18] A. M. Santos, L. Brito and C. Providencia, Phys. Rev. **C 77** (2008) 045805.

[19] C. Ducoin, C. Providencia , A. M. Santos, L. Brito and Ph. Chomaz, Phys. Rev.**C 78** (2005) 055801.

[20] S. Ayik, M. Colonna and Ph. Chomaz, Phys. Lett. **B 353** (1995) 417.

[21] B. Jacquot, S. Ayik, Ph. Chomaz and M. Colonna, Phys. Lett. **B 383** (1996) 247.

[22] B. Jacquot, M. Colonna, S. Ayik and Ph. Chomaz, Nucl. Phys. **A 617** (1997) 356.

[23] M. Colonna, Ph. Chomaz and S. Ayik, Phys. Rev. Lett. **88** (2002) 122701.

[24] V. Baran, M. Colonna, M. Di Tora and A. B. Larionov, Nucl. Phys.**A 632** (1998) 287.

[25] N. Er, "Nuclear Spinodal Instabilities in Stochastic Mean-Field Approaches", PhD Thesis, METU, 2009.

[26] F.Acar,"Spinodal Instabilities in Symmetric Nuclear Matter within a Nonlinear Relativistic Mean-Field Approach", Ms Thesis, METU, 2011.

[27] S. Ayik, O. Yilmaz, N. Er, A. Gokalp, and P. Ring, Phys. Rev. **C 80** (2009) 034613.

[28] G. A. Lalazissis, T. Niksic, D. Vretenar, and P. Ring, Phys. Rev. **C 71** (2005) 024312.

[29] S. Typel and H. H. Wolter, Nuc. Phys.**A656** (1999) 331-364.

[30] T. Niksic, D. Vretenar and P. Ring, Phys. Rev. **C66** (2002) 064302.

[31] T. Niksic, D. Vretenar, P. Finelli, and P. Ring. Phys. Rev. **C 66** (2002) 024306.

[32] U. Badarch ,"Covariant Density Functional Theory for Nuclear Matter", Ph. D. Thesis, Giessen, (2007).

[33] M. Baldo and L. S. Ferreira, Phys. Rev. **C 59** (1999) 682-703.

[34] S. S. Avancini, L. Brito, D. P. Menezes, and C. Providencia, Phys. Rev. **C 70** (2004) 015203.

[35] M. L. Boas, "Mathematical Methods in the Physical Science", John Wiley Sons, (2006).

[36] S. Ayik, O. Yilmaz, F. Acar, B. Danisman, N. Er, A. Gokalp ,Nuc. Phys. **A 859** (2011) 73-86.

[37] A. Rios, Phys. Rev. **C 78** (2008) 044314.

APPENDIX A

AT ZERO TEMPERATURE

When we investigate relativistic problem for symmetric nuclear matter at zero temperature (T=0), there is no correlation; so, we can calculate only phase diagrams, the growth rates and the size of the primary cluster in spinodal region. Chemical potentials at T=0 are given by

$$\mu_0^* = \mu - \frac{\Gamma_v^2}{\mu_v^2}\rho_b^0 \tag{A.1}$$

At finite temperature, we use Fermi Dirac distribution function for the equilibrium phase space distribution function $f_0(\vec{p})$. However, at zero temperature, phase-space distribution function of equilibrium state $f_0(\vec{p})$ is given by step function. For the $T \to 0$ case, and $\mu_0^* = E_F^*$

$$f_0(\vec{p}) = \frac{1}{1+e^{\beta(\varepsilon_0^*-\mu_0^*)}} \to \Theta(\mu_0^* - E_0^*) = \begin{cases} 1, & \mu_0^* > \epsilon_0^* \\ 0, & \mu_0^* < \epsilon_0^* \end{cases} \tag{A.2}$$

At zero temperature

$$\begin{aligned} \vec{\nabla}_p f_0 &= \vec{\nabla}_p \theta\left(\mu_0^* - \sqrt{(c\vec{p})^2 + (M_0^* c^2)^2}\right) \\ &= -c\hat{p}\delta\left(cp - \sqrt{\mu_0^{*2} - (M_0^* c^2)^2}\right) \\ &= -c\hat{p}\delta(cp - cp_1) = \hat{p}\delta(cp - cp_1) \end{aligned} \tag{A.3}$$

here δ is the Kronecker delta and $cp_1 = \sqrt{\mu_0^{*2} - (M_0^* c^2)^2}$ is the momentum vector. By using the baryon density and reduced mass and the self-consistency

conditions at equilibrium,

$$M_0^* c^2 = Mc^2 - \Gamma_s(\rho_b^0)\phi_0 = Mc^2 - \frac{\Gamma_s^2}{\mu_s^2}\rho_s^2 \tag{A.4}$$

where

$$\rho_s^0 = \frac{\gamma}{(2\pi\hbar)^3}\int_0^{p_F} d^3p \frac{M^* c^2}{\sqrt{(c\vec{p})^2 + (M^* c^2)^2}} \tag{A.5}$$

$$\rho_b^0 = \frac{\gamma}{(2\pi\hbar)^3}\int_0^{p_F} d^3p = \frac{\gamma}{6\pi^2}\left(\frac{p_F}{\hbar}\right)^3 = \frac{\gamma}{6\pi^2}k_F^3 \tag{A.6}$$

the chemical potential at zero temperature can be calculated. The final forms of the relativistic Lindhard functions for T=0 and $\omega \to +i\Gamma$ are

$$\begin{pmatrix} \chi_{\rm v}(\vec{k},\omega) \\ \chi_{\rm s}(\vec{k},\omega) \\ \chi_{\rm b}(\vec{k},\omega) \\ \chi_{\rm vs}(\vec{k},\omega) \end{pmatrix} = \frac{2\pi\gamma}{(2\pi\hbar)^3}\frac{(p_1)^3}{\mu_0^*}k^2 \begin{pmatrix} \frac{1}{k}i\Gamma/c \\ \frac{M_0^* c^2}{\mu_0^*} \\ 1 \\ (M_0^* c^2/\mu_0^*)\left(i(\Gamma/c)\frac{1}{k}\right) \end{pmatrix}. \tag{A.7}$$

$$\begin{pmatrix} \tilde{\chi}_{\rm 2s}(\vec{k},\omega) \\ \tilde{\chi}_{\rm s}(\vec{k},\omega) \\ \tilde{\chi}_{\rm v}(\vec{k},\omega) \\ \tilde{\chi}_{\rm b}(\vec{k},\omega) \end{pmatrix} = \frac{2\pi\gamma}{(2\pi\hbar c)^3} \begin{pmatrix} \frac{(cp_1)^3}{\mu_0^*}k^2\left(\frac{M_0^* c^2}{\mu_0^*}\right)^2 L_2(p_1) \\ 2I_4(p_1) - (cp_1)^2\left(\frac{M_0^* c^2}{\mu_0^*}\right)^2\left(\frac{cp_1}{\mu_0^*}\right)k^2 L_2(p_1) \\ \left(\frac{M_0^* c^2}{\mu_0^{*2}}\right)(cp_1)^3 k(i\Gamma/c)L_2(p_1) \\ 2I_2(p_1) - \frac{2}{3}I_4(p_1) - \left(\frac{(cp_1)^2}{\mu_0^*}\right)^2\left(\frac{cp_1}{\mu_0^*}k\right)kL_4(p_1) \end{pmatrix} \tag{A.8}$$

where

$$I_2(p') \equiv \int_0^{p_1'} dp' \frac{p'^2}{[p'^2 + (M_0^* c^2)^2]^{1/2}} \tag{A.9}$$

$$I_4(p') \equiv \int_0^{p_1'} dp' \frac{p'^4}{[p'^2 + (M_0^* c^2)^2]^{3/2}} \tag{A.10}$$

$$\begin{pmatrix} L_0(p^{'}) \\ L_2(p^{'}) \\ L_4(p^{'}) \end{pmatrix} = \int_{-1}^{1} dx \begin{pmatrix} 1 \\ x^2 \\ x^4 \end{pmatrix} \frac{1}{(\Gamma/c)^2 + \left(k\frac{cp}{\varepsilon_0^*}\right)^2 x^2}$$

Eq. 3.45 at T=0 becomes,

$$\begin{pmatrix} A_1 & A_2 & A_3 \\ B_1 & B_2 & B_3 \\ C_1 & C_2 & C_3 \end{pmatrix} \begin{pmatrix} \delta\rho_{\mathrm{v}}(\vec{k},\omega) \\ \delta\rho_{\mathrm{s}}(\vec{k},\omega) \\ \delta\rho_b(\vec{k},\omega) \end{pmatrix} = \begin{pmatrix} 0 \\ 0 \\ 0 \end{pmatrix} \tag{A.11}$$

.

If we use $\omega \to -i\Gamma$, then we have $A_1 \to -A_1, B_1 \to -B_1, C_2 \to C_2, C_3 \to -C_3$. Finally, the determinant of the matrix becomes the same with the case of $\omega \to +i\Gamma$

$$\begin{vmatrix} A_1 & A_2 & A_3 \\ B_1 & B_2 & B_3 \\ C_1 & C_2 & C_3 \end{vmatrix} = A_3(B_1C_2 - C_1B_2) + B_3(C_1A_2 - A_1C_2) + C_3(A_1B_2 - B_1A_2) \tag{A.12}$$

As a result the terms are classified as real or pure imaginary $A_2, A_3, B_2, B_3, C_1, D_2$ and D_2 are real, $A_1 = iA_{11}, B_1 = iB_{11}, C_2 = iC_{12}$ and $D_3 = iD_{13}$ are imaginary.

APPENDIX B

SPECTRAL INTENSITY OF BARYON DENSITY FLUCTUATIONS

The spectral intensity of baryon density function is determined by

$$\begin{aligned}\tilde{\sigma}_{bb}(\vec{k},t)(2\pi)^3\delta(\vec{k}-\vec{k}') &= \overline{\delta\tilde{\rho}_b(\vec{k},t)\delta\tilde{\rho}_b^*(\vec{k}',t)} \\ &= \overline{\delta\rho_b^+(\vec{k})\delta\rho_b^+(\vec{k}')^*}e^{2\Gamma_k t} + \overline{+\delta\rho_b^-(\vec{k})\delta\rho_b^-(\vec{k}')^*}e^{-2\Gamma_k t} \\ &\quad \overline{+\delta\rho_b^+(\vec{k})\delta\rho_b^-(\vec{k}')^*} + \overline{\delta\rho_b^-(\vec{k})\delta\rho_b^+(\vec{k}')^*} \qquad \text{(B.1)}\end{aligned}$$

where time-dependent baryon density fluctuation function for growing and decaying poles is in the form

$$\delta\tilde{\rho}_b(\vec{k},t) = (\delta\rho_b(\vec{k}))^+e^{+\Gamma_k t} + (\delta\rho_b(\vec{k}))^-e^{-\Gamma_k t} \qquad \text{(B.2)}$$

with the initial amplitudes for growing and decaying poles are given by

$$\delta\rho_b^+(\vec{k}) = \frac{S_b^+D_1 + S_s^+D_2 + S_v^+D_3}{iN}. \qquad \text{(B.3)}$$

and

$$\delta\rho_b^-(\vec{k}) = \frac{S_b^-D_1 + S_s^-D_2 + S_v^-D_3}{-iN}. \qquad \text{(B.4)}$$

here short notations are used as the following

$$\begin{aligned} D_1 &= B_1C_2 - B_2C_1 \\ D_2 &= A_2C_1 - A_1C_2 \\ D_3 &= A_1B_2 - A_2B_1 \end{aligned} \tag{B.5}$$

and $\mp iN = \left(\frac{\partial\varepsilon(\vec{k},\omega)}{\partial\omega}\right)_{\omega=\mp i\Gamma}$. The correlation of baryon density initial amplitudes can be written in the following way for growing pole

$$\begin{aligned} \overline{\delta\rho_b^+(\vec{k})\delta\rho_b^+(\vec{k'})^*}|N|^2 &= \overline{S_b^+(\vec{k})S_b^+(\vec{k'})^*}|D_1|^2 + \overline{S_s^+(\vec{k})S_s^+(\vec{k'})^*}|D_2|^2 \\ &+ \overline{S_v^+(\vec{k})S_v^+(\vec{k'})^*}|D_3^{'}|^2 + \overline{S_b^+(\vec{k})S_s^+(\vec{k'})^*}D_1D_2 \\ &- i\overline{S_b^+(\vec{k})S_v^+(\vec{k'})^*}D_1D_3^{'} + \overline{S_s^+(\vec{k})S_b^+(\vec{k'})^*}D_2D_1 \\ &- i\overline{S_s^+(\vec{k})S_v^+(\vec{k'})^*}D_2D_3^{'} + i\overline{S_v^+(\vec{k})S_b^+(\vec{k'})^*}D_3^{'}D_1 \\ &+ i\overline{S_v^+(\vec{k})S_s^+(\vec{k'})^*}D_3^{'}D_2 \end{aligned} \tag{B.6}$$

here D_1, D_2 are real terms but D_3 is imaginary so we use $D_3^{'}$ notation to show real part of this term.

The decaying poles of for the correlation of baryon density initial amplitudes is expressed in the following way

$$\begin{aligned} \overline{\delta\rho_b^-(\vec{k})\delta\rho_b^-(\vec{k'})^*}|N|^2 &= \overline{S_b^-(\vec{k})S_b^-(\vec{k'})^*}|D_1|^2 + \overline{S_s^-(\vec{k})S_s^-(\vec{k'})^*}|D_2|^2 \\ &+ \overline{S_v^-(\vec{k})S_v^-(\vec{k'})^*}|D_3^{'}|^2 + \overline{S_b^-(\vec{k})S_s^-(\vec{k'})^*}D_1D_2 \\ &+ i\overline{S_b^-(\vec{k})S_v^-(\vec{k'})^*}D_1D_3^{'} + \overline{S_s^-(\vec{k})S_b^-(\vec{k'})^*}D_2D_1 \\ &+ i\overline{S_s^-(\vec{k})S_v^-(\vec{k'})^*}D_2D_3^{'} - i\overline{S_v^-(\vec{k})S_b^-(\vec{k'})^*}D_3^{'}D_1 \\ &- i\overline{S_v^-(\vec{k})S_s^-(\vec{k'})^*}D_3^{'}D_2 \end{aligned} \tag{B.7}$$

fixed terms are in the following form

$$\begin{aligned}
\overline{\delta\rho_b^+(\vec{k})\delta\rho_b^-(\vec{k'})^*}(-|N|)^2 &= \overline{S_b^+(\vec{k})S_b^-(\vec{k'},)^*}|D_1|^2 + \overline{S_s^+(\vec{k},)S_s^-(\vec{k'})^*}|D_2|^2 \\
&- \overline{S_v^+(\vec{k})S_v^-(\vec{k'})^*}|D_3^{'}|^2 + \overline{S_b^+(\vec{k})S_s^-(\vec{k'})^*}D_1D_2 \\
&+ \overline{iS_b^+(\vec{k})S_v^-(\vec{k'})^*}D_1D_3^{'} + \overline{S_s^+(\vec{k})S_b^-(\vec{k'})^*}D_2D_1 \\
&+ \overline{iS_s^+(\vec{k})S_v^-(\vec{k'})^*}D_2D_3^{'} + \overline{iS_v^+(\vec{k})S_b^-(\vec{k'})^*}D_3^{'}D_1 \\
&+ \overline{iS_v^+(\vec{k},\omega)S_s^-(\vec{k'},\omega)^*}D_3^{'}D_2 \qquad \text{(B.8)}
\end{aligned}$$

$$\begin{aligned}
\overline{\delta\rho_b^-(\vec{k})\delta\rho_b^+(\vec{k'})^*}(-|N|)^2 &= \overline{S_b^-(\vec{k},)S_b^+(\vec{k'})^*}|D_1|^2 + \overline{S_s^-(\vec{k})S_s^+(\vec{k'})^*}|D_2|^2 \\
&- \overline{S_v^+(\vec{k})S_v^-(\vec{k'})^*}|D_3^{'}|^2 + \overline{S_b^-(\vec{k})S_s^+(\vec{k'})^*}D_1D_2 \\
&- \overline{iS_b^-(\vec{k})S_v^-(\vec{k'})^*}D_1D_3^{'} + \overline{S_s^-(\vec{k})S_b^+(\vec{k'})^*}D_2D_1 \\
&- \overline{iS_s^-(\vec{k})S_v^+(\vec{k'})^*}D_2D_3^{'} - \overline{iS_v^+(\vec{k})S_b^-(\vec{k'})^*}D_3^{'}D_1 \\
&- \overline{iS_v^+(\vec{k})S_s^-(\vec{k'})^*}D_3^{'}D_2 \qquad \text{(B.9)}
\end{aligned}$$

The source terms corresponding to the correlation is given by

$$\begin{pmatrix} S_b^{\pm}(\vec{k},\omega) \\ S_s^{\pm}(\vec{k},\omega) \\ S_v^{\pm}(\vec{k},\omega) \end{pmatrix} \equiv \gamma^2 \int \frac{d^3p}{(2\pi\hbar)^3} \begin{pmatrix} 1 \\ \frac{M_0^*c^2}{\epsilon_0^*} \\ \frac{c\vec{p}}{\epsilon_0^*} \end{pmatrix} \frac{\delta f(\vec{k},\vec{p},0)}{\pm i\Gamma - \vec{v}_0\cdot\vec{k}} \qquad \text{(B.10)}$$

the second moment of the initial phase-space distribution function $\delta\tilde{f}(\vec{k},\vec{p},0)$ is used to write the correlation functions and it can be defined as

$$\overline{\delta\tilde{f}(\vec{k},\vec{p},0)(\delta\tilde{f}(\vec{k'},\vec{p'},t))^*} = (2\pi)^3\delta^3(\vec{k}-\vec{k'})(2\pi\hbar)^3\delta^3(\vec{p}-\vec{p'})f(p)(1-f(p)) \quad \text{(B.11)}$$

we can get the following expression

$$\overline{\tilde{S}_b(\vec{k},\omega)^+(\tilde{S}_b(\vec{k'},\omega)^+)^*} = \gamma^2(2\pi)^3\delta(\vec{k}-\vec{k'})\int \frac{d^3p}{(2\pi\hbar)^3}\frac{f_0(\vec{p})[1-f_0(\vec{p})]}{\Gamma^2+(v_0\cdot\vec{k})^2}. \qquad \text{(B.12)}$$

$$\begin{pmatrix} \overline{S_b^+(\vec{k})S_b^+(\vec{k}')^*} \\ \overline{S_s^+(\vec{k})S_s^+(\vec{k}')^*} \\ \overline{S_v^+(\vec{k})S_v^+(\vec{k}')^*} \\ \overline{S_b^+(\vec{k})S_s^+(\vec{k}')^*} \end{pmatrix} = \begin{pmatrix} \overline{S_b^-(\vec{k})S_b^-(\vec{k}')^*} \\ \overline{S_s^-(\vec{k})S_s^-(\vec{k}')^*} \\ \overline{S_v^-(\vec{k})S_v^-(\vec{k}')^*} \\ \overline{S_b^-(\vec{k})S_s^-(\vec{k}')^*} \end{pmatrix} = \gamma^2(2\pi)^3\delta(\vec{k}-\vec{k}') \begin{pmatrix} K_{11}^{++} \\ K_{22}^{++} \\ K_{33}^{++} \\ K_{12}^{++} \end{pmatrix} \tag{B.13}$$

$$\begin{pmatrix} \overline{S_b^+(\vec{k})S_b^-(\vec{k}')^*} \\ \overline{S_s^+(\vec{k})S_s^-(\vec{k}')^*} \\ \overline{S_v^+(\vec{k})S_v^-(\vec{k}')^*} \\ \overline{S_b^\pm(\vec{k})S_s^\mp(\vec{k}')^*} \end{pmatrix} = \begin{pmatrix} \overline{S_b^-(\vec{k})S_b^+(\vec{k}')^*} \\ \overline{S_s^-(\vec{k})S_s^+(\vec{k}')^*} \\ \overline{S_v^-(\vec{k})S_v^+(\vec{k}')^*} \\ \overline{S_b^\mp(\vec{k})S_s^\pm(\vec{k}')^*} \end{pmatrix} = -\gamma^2(2\pi)^3\delta(\vec{k}-\vec{k}') \begin{pmatrix} K_{11}^{+-} \\ K_{22}^{+-} \\ K_{33}^{+-} \\ K_{12}^{+-} \end{pmatrix} \tag{B.14}$$

$$\begin{aligned} \overline{S_b^+(\vec{k})S_v^+(\vec{k}')^*} &= \overline{S_v^+(\vec{k})S_b^+(\vec{k}')^*} = 0 \\ \overline{S_s^+(\vec{k})S_v^+(\vec{k}')^*} &= \overline{S_v^+(\vec{k})S_v^+(\vec{k}')^*} = 0 \\ \overline{S_b^-(\vec{k})S_v^-(\vec{k}')^*} &= \overline{S_v^-(\vec{k})S_b^-(\vec{k}')^*} = 0 \\ \overline{S_s^-(\vec{k})S_v^-(\vec{k}')^*} &= \overline{S_v^-(\vec{k})S_v^-(\vec{k}')^*} = 0 \end{aligned} \tag{B.15}$$

due to the integral of $\int \frac{x^n dx}{x^2+a^2}$ gives zero for odd n.

with the integrals

$$\begin{pmatrix} K_{11}^{++} \\ K_{22}^{++} \\ K_{33}^{++} \\ K_{12}^{++} \end{pmatrix} \equiv \gamma^2 \int \frac{d^3p}{(2\pi\hbar)^3} \frac{1}{\Gamma^2+(\alpha x)^2} f(p)(1-f(p)) \begin{pmatrix} 1 \\ \left(\frac{M_0^* c^2}{\epsilon_0^*}\right)^2 \\ \left(c\frac{px}{\epsilon_0^*}\right)^2 \\ \left(\frac{M_0^* c^2}{\epsilon_0^*}\right) \end{pmatrix} \tag{B.16}$$

and

$$\begin{pmatrix} K_{11}^{+-} \\ K_{22}^{+-} \\ K_{33}^{+-} \\ K_{12}^{+-} \end{pmatrix} \equiv \gamma^2 \int \frac{d^3p}{(2\pi\hbar)^3} \frac{-\Gamma^2 + (\vec{v}_0 \cdot \vec{k})^2}{[\Gamma^2 + (\vec{v}_0 \cdot \vec{k})^2]^2} f(p)(1 - f(p)) \begin{pmatrix} 1 \\ \left(\frac{M_0^* c^2}{\epsilon_0^*}\right)^2 \\ \left(c\frac{\vec{p}\cdot\hat{k}}{\epsilon_0^*}\right)^2 \\ \left(\frac{M_0^* c^2}{\epsilon_0^*}\right) \end{pmatrix} \quad \text{(B.17)}$$

Finally, The correlation function of baryon density fluctuation becomes for growing poles,decaying poles and mixed terms

$$\begin{aligned} \overline{\delta\rho_b^+(\vec{k})\delta\rho_b^+(\vec{k})^*} &= \gamma^2(2\pi)^3\delta(\vec{k} - \vec{k}') \\ &\quad \times \frac{|D_1|^2 K_{11}^{++} + |D_2|^2 K_{22}^{++} + |D_3|^3 K_{33}^{++} + 2D_1 D_2 K_{12}^{++}}{|N|^2} \end{aligned} \quad \text{(B.18)}$$

in the similar process, we can obtain the decaying pole and the mixed term

$$\begin{aligned} \overline{\delta\rho_b^-(\vec{k})\delta\rho_b^-(\vec{k}')^*}|N|^2 &= \gamma^2(2\pi)^3\delta(\vec{k} - \vec{k}') \left[|D_1|^2 K_{11}^{++} + |D_2|^2 K_{22}^{++} + |D_3|^2 K_{33}^{++}\right. \\ &+ \left. 2D_1 D_2 K_{12}^{++}\right] \end{aligned} \quad \text{(B.19)}$$

$$\begin{aligned} \overline{\delta\rho_b^+(\vec{k})\delta\rho_b^-(\vec{k}')^*}|N|^2 &= \gamma^2(2\pi)^3\delta(\vec{k} - \vec{k}') \left[|D_1|^2 K_{11}^{+-} + |D_2|^2 K_{22}^{+-} - |D_3|^2 K_{33}^{+-}\right. \\ &+ \left. 2D_1 D_2 K_{12}^{+-}\right] \end{aligned} \quad \text{(B.20)}$$

$$\begin{aligned} \overline{\delta\rho_b^-(\vec{k})\delta\rho_b^+(\vec{k}')^*}|N|^2 &= \gamma^2(2\pi)^3\delta(\vec{k} - \vec{k}') \left[|D_1|^2 K_{11}^{+-} + |D_2|^2 K_{22}^{+-}\right. \\ &- \left. |D_3|^2 K_{33}^{+-} + 2D_1 D_2 K_{12}^{+-}\right] \end{aligned} \quad \text{(B.21)}$$

Consequently, the spectral intensity of baryon density correlation function can be found

$$\tilde{\sigma}_{bb}(\vec{k},t)(2\pi)^3\delta(\vec{k}-\vec{k}') = \overline{\delta\tilde{\rho}_b(\vec{k},t)\delta\tilde{\rho}_b^*(\vec{k}',t)}$$

$$\begin{aligned}\tilde{\sigma}_{bb}(\vec{k},t) &= \frac{[K_{11}^+|D_1|^2+K_{22}^+|D_2|^2+K_{33}^+|D_3|^2+2K_{12}^+D_1D_2]}{|\left(\frac{\partial\varepsilon(\vec{k},\omega)}{\partial\omega}\right)_{\omega=i\Gamma}|^2}(e^{2\Gamma t}+e^{-2\Gamma t}) \\ &+ 2\frac{[K_{11}^-|D_1|^2+K_{22}^-|D_2|^2-K_{33}^-|D_3|^2+2K_{12}^-D_1D_2]}{|\left(\frac{\partial\varepsilon(\vec{k},\omega)}{\partial\omega}\right)_{\omega=i\Gamma}|^2} \qquad \text{(B.22)}\end{aligned}$$

with the integrals

$$\begin{pmatrix} K_{11}^{\pm} \\ K_{22}^{\pm} \\ K_{33}^{\pm} \\ K_{12}^{\pm} \end{pmatrix} \equiv \gamma^2 \int \frac{d^3p}{(2\pi\hbar)^3}\frac{\Gamma^2 \pm (\vec{v}_0\cdot\vec{k})^2}{[\Gamma^2+(\vec{v}_0\cdot\vec{k})^2]^2}f(p)(1-f(p)) \begin{pmatrix} 1 \\ \left(\frac{M_0^*c^2}{\epsilon_0^*}\right)^2 \\ \left(c\frac{\vec{p}\cdot\hat{k}}{\epsilon_0^*}\right)^2 \\ \left(\frac{M_0^*c^2}{\epsilon_0^*}\right) \end{pmatrix} \qquad \text{(B.23)}$$

APPENDIX C

SPECTRAL INTENSITY OF SCALAR AND VECTOR DENSITY FLUCTUATIONS

By using three coupled equations with the source terms, baryon, scalar and vector density fluctuations, we obtain the spectral intensity of scalar and vector density fluctuations.

$$\delta\rho_v(\vec{k},\omega)A_1 + \delta\rho_s(\vec{k},\omega)A_2 + \delta\rho_b(\vec{k},\omega)A_3 + = iS_1 \tag{C.1}$$

$$\delta\rho_v(\vec{k},\omega)B_1 + \delta\rho_s(\vec{k},\omega)B_2 + \delta\rho_b(\vec{k},\omega)B_3 + = iS_2 \tag{C.2}$$

$$\delta\rho_v(\vec{k},\omega)C_1 + \delta\rho_s(\vec{k},\omega)C_2 + \delta\rho_b(\vec{k},\omega)C_3 + = iS_3 \tag{C.3}$$

by using these equations scalar and vector density fluctuations can be found in the following form

$$\delta\rho_s(\vec{k},\omega) = i\frac{S_1(B_3C_1 - B_1C_3) + S_2(C_3A_1 - C_1A_3) + S_3(B_1A_3 - B_3A_3)}{[\varepsilon(k,w)]} \tag{C.4}$$

and

$$\delta\rho_v(\vec{k},\omega) = i\frac{S_1(C_3B_2 - C_2B_3) + S_2(C_2A_3 - C_3A_2) + S_3(B_3A_2 - B_2A_3)}{[\varepsilon(k,w)]} \tag{C.5}$$

where $\varepsilon(k,w)$ is the susceptibility and given by $\varepsilon(k,w) = A_3D_1 + B_3D_2 + C_3D_3$. For the scalar and baryon case, $D_1^s = C_1B_3 - i^2B_1C_3$, $D_2^s = i^2A_1B_3 - C_1A_3$, $D_3^s = i(B_1A_3 - A_1B_3)$.

The definition of the spectral intensity for scalar density fluctuations is given

$$\begin{aligned}\tilde{\sigma}_{ss}(\vec{k},t)(2\pi)^3\delta(\vec{k}-\vec{k}') &= \overline{\delta\tilde{\rho}_s(\vec{k},t)\delta\tilde{\rho}_s^*(\vec{k}',t)} \\ &= \overline{\delta\rho_s^+(\vec{k})\delta\rho_s^+(\vec{k}')^*}e^{2\Gamma_k t} + \overline{+\delta\rho_s^-(\vec{k})\delta\rho_s^-(\vec{k}')^*}e^{-2\Gamma_k t} \\ &\quad +\overline{\delta\rho_s^+(\vec{k})\delta\rho_s^-(\vec{k}')^*} + \overline{\delta\rho_s^-(\vec{k})\delta\rho_s^+(\vec{k}')^*} \qquad \text{(C.6)}\end{aligned}$$

By following the same procedure in appendix B, the results can be obtained by

$$\begin{aligned}\tilde{\sigma}_s(\vec{k},t) &= \frac{[K_{11}^+|D_1^s|^2 + K_{22}^+|D_2^s|^2 + K_{33}^+|D_3^s|^2 + 2K_{12}^+D_1^sD_2^s]}{\left|\left(\frac{\partial\varepsilon(\vec{k},\omega)}{\partial\omega}\right)_{\omega=i\Gamma}\right|^2}(e^{2\Gamma t}+e^{-2\Gamma t}) \\ &\quad +2\frac{[K_{11}^-|D_1^s|^2 + K_{22}^-|D_2^s|^2 - K_{33}^-|D_3^s|^2 + 2K_{12}^-D_1^sD_2^s]}{\left|\left(\frac{\partial\varepsilon(\vec{k},\omega)}{\partial\omega}\right)_{\omega=i\Gamma}\right|^2} \qquad \text{(C.7)}\end{aligned}$$

however, vector case has different form. $D_1^v = i(B_2C_3 - C_2B_3), D_2^v = i(C_2A_3 - A_2C_3), D_3^v = A_2B_3 - B_2A_3$. and the vector density fluctuations is found as

$$\begin{aligned}\tilde{\sigma}_{vv}(\vec{k},t)(2\pi)^3\delta(\vec{k}-\vec{k}') &= \overline{\delta\tilde{\rho}_v(\vec{k},t)\delta\tilde{\rho}_v^*(\vec{k}',t)} \\ &= \overline{\delta\rho_v^+(\vec{k})\delta\rho_v^+(\vec{k}')^*}e^{2\Gamma_k t} + \overline{+\delta\rho_v^-(\vec{k})\delta\rho_v^-(\vec{k}')^*}e^{-2\Gamma_k t} \\ &\quad +\overline{\delta\rho_v^+(\vec{k})\delta\rho_v^-(\vec{k}')^*} + \overline{\delta\rho_v^-(\vec{k})\delta\rho_v^+(\vec{k}')^*} \qquad \text{(C.8)}\end{aligned}$$

the vector correlation of growing pole is given by,

$$\begin{aligned}\overline{\delta\rho_v^+(\vec{k})\delta\rho_v^+(\vec{k}')^*}|N|^2 &= \overline{S_b^+(\vec{k})S_b^+(\vec{k}')^*}|D_1'|^2 + \overline{S_s^+(\vec{k})S_s^+(\vec{k}')^*}|D_2'|^2 \\ &+ \overline{S_v^+(\vec{k})S_v^+(\vec{k}')^*}|D_3|^2 + \overline{S_b^+(\vec{k})S_s^+(\vec{k}')^*}D_1{}'D_2' \\ &+ i\overline{S_b^+(\vec{k})S_v^+(\vec{k}')^*}D_1{}'D_3 + \overline{S_s^+(\vec{k})S_b^+(\vec{k}')^*}D_2{}'D_1{}' \\ &+ i\overline{S_s^+(\vec{k})S_v^+(\vec{k}')^*}D_2{}'D_3 + \overline{S_v^+(\vec{k})S_b^+(\vec{k}')^*}D_3(-iD_1{}') \\ &+ \overline{S_v^+(\vec{k})S_s^+(\vec{k}')^*}D_3(-iD_2{}') \qquad \text{(C.9)}\end{aligned}$$

and the decaying and mix poles for correlation functions are given

$$\begin{aligned}
\overline{\delta\rho_v^-(\vec{k})\delta\rho_v^-(\vec{k'})^*}|N|^2 &= \overline{S_b^-(\vec{k})S_b^-(\vec{k'})^*}|D_1^{'}|^2 + \overline{S_s^-(\vec{k})S_s^-(\vec{k'})^*}|D_2^{'}|^2 \\
&+ \overline{S_v^-(\vec{k})S_v^-(\vec{k'})^*}|D_3^{'}|^2 + \overline{S_b^-(\vec{k})S_s^-(\vec{k'})^*}D_1^{'}D_2^{'} \\
&- i\overline{S_b^-(\vec{k})S_v^-(\vec{k'})^*}D_1^{'}D_3 + \overline{S_s^-(\vec{k})S_b^-(\vec{k'})^*}D_2^{'}D_1^{'} \\
&- i\overline{S_s^-(\vec{k})S_v^-(\vec{k'})^*}D_2^{'}D_3 - i\overline{S_v^-(\vec{k})S_b^-(\vec{k'})^*}D_3D_1^{'} \\
&- i\overline{S_v^-(\vec{k})S_s^-(\vec{k'})^*}D_3D_2^{'} \qquad \text{(C.10)}
\end{aligned}$$

$$\begin{aligned}
\overline{\delta\rho_v^+(\vec{k})\delta\rho_v^-(\vec{k'})^*}(-|N|)^2 &= \overline{S_b^+(\vec{k})S_b^-(\vec{k'})^*}|D_1^{'}|^2 - \overline{S_s^+(\vec{k})S_s^-(\vec{k'})^*}|D_2^{'}|^2 \\
&+ \overline{S_v^+(\vec{k})S_v^-(\vec{k'})^*}|D_3|^2 - \overline{S_b^+(\vec{k})S_s^-(\vec{k'})^*}D_1^{'}D_2^{'} \\
&+ i\overline{S_b^+(\vec{k})S_v^-(\vec{k'})^*}D_1^{'}D_3 - \overline{S_s^+(\vec{k})S_b^-(\vec{k'})^*}D_2^{'}D_1^{'} \\
&+ i\overline{S_s^+(\vec{k})S_v^-(\vec{k'})^*}D_2^{'}D_3 + i\overline{S_v^+(\vec{k})S_b^-(\vec{k'})^*}D_3D_1^{'} \\
&+ i\overline{S_v^+(\vec{k})S_s^-(\vec{k'})^*}D_3D_2^{'} \qquad \text{(C.11)}
\end{aligned}$$

$$\begin{aligned}
\overline{\delta\rho_v^-(\vec{k})\delta\rho_v^+(\vec{k'})^*}(-|N|)^2 &= -\overline{S_b^-(\vec{k})S_b^+(\vec{k'})^*}|D_1^{'}|^2 - i\overline{S_s^-(\vec{k})S_s^+(\vec{k'})^*}|D_2^{'}|^2 \\
&+ i\overline{S_v^+(\vec{k})S_v^-(\vec{k'})^*}|D_3|^2 - \overline{S_b^-(\vec{k})S_s^+(\vec{k'})^*}D_1^{'}D_2^{'} \\
&- i\overline{S_b^-(\vec{k})S_v^-(\vec{k'})^*}D_1^{'}D_3 - \overline{S_s^-(\vec{k})S_b^+(\vec{k'})^*}D_2^{'}D_1^{'} \\
&- i\overline{S_s^-(\vec{k})S_v^+(\vec{k'})^*}D_2^{'}D_3 - i\overline{S_v^+(\vec{k})S_b^-(\vec{k'})^*}D_3^{'}D_1 \\
&- i\overline{S_v^+(\vec{k})S_s^-(\vec{k'})^*}D_3D_2^{'} \qquad \text{(C.12)}
\end{aligned}$$

Finally, the correlation function of baryon density fluctuation are obtained for growing poles,decaying poles and mixed terms

$$\begin{aligned}\overline{\delta\rho_v^+(\vec{k})\delta\rho_v^+(\vec{k})^*} &= \overline{\delta\rho_v^-(\vec{k})\delta\rho_v^-(\vec{k'})^*} \\ &= (2\pi)^3\delta^3(\vec{k}-\vec{k'}) \\ &\quad\times\frac{|D_1|^2K_{11}^{++}+|D_2|^2K_{22}^{++}+|D_3|^3K_{33}^{++}+2D_1D_2K_{12}^{++}}{|N|^2}\end{aligned} \tag{C.13}$$

in the similar process, we can obtain the decaying pole and the mixed term

$$\begin{aligned}\overline{\delta\rho_v^+(\vec{k})\delta\rho_v^-(\vec{k'})^*} &= \overline{\delta\rho_v^-(\vec{k})\delta\rho_v^+(\vec{k'})^*} \\ &= (2\pi)^3\delta^3(\vec{k}-\vec{k'}) \\ &\quad\times\frac{[-|D_1|^2K_{11}^{+-}-|D_2|^2K_{22}^{+-}+|D_3|^2K_{33}^{+-}-2D_1D_2K_{12}^{+-}]}{(-|N|)^2}\end{aligned} \tag{C.14}$$

Finally, vector density fluctuation is found as

$$\begin{aligned}\tilde{\sigma}_v(\vec{k},t) &= \frac{[K_{11}^+|D_1^v|^2+K_{22}^+|D_2^v|^2+K_{33}^+|D_3^v|^2+2K_{12}^+D_1^vD_2^v]}{|\left(\frac{\partial\varepsilon(\vec{k},\omega)}{\partial\omega}\right)_{\omega=i\Gamma_k}|^2}(e^{2\Gamma t}+e^{-2\Gamma t}) \\ &\quad -2\frac{[K_{11}^-|D_1^v|^2+K_{22}^-|D_2^v|^2-K_{33}^-|D_3^v|^2+2K_{12}^-D_1^vD_2^v]}{|\left(\frac{\partial\varepsilon(\vec{k},\omega)}{\partial\omega}\right)_{\omega=i\Gamma_k}|^2}\end{aligned} \tag{C.15}$$